INFORMATION TO USERS

This manuscript has been reproduced from the microfilm master. UMI films the text directly from the original or copy submitted. Thus, some thesis and dissertation copies are in typewriter face, while others may be from any type of computer printer.

The quality of this reproduction is dependent upon the quality of the copy submitted. Broken or indistinct print, colored or poor quality illustrations and photographs, print bleedthrough, substandard margins, and improper alignment can adversely affect reproduction.

In the unlikely event that the author did not send UMI a complete manuscript and there are missing pages, these will be noted. Also, if unauthorized copyright material had to be removed, a note will indicate the deletion.

Oversize materials (e.g., maps, drawings, charts) are reproduced by sectioning the original, beginning at the upper left-hand corner and continuing from left to right in equal sections with small overlaps.

Photographs included in the original manuscript have been reproduced xerographically in this copy. Higher quality 6" x 9" black and white photographic prints are available for any photographs or illustrations appearing in this copy for an additional charge. Contact UMI directly to order.

Bell & Howell Information and Learning
300 North Zeeb Road, Ann Arbor, MI 48106-1346 USA
800-521-0600

The Development of Laminar Morphology in a Co-Rotating Twin Screw Extruder

by

Oscar Alberto Rodriguez Veloz

A Thesis submitted to the Faculty of Graduate Studies and Research in partial fulfilment of the requirements of the degree of Master of Engineering

June 1998
Department of Chemical Engineering
McGill University, Montreal

ABSTRACT

Laminar morphology of high density polyethylene (HDPE) / polyamide-6 (PA-6) blends was obtained, for the first time, in a co-rotating twin screw extruder. The morphology analysis in the interior of the adapter, which connects the extruder with a slit die, revealed that, under specific processing conditions, it is possible to produce layers of PA-6 in the end of the screw zone of the extruder. These layers were visible at very low magnification (6.7X). It was also observed that a high adapter converging angle (70°) produced breakup of the layers, due to the high elongational and shear flow.

The micrographs of the extruded final products showed distributed layers across the sample thickness and along the flow direction. The effect of design variables such as adapter angle and die gap on the final product morphology was studied. It was noted that a low die gap resulted in high stretching, leading to particle breakup that resulted in an increase of toluene permeability. On the other hand, the adapter angle did not have significant influence on the final product morphology. The effects of processing variables, including temperature profile, feed rate, and screw speed, were evaluated. It was observed that a low temperature profile along the barrel, but high enough to melt the nylon-6, is required to obtain elongated platelets. The formation of laminar morphology of the extruded blend depends strongly on the feed rate. Low feed rates increase residence time that produces premature melting of the dispersed phase and causes rupture of the layers. Conversely, very high feed rates contribute to the appearance of unmelted pellets in the extrudate. It was also observed that high extruder screw rotation speeds enhance laminar morphology development, but apparently reduce the contact time between the two phases that results in poor mechanical properties.

There is a strong relation between the morphology, permeability and impact properties of the blend. Good laminar morphology results in low permeability and poor impact properties. In this work, blends with improved toluene permeability up to 113 times the permeability of the matrix were obtained. This value is 2.5 times better than the best value reported for products of single screw extrusion. For coextruded products, the

estimated improvement is 262 times for the same system and composition. Mechanical tests showed that the HDPE/PA-6 extrudates maintain stiffness and tensile strength values comparable to those of polyethylene. In order to obtain products with optimum balance between the permeability and the mechanical properties, a statistical analysis was carried out. It produced useful information regarding the important processing and design factors that affect the product properties.

RÉSUMÉ

La morphologie laminaire du mélange de polyéthylène haute densité (HDPE) et de polyamide-6 (PA-6) a été obtenue, pour la première fois, dans une extrudeuse co-rotative à double vis. L'analyse de la morphologie à l'intérieur de l'adaptateur, lequel raccorde l'extrudeuse à la filière, a révélé que, sous des conditions de fonctionnement spécifiques, des lamelles de polyamide-6 peuvent être formées a la fin de la zone de la vis. Ces lamelles ont été visibles à faible grossissement (X6.7). Il a été observé qu'un adaptateur avec un grand angle convergent (70°) produisait la rupture des lamelles à cause du haut flux au cisaillement et à l'allongement.

Les photographies de microscope des produits extrudés ont montré une distribution des lamelles sur toute l'épaisseur de l'échantillon et le long de la direction d'écoulement. L'effet des variables géométriques comme l'angle de l'adaptateur et l'écartement de filière sur la morphologie des produits finis a été etudié. Il a été remarqué qu'un petit écartement de filière provoque un grand étirage des lamelles ce qui cause leur rupture et accroît la perméabilité au toluene du mélange. D'un autre côté, l'angle de l'adaptateur n'a pas montré de résultats notables sur la morphologie du produit final. Les effets des variables du procédé de transformation, qui comprennent le profil de température, la vitesse de vis et d'alimentation, ont été evalués. Il a été observé qu'il est nécessaire d'avoir un profil de température bas, mais aussi suffisamment haut pour permettre la fusion du nylon-6, le long du cylindre d'extrusion, afin d'obtenir des plaquettes allongées. La formation de la morphologie laminaire du mélange extrudé dépend fortement de la vitesse d'alimentation. Une vitesse d'alimentation lente augmente le temps de séjour, lequel provoque la fusion prématurée de la phase dispersée et la rupture des lamelles. Au contraire, une vitesse d'alimentation rapide contribue à l'apparition de granulés non fondus dans les produits extrudés. Il a aussi été noté aussi qu'une vitesse rapide de rotation de vis améliore le développement de la morphologie laminaire, mais apparemment réduit le temps de contact entre les deux phases qui résulte en des propriétés mécaniques déficientes.

Il existe une importante relation entre la morphologie, la perméabilité et les propriétés d'impact des mélanges de polymères. Une bonne morphologie laminaire provoque une faible perméabilité et de mauvaises propriétés mécaniques. Dans le cadre de cette recherche, une perméabilité au toluene jusqu'à 113 fois supérieure à la matrice a été obtenue pour certains mélanges. Cette valeur est 2.5 fois supérieure à la valeur maximale rapportée dans le cas de l'extrusion monovis. Pour le procédé de coextrusion, on estime une amélioration de la perméabilité de 262 fois pour le même système et la même composition. Les tests mécaniques ont montré que les produits d'extrusion à double vis du mélange de HDPE et de PA-6 ont des valeurs de rigidité et de force de tension similaires à celles du HDPE seul. Une analyse statistique a été effectuée, afin d'obtenir des produits avec une balance optimale entre la perméabilité et les propriétes mécaniques,. Cette analyse a apporté des informations utiles pour les paramètres de transformation et pour la géometrie de l'extrudeuse qui affectent les propriétés du produit final.

RESUMEN

Por primera vez se obtuvo la morfología laminar en la mezcla de polietileno de alta densidad (HDPE) y poliamida-6 (PA-6) en un extrusor co-rotativo de doble tornillo. El análisis de la morfología en el interior del adaptador, que conecta el extrusor con el dado, reveló que bajo ciertas condiciones de procesamiento, es posible producir láminas de poliamida-6 al final de la zona de tornillos del extrusor. Las láminas de poliamida-6 se observaron a muy bajas magnificaciones (6.7X). También se notó que un ángulo convergente grande (70°) en el adaptador ocasionó la ruptura de las láminas, debido a los altos flujos de corte y alargamiento.

Las fotos de microscopía de los productos finales mostraron la presencia de láminas distribuidas a lo ancho del espesor de la muestra y a lo largo de la dirección de flujo. Se estudiaron los efectos de las variables de diseño, como son el ángulo del adaptador y la abertura del dado en la morfología de los productos finales. Se observó que una abertura de dado pequeña origina un gran estiramiento de las láminas, lo que causa su ruptura e incrementa la permeabilidad del tolueno en la mezcla. En cambio, las variaciones en el ángulo del adaptador no mostraron resultados significativos en la morfología del producto final. Se evaluaron los efectos de las variables de proceso, en las que se incluyen el perfil de temperatura, la rapidez de alimentación y la velocidad de los tornillos. Se observó que se requiere un perfil de temperaturas bajo, pero suficientemente alto para fundir el nylon-6, a lo largo del cilindro de extrusión, con el fin de obtener plaquetas elongadas. La formación de morfología laminar en la mezcla extruida depende altamente de la rapidez de alimentación. Las bajas velocidades de alimentación incrementan el tiempo de residencia, el cual produce la fusión prematura de la fase dispersa y la ruptura de las láminas. Por el contrario, las velocidades de alimentación altas contribuyen a la aparición de gránulos sin fundirse en los productos extruidos. También se observó que altas velocidades de rotación de tornillo mejoran el desarrollo de la morfología laminar, pero aparentemente reducen el tiempo de contacto entre las dos fases, lo que resulta en propiedades mecánicas deficientes.

Existe una fuerte relación entre la morfología, permeabilidad y las propiedades de impacto de las mezclas poliméricas. Una buena morfología laminar produce una baja permeabilidad pero pobres propiedades mecánicas. En este estudio, se obtuvieron mezclas con permeabilidades al tolueno hasta 113 veces la permeabilidad de la matriz. Este valor es 2.5 veces mayor que el mejor valor reportado para mezclas obtenidas por extrusion de un solo tornillo. En el proceso de coextrusion se estima una mejora en la permeabilidad de 262 veces para el mismo sistema y composición. Las pruebas mecánicas mostraron que los productos de extrusión de la mezcla de polietileno de alta densidad (HDPE) y poliamida-6 (PA-6) tienen valores similares de rigidez y fuerza de tensión que aquellos que se observan en el polietileno solo. Finalmente, en este trabajo, se llevó a cabo un análisis estadístico con el fin de obtener productos que contaran un balance óptimo entre la permeabilidad y las propiedades mecánicas. Este análisis produjo información útil con respecto a factores de proceso y diseño importantes que afectan las propiedades de la mezcla.

ACKNOWLEDGEMENTS

I would like to express my gratitude to the following people who contributed in the development of the present work:

Firstly, I extend my thankfulness to my research supervisor, Professor M. R. Kamal, for giving me the opportunity to discover the great world of research in polymers and for his guidance and encouragement throughout this project.

I would also like to thank:

- Dr. Hamid Garmabi and Dr. Richard Lai-Fook for teaching me all the processing and analytical techniques required in this study.
- Mr. Yong Gyun Cho for sharing some of his knowledge about polymer blends and his friendship.
- The staff of the Chemical Engineering Store and Machine Shop, in particular Mike Harrigan, Charles Dolan and Walter Greenland.
- Mr. Lou Cusmich for helping with the electronic problems of the twin screw extruder and stealing my screw driver.
- Ms. Helen Campbell for her advice on scanning electron microscope.
- My colleagues in the polymer group: Oi Wun Lee, Edgar Ramírez, Lei Wang, Yalda Farhoudi, Marie Claude Heuzey, Ludovic Capt, Kevin Alam, François Koran and Antonio Gallardo for their scientific advice and friendship.
- The Consejo Nacional de Ciencia y Tecnología (CONACYT) for the financial support
- My parents, sisters, brother, "Hidalguense" family and god for being always in my heart.
- Ahhh!, and Mr. Twin Screw Extruder for being my favorite machine.

TABLE OF CONTENTS

LIST OF FIGURES

LIST OF TABLES

NOMENCLATURE

Symbols

A	area of sample
a	droplet diameter
a_α	droplet radius
c	concentration
d	drops diameter
de	desired value
d_{std}	desirability standard function
D	difussion coefficient
D_{crit}	critical value of drop deformability
E	tensile modulus
F	flow rate in permeability
f	shape factor
h_c	critical separation distance
KB	kneading block element in twin screw extrusion
L	length of platelets
LI	left-handed element
$N_{2\alpha}$	second normal stress function for phase α
$N_{2\beta}$	second normal stress function for phase β
P	permeability
P_b	permeability of blend
P_d	permeability of dispersed phase
P_m	permeability of the matrix
Q	permeation rate
S	solubility
SW	self wiping element in twin screw extruder
T	thickness of platelets
t	time
t_b	breakup time for threads
t_c	critical coalescence time
w_i	weight fraction in Nielsen formula
y	actual data from desirability function
y'	transformed data from desirability function

ΔH_{mix}	heat of mixing
ΔG_{mix}	free energy of mixing
ΔS_{mix}	entropy of mixing
β_{12}	Nielsen empirical parameter
χ_{ij}	polymer/polymer thermodynamic interaction coefficient
ϕ_c	critical volume concentration

ϕ_d	concentration of minor phase
ϕ_i	volume fraction of i.
$\dot{\gamma}$	shear rate
$\gamma_{\alpha\beta}$	interfacial tension of a droplet of phase α in the matrix β
η_d	viscosity of the dispersed phase
η_m	viscosity of the matrix
κ	capillary number
κ_{crit}	critical capillary number
λ	viscosity ratio
τ	tortuosity
ν	interfacial tension

1.0 INTRODUCTION

Polymers offer a number of advantages in comparison to metals, ceramics, glass and paper in a variety of applications, because of their low cost, relative ease of processing, flexibility, light weight, good physical properties and recyclability. However in most cases, one polymeric material cannot offer all the properties required or the cost of the polymer is very high. Hence, it is common to use a blend of polymers. Through the choice of suitable components, it is possible to selectively adjust the properties of the blend to meet specific requirements. Thus, polymer blends help to fill some gaps in the property profiles of individual polymers. [1-4]

The use of polymer combinations to obtain a good barrier (i.e. low permeability) to hydrocarbons and gases has been of considerable interest recently [1,5-15]. Currently, plastic containers with high barrier properties are produced with a multilayer structure using co-extrusion technology. Although multilayer extrusion products satisfy many of the needs for applications in the automotive and packaging industry, they still require heavy commitment in capital investment and involve difficult process optimization and control. One alternative to multilayer extrusion could be based on the use of polymer blend systems having dispersed lamella (layers) of impermeable polymers, i.e. laminar morphology. The properties of such a blend will depend on the interaction between the phases, and the shape and size of the layers.

Viscosity and elasticity ratios, and interfacial tension between the matrix and dispersed phase are important parameters in the development of morphology of blends [17]. The morphology is also influenced by extruder processing conditions such as feed rate, screw speed, and temperature profile, which determine the level of stretching, residence time and shear rate [31]. Understanding of the deformation and breakup behavior of the dispersed phase is essential for manipulation and control of the laminar morphology of the blend. Ideally, it is desirable to have maximum area deformation or enlargement without breakup, in order to develop a large number of dispersed phase thin layers in the

matrix. Such structure will represent a long tortuous path for the gas or solvent penetrating the blend [60].

Laminar morphology has been demonstrated in single screw extruders and blow molding machines. Both processes have shown that high screw speed, low temperature profile, and the use of a metering screw prevent excessive mixing and favor the formation of a well-developed laminar structure [1,5-15,41,56-57]. To our knowledge, no studies have been done regarding the development of laminar morphology in twin screw extruders. Such a possibility might provide a number of advantages, such as product uniformity and high production speeds.

2.0 LITERATURE REVIEW

2.1 Polymer Blends, Principles and Morphology

Polymer blends are materials made by combining two or more polymers, through processing steps, in order to obtain physical mixtures exhibiting random or structured arrangements. [1]

The thermodynamics of polymer-polymer mixtures plays a major role in the molecular state dispersion, the morphology of two-phase mixtures, and the adhesion between phases. Consequently, it influences most properties and applications [2, 3]. The large molecular weight of both components is a critical factor that affects the thermodynamics of polymer blends, when compared to other systems. The rules, which govern the behavior of miscibility or immiscibility of polymer blends, are best understood through a thermodynamic approach involving the Gibbs free energy of mixing, ΔG_{mix}.

According to miscibility, polymer blends can be: a) Miscible polymer blends; these blends are homogenous down to the molecular level and they exhibit a negative value of free energy of mixing value ($\Delta G_{mix} \leq 0$); b) Immiscible polymer blends for which $\Delta G_{mix} > 0$; the properties of such two-phase blend are usually poor. c) Compatible polymer blends, which are two-phase systems but exhibit very interesting properties combining the behavior of the individual components.

Generally, the qualitative thermodynamic argument, which indicates that miscibility is a rare occurrence in polymer blends, recognizes that the entropy of mixing, ΔS_{mix}, in the free energy of mixing expression (equation 2.1) is very small. This is due to the small number of moles of each polymer in the blend, because large molecular weights are involved.

$$\Delta G_{mix} = \Delta H_{mix} - T\,\Delta S_{mix} \qquad (2.1)$$

While the sign of the combinatorial entropy favors mixing, it is usually too small to result in the necessary negative free energy. This is because the heat of mixing, ΔH_{mix}, is generally positive, at least for relatively non-polar systems. Thermodynamic stability of a one phase mixture exists only when:

$$\Delta G_{mix} < 0, \qquad \chi_{ij} < 0 \tag{2.2}$$

and,

$$(\partial^2 \Delta G_{mix} / \partial \phi^2)_{T,P} > 0 \tag{2.3}$$

where ϕ_i is the volume fraction of species i and χ_{ij} is an interaction parameter related to the heat of mixing, which is positive for endothermic systems. There are different interactions that intervene in blends: dispersive (Van der Waals) forces, free volume contributions, and specific interactions, such as hydrogen bonding, ionic, and dipolar interactions.

2.1.1 Morphology of Polymer Blends

Blend morphology is understood as the spatial arrangement of the blend component phases. Four different morphologies may be identified: disperse, fibrillar, stratified (lamellae, sandwich), and co-continuous phases (interlocked). In the first case, the matrix phase generally dominates the properties. In the fibrillar morphology the dispersed phased is stretched in the form of cylinders. Lamella arrangements allow both phases to contribute to many properties in direct proportions to their concentration in the blend. In the co-continuous morphology, both polymers are simultaneously continuous, forming interpenetrating networks (IPN) of the phases. For mechanical properties, adhesion between phases is an issue that is more critical for some morphologies than others. [4]

Many properties, and subsequently uses, of a blend depend critically on the nature of the arrangement of the two phases. One phase may be dispersed in a matrix of the other, and in this case, the matrix phase dominates the properties. Uniform, fine dispersions generally

result in average properties, while laminar morphology (EVOH, polyamides and polyesters with polyolefins), where small amounts of the minor phase are dispersed as essentially parallel, thin, and large layers produce substantial reduction of permeability in blow molded/extruded articles [1,5-15].

It has been reported that domain structure and size strongly depend on the amounts of the dispersed phase. For blends of PP/EVOH, Lepoutre [16] observed that an increase in the concentration of the minor component led to a significant increase in the average domain diameter. The morphology in a molten polymer blend depends on the viscosity ratio (size) and elasticity ratio (shape) of the phases, which are based on the stress (or shear rate) level, as well as on the initial size of the components (melt mixing process). The fineness of the dispersed phase is determined by the viscosity ratio (λ) and the interfacial tension. These aspects will be discussed below.

2.1.1.1. Viscosity Ratio Effect

Currently, there is conflicting information about the optimum viscosity ratio for achieving the highest degree of dispersion. Most of the researchers in this area suggest that at viscosity ratio of one ($\lambda = 1$), the smallest particle size is obtained. Taylor [21] defined the viscosity ratio and capillary number as follows:

$$\lambda = \frac{\eta_d}{\eta_m} \qquad \kappa = \frac{\dot{\gamma}\,\eta_m a}{\upsilon} \qquad (2.4)$$

where η_d and η_m refer to the viscosities of the dispersed and matrix phases, $\gamma^{\bullet}$ is the shear rate, a is the droplet diameter and ν is the interfacial tension. Wu [17] investigated the formation of the dispersed phase in blends during melt extrusion with a co-rotating twin screw extruder, using nylon (N66) or polyester (PET) as the matrix, and ethylene-propylene rubbers (EP) as the dispersed phase. All blends contained 15wt% rubber and 85wt% polymer. He showed that a master curve of the capillary number (also called

Weber number) vs. viscosity ratio could be drawn (Figure 2.1). The master curve can be expressed by

$$\kappa = 4\,(\eta_d/\eta_m)^{0.84} \quad \text{for} \quad \lambda > 1 \tag{2.5}$$

$$\kappa = 4\,(\eta_d/\eta_m)^{-0.84} \quad \text{for} \quad \lambda < 1 \tag{2.6}$$

The capillary number and viscosity ratio calculations for the curve were based on a circular die temperature of 280 °C and a fixed shear rate of 100 s^{-1} for all the blends. The capillary number appeared to have the lowest value at $\lambda \approx 1$. It means that the smallest particle size is obtained when the viscosity ratio is about unity. But at $\lambda = 4$, breakup of the particles occurred during the extrusion process.

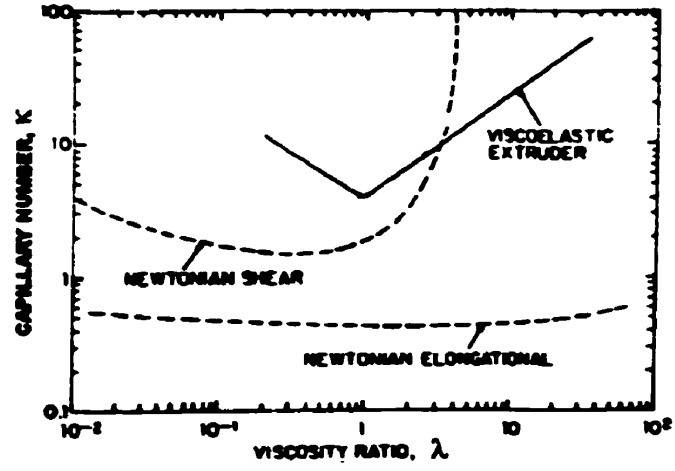

Figure 2.1. Comparison of the master curve for viscoelastic blends in a co-rotating twin screw extruder with those for Newtonian liquids in steady uniform shear and in elongational flow.[17]

Wu [17] compared his master curve with those obtained for Newtonian liquids in steady uniform shear and elongational flow (Figure 2.1). He observed that the viscoelastic curve becomes more V-shaped compared to the Newtonian shear curve but it follows a similar trend, i.e. the breakup occurs at $\lambda = 4$. He also observed that in the Newtonian

elongational system the drop breakup occurs much more easily, even for $\lambda \geq 4$, compared to the viscoelastic and Newtonian shear fields. The elongational curve was determined experimentally, but can be calculated dividing by two the shear rate of the simple shear flow.

2.1.1.2 Interfacial Tension Effect

The dispersion, morphology and adhesion of the component phases are greatly affected by the interfacial tension and elastic properties, which play an important role in determining the mechanical properties of multiphase polymer blends. Interfacial tension prevents further deformation of the dispersed droplets when the domain size is in the micron range. [2]

According to VanOene's theory [18], the elastic properties and interfacial tension determine droplet formation and equilibrium particle size, and provide a criterion for transformation from dispersed to stratified morphology. VanOene mentioned that morphology is unaffected by temperature, residence time and shear stress conditions because they only influence the homogeneity of the dispersion but not the mode of dispersion. He derived an equation for the dynamic interfacial tension between phase α and β during flow:

$$\gamma_{\alpha\beta} = \gamma^{\circ}_{\alpha\beta} + \left(\frac{1}{6}\right) a_{\alpha} \left[N_{2\alpha} - N_{2\beta}\right] \qquad (2.7)$$

where $\gamma_{\alpha\beta}$ is the dynamic interfacial tension during flow of a droplet of phase α in the matrix β, $\gamma^{o}_{\alpha\beta}$ is the interfacial tension in the absence of flow, a_{α} is the droplet radius, and $N_{2\alpha}$, and $N_{2\beta}$ are the second normal stresses for phase α and β, respectively. Since the interfacial tension is a positive quantity, the above equation is always satisfied when:

$$N_{2\alpha} > N_{2\beta} \qquad \text{or} \qquad \gamma^{\circ}_{\alpha\beta} > (1/6)\, a_{\alpha} [N_{2\alpha} - N_{2\beta}] \qquad (2.8)$$

If the phase dimension of the phase β is larger than 1 μm, as may be accomplished by incomplete mixing, phase β does not form droplets but stratifies. A further consequence is that in the submicron region, phase α will form single droplets; droplet formation of phase β leads to composite droplets, i.e. droplets of β containing smaller droplets of α. Differences in viscosity, shear rate, extrusion temperature, and residence time in the capillary influence only the homogeneity of the dispersion and not the mode of dispersion.

Demarquette [19] studied the interfacial tension for various polymer blends with two different instruments based on the pendant and spinning drop methods. Garmabi [15] using the same instruments, obtained an optimum maleation level value (0.014-0.028%) for the High-Density Polyethylene (HDPE) / Polyamide-6 (PA-6) system. Others methods have been also used to measure the interfacial tension of polymer [20].

2.1.1.3 Drop Deformation

When a neutrally buoyant, initially spherical droplet is suspended in another liquid and subjected to shear or extensional stress, it deforms and then breaks up into smaller droplets. Several studies have been carried out involving theoretical and experimental work on droplet deformation. The majority dealt with the deformation of Newtonian fluids subjected to either uniform shearing flow or uniaxial elongational flow. The studies confirmed that at low deformation, κ is the controlling parameter [21-23]

Taylor [21] found that in simple shear flow and at low stress, the subcritical deformation of a droplet results from balancing the interfacial tension forces (tending to keep the droplet spherical) with the viscous forces (tending to elongate the droplets). When the balance was absent, breakup occurred. He showed that the parameter describing the critical condition at breakup was the critical capillary number, κ_{crit}.

The capillary number for breakup κ_{crit}, correspond to the smallest steady state shear rate for which the drop is unable to maintain a steady shape and consequently undergoes a transient continuo stretching. The drop attains a threadlike shape and eventually breaks into smaller drops. The critical capillary number is determined experimentally, although interfacial tension value at equilibrium can be used to get an approximation.

Taylor studied the deformability, D, for Newtonian systems at low strains (the interfacial tension-effect dominates the viscous forces). He found the following expression for this case:

$$D = (\kappa/2)\,[(19\lambda + 16) / (16\lambda + 16)] \qquad (2.9)$$

Since the quantity in the square brackets ranges from 1.00 to 1.18 for $1 < \lambda < \infty$, the drop deformability, D, is nearly equal to $\kappa/2$. When the interfacial tension is relatively small in comparison to viscosity (high value of λ), the analysis gives $D = 5\kappa/8$. The breakup occurs when $D > D_{crit}$. An extended treatment for a Newtonian system with a full range of viscosities was studied by Cox [22].

Tomotika [23] proposed another mechanism for dispersing one liquid in another via the capillary instability of a long cylindrical column. He showed that the degree of instability can be described by the growth rate parameter of sinusoidal distortion, q. He also defined the time required to break up the threads, t_b. He concluded that t_b and κ_{crit} are two important parameters describing the breakup process, and that $\kappa > \kappa_{crit}$ is the requirement for breakup, but to achieve it, $t \geq t_b$ must be satisfied.

Stone et al. [24] showed that the breakup process is gradual, so it leads to a distribution of particle sizes (Figure 2.2). On the other hand, Utracki et al [31] observed that the systems that are easier to disperse in a simple shear field are those with the viscosity ratios within

the range $0.3 \leq \lambda \leq 1.5$. They concluded that within the entire range of λ, elongational flow was found to be more efficient than shear for breaking the drops.

In the case of non-Newtonian systems, the viscoelastic behavior is an important factor. Palierne [25] developed a theory for deformation of a viscoelastic drop in a viscoelastic matrix, considering uniaxial flow. Delaby [26] extended Palierne's theory to study drop behavior in elongational flow. He observed that the drop deformed less when the matrix was viscoelastic rather than viscous, and a higher deformation was reached when $\lambda < 1$. His studies were limited to small deformations and did not take into account the interfacial tension.

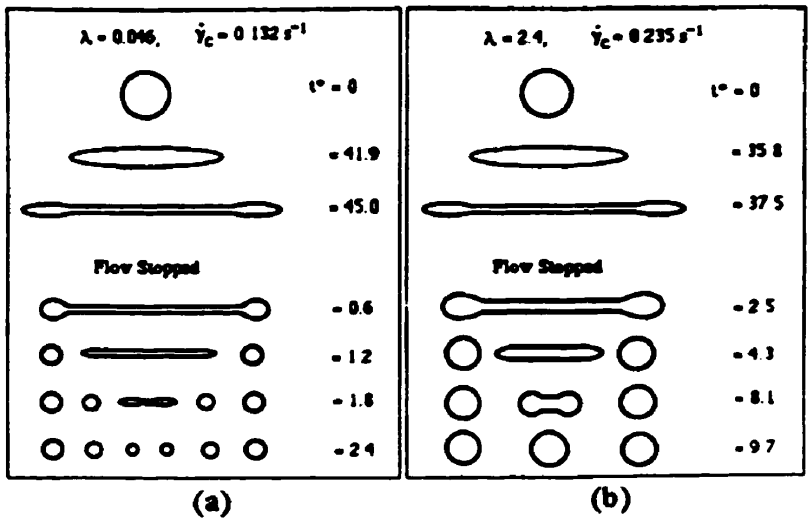

Figure 2.2. Non-uniform breakup [24]

Elmendorp [27] studied the formation and breakup of filaments. He observed that a sinusoidal deformed filament was produced in a blend of a Newtonian matrix with a Newtonian dispersed phase. The interfacial area decreased when the distortion amplitude increased, but when the distortion wavelength of the filament exceeded the circumference of the thread, an unstable thread was produced. It originated an increase in the distortion amplitude compared to the average radius of the thread therefore the thread broke. For

non-Newtonian dispersed and continuous phases, an elongated sinusoidally distorted thread did not break when the yield stress was greater than or equal to the pressure difference between the positions in the thread.

Recently, Bourry et al. [28] studied drop deformability in convergent slit flow of Newtonian and viscoelastic drops using an extensional flow mixer. They concluded that, initially, Newtonian drops are easier to deform than viscoelastic ones, but after some time, the opposite behavior is observed. They also showed that in a convergent zone, the drop deforms into a fiber, but when it reaches a divergent zone, the drop reverts to the spherical symmetry.

2.1.14 Coalescence

The melt morphology during mixing multiphase polymer systems results, in part, from the competition between breakup and coalescence of dispersed particles. Mason et al. [29,30] described three steps that illustrate the coalescence in shear flow for Newtonian fluids. Firstly, the dispersed droplets approach each other and form a rotating collision doublet. Secondly, there is a time when the drainage of the thin film of fluid between the droplets occurs. This time determine the coalescence. In case of short contact times due to high flow rates, the droplets do not coalesce and separate. Thirdly, as soon as the film thickness reaches a critical value h_c, interaction forces between the drops cause film rupture and coalescence takes place. He observed that the flow that induces coalescence in polymer blends is less pronounced than in Newtonian system, because the viscoelastic properties of the matrix retard film drainage.

Coalescence can be accelerated by the same factors that favor drop breakup (e.g., higher shear rates, low dispersed-phase viscosity). The drop collisions, which can lead to coalescence, occur not only in flow but also in quiescent systems; they are caused by Brownian motion, dynamics of concentration fluctuation, etc. When the concentration of

the minor phase exceeds a critical value of volume concentration, $\phi_d > \phi_c = 0.005$, the effect of the coalescence must be taken into account [31].

Elmendorp [27] considered coalescence as a dynamic process. Assuming that coagulation results from the collision of two spherical drops of diameter, d, which approach each other to a smaller than the critical separation distance, h_c, the critical coalescence time for systems with a mobile interface is expected to follow the relation:

$$t_c = 3k\left[\ln\left(d/4h_c\right)\right]/4\dot{\gamma}^2 \qquad (2.10)$$

This equation does not take into account the concentration effect. It predicts that the coagulation time might increase with the viscosity of the matrix and with the drop diameter but decrease with an augmentation of the interfacial tension coefficient. Elmendorp also showed that in finely dispersed systems, the interparticle collisions have a greater probability of resulting in coalescence.

Fortelny [32] gave an explanation of coalescence effect based on the assumption that the dispersed phase is above or close to the percolation threshold. This led to a concentration-dependant number of neighbor droplets that coalesced due to weak driving forces, most probably van de Waals forces. He used another approach where the viscous flow (interfacially driven coalescence, reshaping agglomeration) led to the reduction of the interfacial area. In the case of irregularly shaped droplets, which were usually produced by melt mixing, the droplets returned to a spherical shape when the system was remelted. High contents of dispersed phase led to the contact and coalescence of neighboring droplets.

Lohfink [8,9] studied the convergence zone of an adapter between the extruder and slit die to produce ribbons of polypropylene and ethylene vinyl-alcohol copolymer blends. He showed that the dispersed phase in the converging part of the adapter was streamlined and

forced into coalescence towards the center axis (Figure 2.3a). The particles remained in the center of the stream after the stretching in a slit die (Figure 2.3b), and formed a laminar structure of the dispersed phase, mainly in the center of the final extrudate.

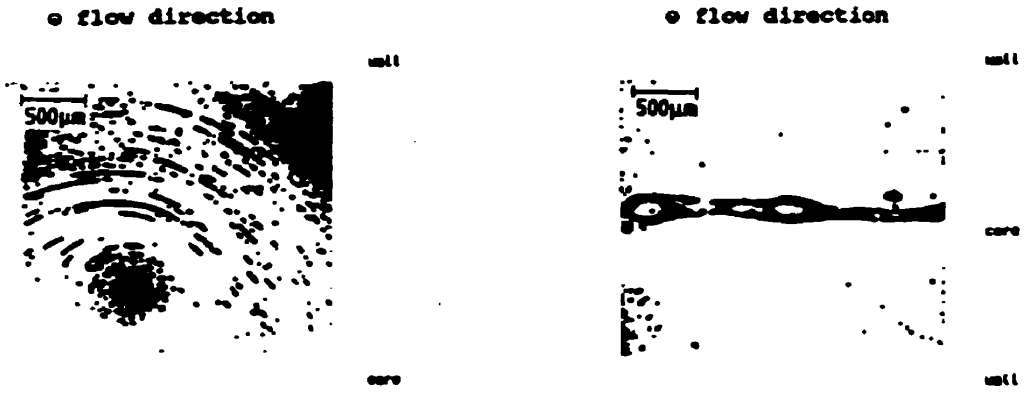

(a) (b)

Figure 2.3. Morphology development in (a) adapter and (b) slit die. [8]

Wallheinke et al. [33] studied the coalescence in quiescent melt of blends of thermoplastic polyurethane and polyolefins. They showed that during blending process in a twin screw extruder, coalescence began to occur at dispersed phase contents of about 1 wt%. They observed two different mechanisms of coalescence according to Scanning Electron Microscopy (SEM) and light microscopy. In the first mechanism, the reshaping of elongated droplets and breakup of fibers led to interparticle contacts and resulted in coalescence. In the second, a "domino effect", where the coalescence of two neighboring droplets resulted in a larger particle that became close to another particle and coalesced, was observed.

2.1.1.5 Compatibilizer Effect

Polymer compatibility is defined in a variety of different ways, depending on the application. At the microscopic level, one defines compatibility as the total miscibility on a

molecular scale of polymers with each other in various combinations. The second definition describes compatible polymers as polymer mixtures that exhibit desirable physical properties when blended. Others define compatibility in polymers as the condition when polymer mixtures do not exhibit gross symptoms of phase separation when blended. These three definitions of polymer compatibility are somewhat interrelated, since it is only reasonable to suppose that polymer blends exhibiting no gross symptoms of phase separation on blending and having desirable properties show at least some mixing of polymer segments on a microscopic scale [4]. Compatibility implies either a certain amount of thermodynamic compatibility or a physical constraint that prevents demixing. Typical mechanisms include grafting, cross-linking, the presence of block copolymers, interpenetrating network (IPN) formation, or the quenching of a mixed system to a temperature at which demixing is thermodynamically, but not kinetically, favored.

Incompatible polymers, when blended together, produce a dispersed phase that is large and lacks adhesion to the matrix. Adhesion can be enchanced by a component, usually called compatibilizer or interfacial agent. It has been found that compatibilizers significantly increase the rate of mixing, reduce the scale of morphology, stabilize the phase dimensions and improve the final properties of the blend [34].

Setua et al. [35] investigated the LDPE/Nylon-6 system, using maleated polystyrene-poly(ethylene-co-butylene) as an interfacial agent in a twin screw extruder. They found that the domain size of polyamide-6 was rapidly decreased after the first kneading block of the screw and gradually became smaller. They concluded that the addition of compatibilizing agents to the blend does not only reduce the scale of the dispersed phase, but significantly enhances the rate of mixing.

Lepoutre[16] studied PP/EVOH blends, using small amounts of maleic anhydride grafted polypropylene compatibilizer (less than 10%wt , based on the minor phase), and observed no effect on the domain size or adhesion. Lohfink [8,9] used the same blend with concentrations between 5 and 20% wt, and noticed an improvement in adhesion. Hozhabr

[12] observed for the same system that samples with a higher content of maleic anhydride showed better compatibility, reflected in their morphology and mechanical properties. He also observed that the layered structure that could be achieved in a single screw extruder became diffuse at high levels of maleation.

Lim and White [36] studied the morphology of PE/PA-6 blends in the screw zone of a co-rotating twin screw extruder. They observed that the addition of a compatibilizing agent causes the phase morphology scale to be reduced more rapidly along the length of the screw. Increasing the amount of compatibilizing agent both accelerated the adhesion of the dispersed phase and decreased the scale of the ultimate morphology.

Lacasse and Favis [40] showed the influence of extrusion on the morphology of PA-6/ABS blends. They observed that by increasing the compatibilizer, a more homogeneous blend was obtained when a twin screw extruder was used. The intense mixing in the twin screw extruder helped the compatibilizer to migrate to the interface. They also showed that a significant reduction of the average diameter, d_v, is produced when using twin screw extrusion compared to single screw extrusion.

Garmabi [14,15] extruded HDPE/PA-6 blends in a single screw extruder and found that 10% wt of maleated polyethylene (0.014%wt MAH content, based on total polyethylene content) was the optimum value to obtain a good combination of mechanical and barrier properties. He showed that high levels of MAH improve the mechanical properties but decrease the size of the dispersed phase.

2.1.1.6 Processing Effects

Understanding the development of phase morphology is facilitated by analyzing a solid blend sample during and after it has been processed. Morphological development can then be inferred by combining these observations with knowledge about melting, heating and mixing processes, which take place during processing, while keeping in mind the influence

of material properties such as viscosity, elasticity, and interfacial tension. It has been found that the processing variables that have the greatest influence on the blend morphology are the type of mixer, residence time, shear rate, temperature profile, screw configuration, and flow rate.

Shi and Utracki [37] studied PS/HDPE blends in a co-rotating twin screw extruder. They found that increasing the screw speed caused an increase in the shear stress, thus making the drop breakup more efficient. They also found that the diameter decreased when the throughput increased.

Teh and Rudin [38] studied the PS/LLDPE blend in a co-rotating twin screw extruder. They observed that by increasing the screw speed at constant mass flow rate, the extrusion pressure and torque decreased due to a reduction in the melt viscosity produced by the shear heating. On the other hand, increasing the mass flow rate at constant screw speed resulted in an increase in extrusion pressure as well as screw torque. The extrusion pressure and screw torque also decreased when the screw configuration was changed to give less shearing and mixing.

Yang et al. [39] studied the morphology of LLDPE and PS in a counter-rotating twin screw extruder using different screw configurations. They found that using reverse elements at high screw speed under constant flow conditions enhances the size reduction of the dispersed phase due to the longer time spent in the feed zone of the screw, where the most significant changes of phase morphology occur.

Lohfink [8,9] used a single screw extruder to obtain laminar morphology of a PP/EVOH blend through a slit die. He observed that using a high extrusion temperature profile, high flow rate and a metering screw produced better laminar morphology. Arghyris [13], Hozhabr [12] and Garmabi [14,15] used twin screw extrusion as an intermediate step, prior to producing laminar morphology in PP/EVOH and PE/PA-6 blends in a single screw extruder with the same die used by Lohfink. They observed reduced laminar morphology

when a twin screw extrusion step was used compared with the results obtained with the single screw extruder alone.

Lee at al. [41] used a single screw blown film extrusion system to produce laminar morphology. They observed that large predeformed domains at the extruder outlet are obtained with short residence times, high screw speeds, and low viscosity ratios. They also observed a reduction in the size of the dispersed phase, when a twin screw extruder was used as a pre-compounder.

Delamare and Vergnes [42] studied the morphology changes of a polymer blend in a twin screw extruder. They showed that by increasing the feed rate, the filling ratio of the screw is increased, but the residence time is decreased. The latter effect was predominant and limited the breakup at high feed rate, producing larger particles. On the other hand, an increased screw speed led to shorter residence times and higher shear rates, and modified the viscosity ratios (Figure 2.4)

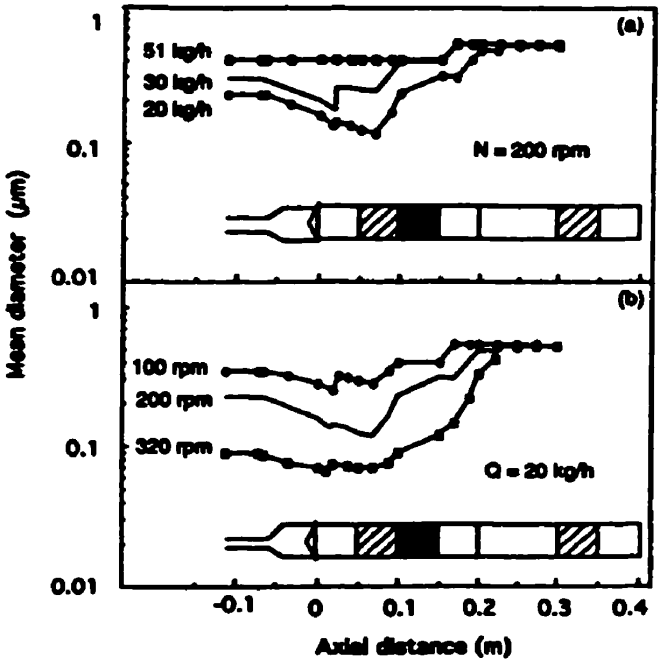

Figure 2.4. Influence of (a) feed rate and (b) screw speed on morphological change

2.2 Morphology Development of Polymer Blends

2.2.1 Mechanism

The morphology of the dispersed phase is modified very rapidly under dynamic conditions in the melt. The dispersed phase of a polymer blend that enters to the mixer or extruder in the form of pellets (1-3 mm) may produce layers, fibers or sub-micron size particles, depending on material properties and processing conditions.

Scott and Macosko [43] studied morphology development in a batch mixer. They found that initially the mechanism is intimately connected with the melting or softening process. They showed that the dragging of a dispersed phase particle against a hot surface causes the formation of a sheet. Subsequently, holes are formed in the sheet due to the interfacial and shearing forces. The holes grow until a lace structure is formed. This lace is broken down into irregularly shaped particles, and finally produces spherical particles. (Figure 2.5).

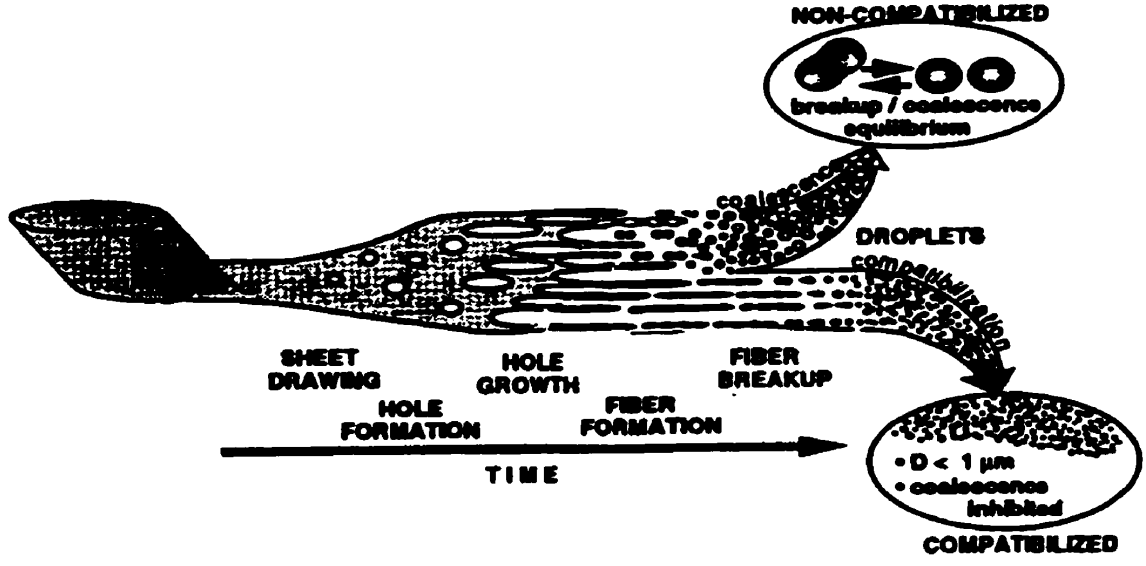

Figure 2.5 Dispersion of the minor phase during blending [43]

Later, Sundararaj and Macosko [44] showed that the same dispersed phase sheeting mechanism occurred in the first part of a co-rotating twin screw extruder. They observed lacy sheets and fragments whose length and width are in the order of ten microns and the thickness in the order of one micron (Figure 2.6). This first part of the extruder had only conveying elements. They showed that the most pronounced morphology change occurred during the early melting stage. Vainio et. al [45] obtained similar results when they studied the morphologies of a blend in the first part of the extruder using only conveying elements. Even when a kneading block was added to this section of conveying elements, lamellar morphology was observed. These studies showed that laminar morphology exists and can be developed in a twin screw extruder under certain processing conditions.

Figure 2.6. Sheets of Nylon from the initial morphology development in a twin screw extruder [44].

Lindt and Ghosh [46] studied the earlier stages of blend morphology development in a single screw extruder as a function of the physical properties of the polymers involved and the processing conditions. They used the three-layer model to explain that molten layers deform due to a combination of drag, pressure and squeezing flow in the extruder. According to their analysis, the lamellae tend to thin down into threads, and finally break up to form droplets (Figure 2.7a). The authors used Monte-Carlo simulation to develop a theory for the primary striation produced by melting the single pellets at the melt solid

interface. They suggested that neighboring primary striations of the same component are combined into a single striation in the flow field (Figure 2.7b).

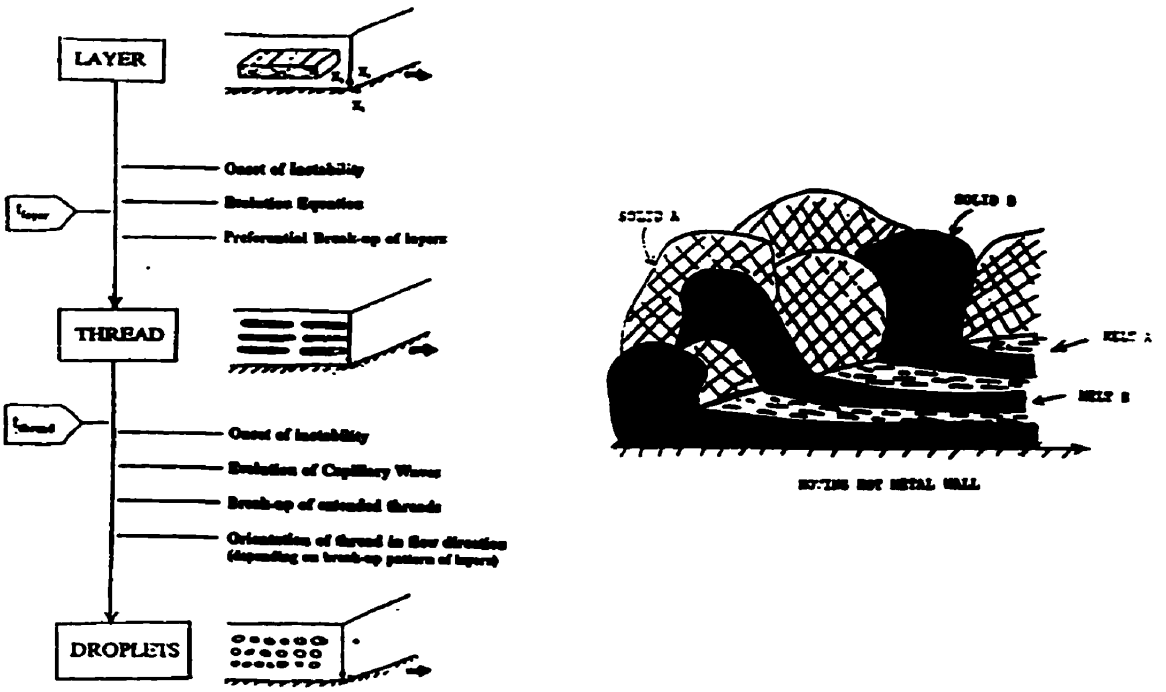

(a) *(b)*

Figure 2.7. (a) The transition from lamellar structure to dispersed drops. (b) Conversion of pellets into striation [46].

Levitt et. al [47] mapped the morphology development of different polymer blends using a new visualization apparatus. The largest stretching of the dispersed phase was observed for the pair of polymers with closely matching viscosities and small interfacial tension. In the case of amorphous polyamide, with maleated polystyrene as the matrix, a modest extended area of the dispersed phase was seen compared to other blends (e.g. PP/PS).

They explained that this behavior was due to the presence of reaction at the interface that decreased the interfacial tension.

2.2.2 Laminar Morphology

Polyamides exhibit high barrier to permeation of organic solvents and gases, and excellent physical properties such as mechanical strength, heat resistance and thermal moldability. However, this polymer is expensive and does not provide barrier to water. On the other hand, polyolefins exhibit excellent barrier to permeation of water and polar solvents, good impact resistance, easy processability, and low cost. Generally, polyolefins and polyamides (Nylons) are incompatible. Under the proper processing conditions, coextruded articles or laminar blends of these materials can have many applications in food packaging, gasoline tanks, fuel tubing, photodegradable polymers and drugs packaging. [1,5-15,48-51]

Subramanian [1,5-7] employed a modified nylon in blends with high-density polyethylene (HDPE) in annular and slit flow to obtain a laminar morphology that yields good barrier properties. Biaxially stretched nylon dispersed in the polyolefin matrix and bound to it by an appropriate compatibilizer, produced overlapping multilayer or lamellar structure, which exhibited significantly reduced oxygen and/or hydrocarbon permeability. Toluene weight loss in blend bottles, showed an improvement of the order of 200 times compared to the permeability of the HDPE. Subramanian observed that cooling rates outside the die affect the shape of the dispersed phase. Lower cooling rates led to longer relaxation times and eventually to more coalescence. According to Subramanian, shear stress, interfacial tension, coalescence, viscosity, die and extruder temperatures must be taken into account in producing laminar morphology.

Kamal et al [52] and Utracki et al. [53] studied the behavior of HDPE/PA-6 blends in capillary flow in a twin screw extruder. Their main goal was to improve the barrier properties of polyethylene films. The best results in reducing of oxygen permeability

showed a factor of 3.6. The morphology of the rod at 250 °C, obtained by capillary extrusion showed a tree-ring structure, produced by shear-induced interlayer slip. They observed that at 150 °C, the dispersed PA-6 migrated to the center, while at 250 °C, the opposite was true. At 200 °C an intermediate behavior was observed.

Lohfink and Kamal [8,9] obtained laminar structure of polypropylene/ethylene vinyl alcohol copolymer, using a slit die to produce ribbons in a single screw extruder and the die shown in Figure 2.8. When a metering screw was used, a small streamlined flow angle was sufficient to cause coalescence and produce layered structures in the adapter. A mixing screw combined with a large entrance angle of the adapter enhanced coalescence, resulting in large dispersed phase agglomerates which exhibited a layered structure throughout the downstream sections of the die unit. Their results showed an improvement in oxygen permeability of about 2.6 times the permeability of polypropylene (PP). Hozhabr [12] and Arghyris [13] worked with the same extrusion system using a twin screw extruder to premix the compatibilizer and matrix phases. Hozhabr improved the adhesion at the interface using a maleated polypropylene, while Arghyris improved the mechanical properties by the incorporation of a rubber phase. Later, Walling and Kamal [54,55] observed laminar morphology in injection-molding samples of PP/EVOH. They identified three different zones across the thickness of the sample: core, intermediate and skin. The samples showed moderate improvement in toluene permeability (3.9 times) but poor impact properties.

Lee and Cho [56] obtained laminar morphology for HDPE/PA-6 system by in situ reactive compatibilization that enhances the adhesion between the phases during blow molding of bottles. They calculated permeability improvement by a factor of 78 based on the solvent weight loss in the matrix alone compared to the blend. They observed that the potential maximum factor using this system was 240.

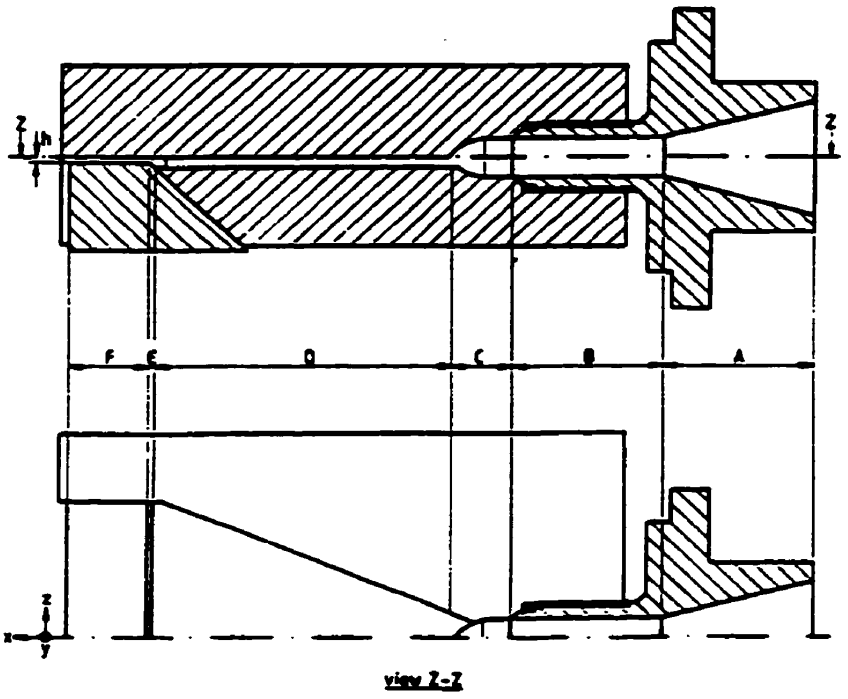

Figure 2.8. Schematic of slit die unit and adapter used by Lohfink to produce laminar morphology [8].

San-Young et al. [41,57] studied the laminar morphology in LDPE/EVOH blends, when extruded through an annular blown film die. They found that short residence times combined with high screw speed and lower viscosity ratios in the die temperature favored the formation of a well developed laminar structure that resulted in good oxygen barrier properties. They showed a reduced oxygen permeability factor of 740 compared to a maximum potential value of 25,000.

Garmabi and Kamal [14,15] obtained laminar morphology of HDPE/PA-6 blends using maleated polyethylene as a compatibilizer. They used a single screw, and in some cases a twin screw extruder for premixing, to produce ribbons. The authors suggested that a low temperature profile along the extruder might avoid the formation of lace structure and reduce breakup of the dispersed phase during the extrusion process, because the deformed layers are tough and not easy to break. Therefore, larger particles can be obtained and then

stretched in a slit die. The samples showed a reduction up to 45 times in toluene permeability. The lowest permeability values for this blend were close to the co-extruded ribbon permeability levels predicted by the Series Model (Figure 2.9).

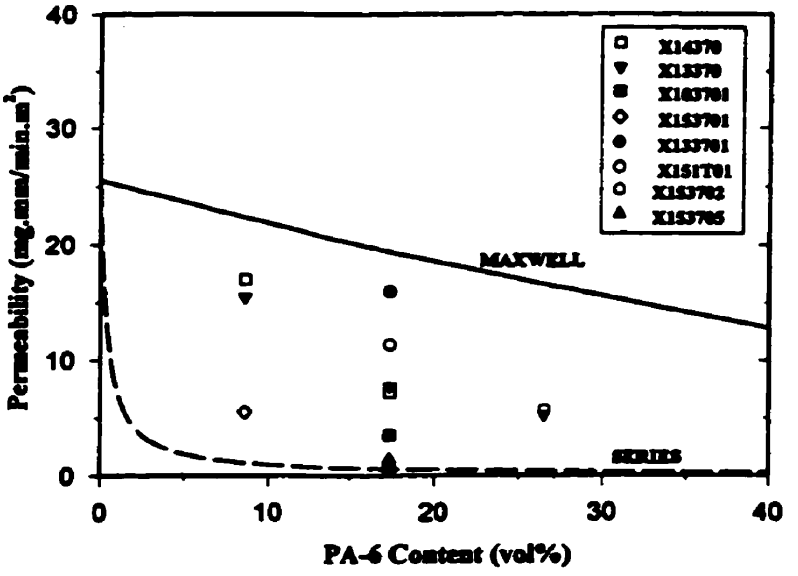

Figure 2.9. Variation of toluene permeability with respect to PA-6 content along with Maxwell and series model predictions for HDPE/PA-6 blends [15].

2.3 Permeability of Polymer Blends

Blends of dissimilar polymers have considerable technological importance, since blending provides a mean for combining their physical and mechanical properties. The analysis of the phase morphology of blends can be achieved directly via microscopic techniques or by dissolving one of the phases. It can also be inferred from material properties, such as gas or solvent permeability, which are strongly dependent on the phase morphology.

Low permeability is very important for blends used in the packaging, pharmaceutical and automotive industries [48-51]. The permeability, P, is defined as the product of solubility,

S, of the permeant and the diffusion coefficient, D, of permeant through the barrier material. The rate at which a gas, vapor or liquid will pass through a polymeric material is governed by several factors, some of which are dependent on the properties of the diffusing species while others are controlled by the properties of the polymer (polymer-liquid or polymer-gas interaction). In order to be a suitable barrier material, the polymer must have: some degree of polarity, high chain stiffness, close chain-to-chain packing ability, inertness to permeating species, some bonding between chains and high glass transition temperature [58].

Reduction of solubility or increase of the length of the diffusion path (tortuosity) caused by the presence of lamellar structure can decrease permeability (Figure 2.10). The tortuosity factor, τ, is defined as the ratio of the effective path length required for permeation divided by the actual film thickness.

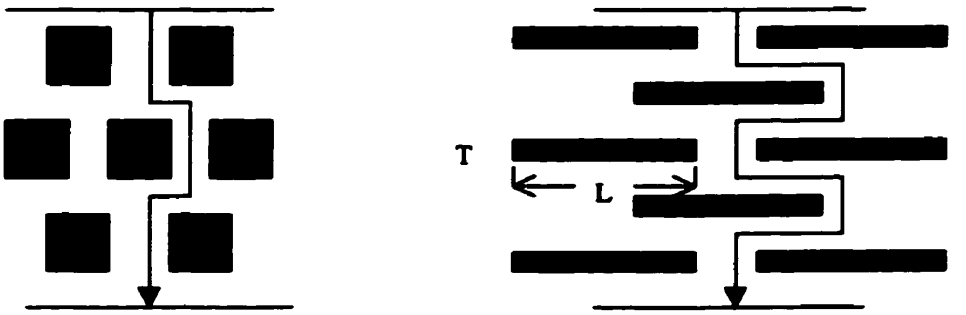

Figure 2.10. Model for a path of a diffusing molecule through a polymer filled with square plates.

An estimation of barrier properties of homogenous blends can be based on the analysis of conductivity proposed by Maxwell [59] for a dispersion of a non-conductive spherical particle in a conductive matrix. Maxwell's analysis yields:

$$\tau = 1 + \phi_d/2 \qquad (2.11)$$

where τ is tortuosity and ϕ_d is the volume fraction of dispersed phase. For the morphology of square laminates oriented parallel to the sample surface, Nielson [60] proposed the following equation:

$$\tau = 1 + (L/2T)\,\phi_d \qquad (2.12)$$

where L and T are length and thickness of the platelets, respectively. The above equation show that samples with impermeable particles displaying a large aspect ratio will result in a large tortuosity factor, and consequently lower permeability or improved barrier properties. Particle size does not appear to explicitly influence the permeability. However, if the length and width of the low permeability platelet were infinitely large, the sample would be virtually impermeable, and its structure would be comparable to a multilayered system. Thus, the size of the dispersed phase is also likely to influence the permeability of samples.

For systems with a uniform spherical dispersion of the minor phase, the overall permeability of the composite, P_c, is given by:

$$p_b = p_m\left(\frac{p_d + 2p_m - 2\phi_d(p_m - p_d)}{p_d + 2p_m + \phi_d(p_m - p_d)}\right) \qquad (2.13)$$

where P_b , P_m and P_d are the permeabilities of the blend, matrix and dispersed phase and ϕ_d is the volume fraction of the dispersed phase. This equation is also known as the Maxwell Model.

Roberson's [61] model for continuous multilayer or laminar structures consists of treating the different layers as different resistances, by analogy with electrical conduction. The resulting permeability of a binary system is given by the following equation:

$$1/P_b = \phi_d/P_d + \phi_m/P_m \qquad (2.14)$$

where ϕ_m is the volume fraction of the matrix. This equation is also called the series model. The reduction of permeability in homogenous blends is small, even with a large volume fraction of the minor phase.

Recently, Cussler [62] presented an equation to predict the barrier properties of platelet structures. For platelets with rectangular geometry, the equation is:

$$\frac{P_m}{P_b} = 1 + \left(\frac{L}{T}\right)^2 \left(\frac{\phi_d^{\,2}}{1-\phi_d}\right) \qquad (2.15)$$

where T can also be taken as cross-sectional average of individual striation thickness of the dispersed phase.

2.4 Processing

2.4.1 Twin screw extruder (TSE)

Extrusion is the commonly used plastics processing operation. While single screw extrusion has been the predominant process, recently the use of multiple screw and specially the twin screw extruders has grown substantially. [63]

The theoretical analysis of twin-screw extruder operation remains undeveloped. This situation has led to development of twin screw extruders of modular design with interchangeable screw and barrel elements. Thus, the screw design can be altered by changing the sequence of elements along the shaft, on the basis of empirical tests, but the

optimization of screw configuration for each application requires extensive experimental studies.

Two main areas of application for twin screw extruders are profile extrusion of thermally sensitive materials and specialty polymer processing operations such as compounding, devolatilization, chemical reactions, etc. Twin screw extruders represent not only one technology but several. The screws may be co-rotating or counter-rotating. They may be intermeshing, tangential, or separated. These machines offer several advantages over single screw extruders. Some of these advantages are given below [63,64].

- Positive feed characteristics, which allow the machine to process hard-to-feed materials.
- Short residence times and a narrow residence time distribution (RTD) spectrum.
- Low shear in the channel, leading to mainly conductive heating.
- Better distributive mixing and larger heat transfer area, which allow good control of the stock temperatures.
- Easier scale-up
- Large output.

There are few direct comparisons of different types of twin screw extruders. These comparisons are mainly made for intermeshing machines. Rauwendaal [65] compared a Leistritz modular counter-rotating machine and a 28-mm Werner and Pfleiderer modular co-rotating machine. He found that the intermeshing counter-rotating machine had much better pumping capacity than the co-rotating one, but the co-rotating machine had a much broader distribution of residence times. Rauwendaal concluded that the modular intermeshing co-rotating extruder does a better job in distributive mixing and argued that it was better for blending. The modular intermeshing counter-rotating twin screw extruder was found to be better in dispersing small particles.

White [63] noted that intermeshing counter-rotating machine had narrower residence time distributions than the co-rotating one. He later compared the ability of both types of machines to disperse small particles and to mix glass fibers without breakage. He found the intermeshing counter-rotating extruder to be superior in the former task, but the co-rotating machine was better in the latter.

Three main zones are found in twin screw extruders: feeding, melting, and pumping. However, screws with as many as eight or nine zones are being used. Each zone, while intended for a particular function, performs other functions as well. Hunneault et al. [66] and Maier et al. [67] observed the morphology of different blends in a co-rotating twin screw extruder (TSE) and concluded that the melting zone in the extruder plays a major role in the dispersion of the minor phase. On the other hand, Bordereau et al. [68] showed that in a co-rotating twin screw extruder, the function that each zone performs is better defined than in a counter-rotating one. Thus, analysis of morphology development is easier in a co-rotating twin screw extruder.

2.4.2 Mixing Mechanism in Extrusion

The mixing of various components is a basic processing step, which is encountered in many industries. Among continuous plastic processing machinery, the single and twin screw extruders are the most commonly used. Before discussing mixing in these devices, some concepts about mixing are discussed below.

In the mixing of immiscible polymers, the minor component is generally present as the dispersed phase (drops, filaments, layers) in a continuous phase of the major component. An elementary step in the mixing process is the deformation of dispersed drops in the flow field, yielding an increase in the interfacial area between the two components accompanied by a decrease in local dimensions perpendicular to the flow direction, called striation thickness.

The mixing process can be classified according to the value of the capillary number, κ, which continuously decreases during the process as a result of the decrease of the characteristic length scale [69].

a) Distributive mixing occurs when $\kappa > \kappa_{crit}$ (large dispersed domains, passive interfaces); drops are extended affinely within the matrix but do not develop capillary waves leading to breakup, since the interfacial stress is dominated by the shear stress.
b) Dispersive mixing occurs when $\kappa \cong \kappa_{crit}$ (local small radii of curvature, active interfaces); the interfacial stress, ν/a, competes with the shear stress, $\tau = \gamma\eta_m$, and causes disturbances at the interface to grow, leading to breakup into smaller droplets and thus to a finer dispersion.

In order to develop laminar morphology, distributive mixing is desired. Lawal and Kaylon [70] compared the mechanisms of mixing in single and co-rotating twin screw extruders. They found that the distributive mixing capability of an extruder depends on the level of strain that it is capable of generating, as well as on how much of the material experiences a particular strain level, i.e., the residence time distribution. Of equal importance in this kind of mixing, is the ability of the equipment to progressively orient the material interfaces as the components to be mixed pass through the processor. They showed that even though high strain levels can be generated in single screw extruders by manipulating operating variables and geometrical parameters, there was an absence of a mechanism of reorientation that prevents interfacial growth. On the other hand, when they worked with a intermeshing co-rotating twin screw extruder with regular conveying elements, they found that the nip region, where the two screws intermesh, increased the deformation rate and stresses, and enhanced the distributive mixing capability.

A recent analysis of mixing is based on the theory of chaotic mixing. The simplest flow that can exhibit chaotic mixing is a two-dimensional flow. In steady two-dimensional flow, the streamlines are fixed and the trajectories of fluid particles do not cross. Thus, in this

flow, the flow particles cannot become mixed. However, if the flow is made to change with time, the character of the flow can change dramatically. A convenient way to accomplish this is to force the flow to vary with the time in a periodic manner. To accomplish effective mixing, such a flow should stretch and fold a region of fluid and return it to its initial location. This process of stretching and folding is referred to as a horseshoe map (Figure 2.11) [71,72].

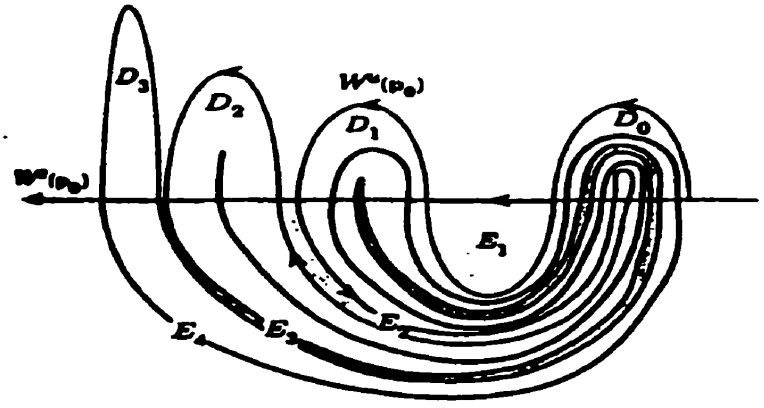

Figure 2.11 Representation of stretching and folding (horseshoe map)

Ottino [71] and Aref [73] studied the blinking vortex system, consisting of two alternating co-rotating vortices (Figure 2.12), each of them switched on and off for half the cycle time. They observed that the trajectory in such a system developed a pattern described by Poincaré sections (Figure 2.13). In these sections for co-rotating vortices, there are elliptic points located in the center of each co-rotating vortex, and a hyperbolic point located in the center of the section for one period. At the hyperbolic point, the fluid moves toward it in one direction and away from it in another direction. When a fluid particle in a periodic flow returns to its exact initial position, that particle defines a periodic point. Periodic elliptic points tend to form regions where mixing is slow. Intersections between hyperbolic points, depending on the nature of intersection, can form homoclinic or heteroclinic points. It is said that a system can be described as chaotic when it is able to produce horseshoe maps or transverse homoclinic and heteroclinic intersections.

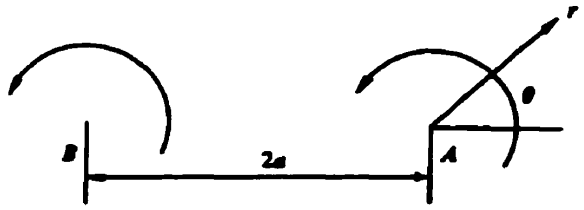

Figure 2.12 Schematic of the blinking vortex system

Recently, Raynal and Gence [78] studied laminar flow in a cylindrical tank with two agitators using viscous or non-viscous fluids. They found that similar streamline patterns to those of the Poincaré section were developed for both fluids. Lawal et al. [74] showed by simulation, that the flow in conveying and kneading elements of an intermeshing co-rotating twin screw extruder produced distributive mixing. This flow was governed by chaotic mixing.

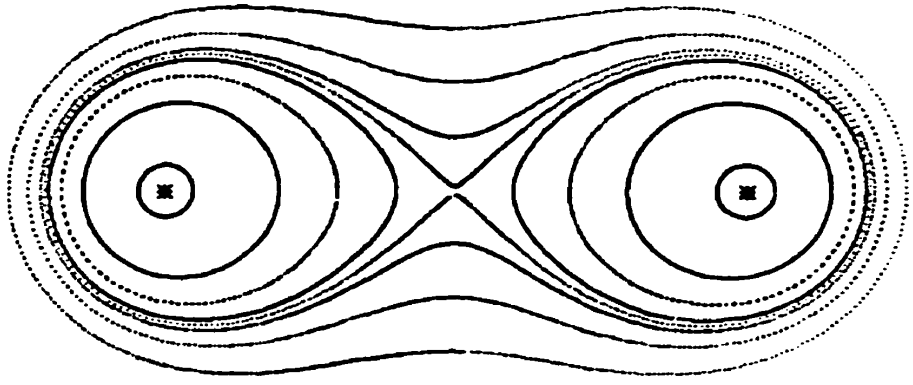

Figure 2.14 Poincaré section for two co-rotating vortex-lines

3.0 OBJECTIVES

The bulk of work aimed at the development of laminar blends has involved single screw extruders. However, it is frequently important to employ twin screw extrusion for purposes of premixing and/or compounding. In some cases at least, it may be possible and desirable to replace the two steps with one step involving only twin screw extrusion.

The main objective of this research was to obtain laminar morphology for HDPE/PA-6 blend in a co-rotating twin screw extruder. In order to achieve this objective, the following specific tasks were defined:

1. Design an adapter to connect a specially designed converging-diverging die to a twin screw extruder.

2 Evaluation of different processing conditions to produce laminar morphology in the extrudate.

3 Characterization of the morphology development after the molten blend leaves the screw zone.

4 Characterization of the final products to evaluate their barrier and mechanical properties.

4.0 EXPERIMENTAL

4.1 Materials

The following three resins were used in this research:

1. Ultramid B5 Natural for the dispersed phase. This is a blow-molding grade polyamide (PA-6). The polyamide is tough and hard, and yields products that efficiently suppress vibration, and are extremely shockproof even if they are in the dry state. It also has considerable resistance to hydrocarbons. This product was purchased from BASF Corporation.

2. Sclair 58A as the matrix phase. This is a blow-molding grade high density polyethylene (HDPE). This material was specifically designed to have an appropriate combination of environmental stress crack resistance (ESCR), stiffness and impact strength, which make it ideally suited for use in most food, pharmaceutical, household and industrial chemical applications. This product was donated by Novacor Chemicals Ltd.

3. Bynel 4006 as the compatibilizer. This is an anhydride-modified, high-density polyethylene (MAPE). It is a good moisture barrier and has good hydrocarbon resistance. This resin was supplied by Du Pont Canada Inc.

The physical and mechanical properties of the above products are summarized in Table 4.1.

Table 4.1 Properties of the resins

Property	HDPE	PA-6	MAPE
Solid density (g/cm3)	0.955	1.130	0.950
Melt Index (dg/min)	0.43 (190 °C)	na	0.6 (190 °C)
Vicat Softening Point (° C)	125	na	128
Melting Point (° C)	135	220	136
Toluene Permeability (mg.mm/m2.day)	27.08 @ 22.8 °C 24.03 @ 22.0 °C**	0.0162** (22 °C)	32.9*
Oxygen Permeability (cm3.mm/m2.day.atm)	26.25 (25 °C)	0.71 (23 °C)	25.0*
Impact Strength (J/mm)	2.8**	7.1**	1.8*
Elastic Modulus (MPa)	709**	1017**	na
Tensile Yield Strength (MPa)	25.9**	67.4**	na
Maleation Content* (wt%.)	0.0	0.0	0.113

* Measured values from reference [15]

** Measured values in this research

na = not available

4.2 Blend Preparation

Before processing, the Nylon-6 and MAPE were dried overnight in a vacuum oven at 80 °C to eliminate moisture. According to the manufacturer, these pellets are very sensitive to heat and must be dried under mild conditions (at temperatures not exceeding 80 °C), in order to avoid yellowing.

4.2.1 Dry Blending

This term refers to the blends prepared by simply tumbling and mixing the pellets together at room temperature. The HDPE pellets have the shape of lentils, the Nylon-6 pellets are cylindrical and the MAPE granules are spherical.

On the basis of earlier work [15], the following blend composition was employed, unless otherwise specified: 70 %wt of HDPE, 20% wt of PA-6 and 10 %wt of MAPE. After weighing, the resins were placed in a container where they were dry mixed. This dry blend was then ready for further processing.

4.2.2 Processing Equipment

4.2.2.1 Twin Screw Extruder

The experiments were carried out in a Berstoff co-rotating twin screw extruder with intermeshing screws, model ZE 25 (1990). Other specifications are listed on Table 4.2. The intermeshing screw configuration consisted mainly of conveying elements and one kneading element in the end of the screws (Figure 4.1). The kneading element was placed just before the adapter. This configuration was selected in order to avoid or minimize disperse mixing while enhancing distributive mixing of the blend.

Table 4.2. Twin Screw Extrusion Specifications

MODEL	ZE 25 * 28
External diameter of screw	25 mm
Core diameter	17 mm
Center distance	21.5 mm
Shaft	Square polygon
Max. admissible screw speed	550
Max. driving power	10.5 kW
Dynamic load capacity	14 400 N
Voltage/Frequency	3 x 230 V/ 60 Hz

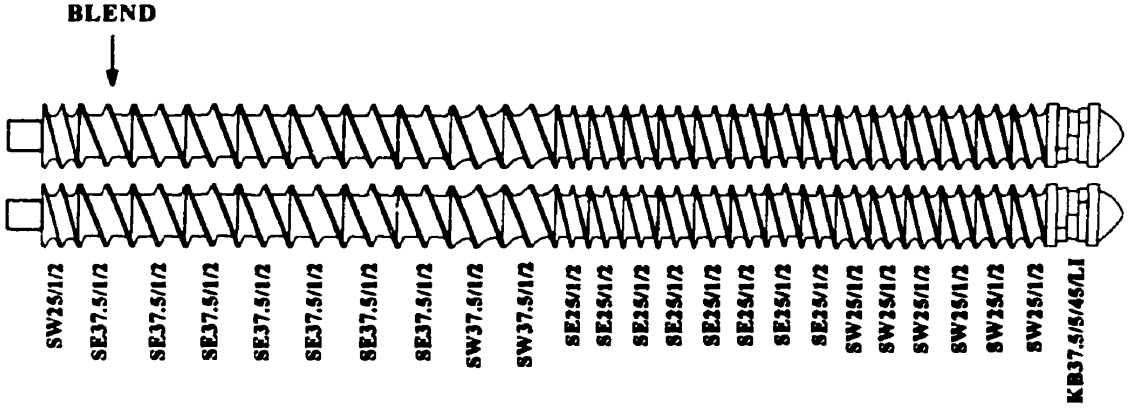

Figure 4.1 Screw configuration for co-rotating twin screw extruder.

The numbering system for the elements is explained below.

Conveying elements:		Kneading element:	
S.W.:	self-wiping	K.B.:	kneading block
S.E.:	simple element	1st digit:	length of the block
1st digit:	pitch distance	2nd digit:	kneading disks
2nd digit:	number of pitches	3rd digit:	angle between disks
3rd digit:	number of double threads	LI:	left-hand thread

4.2.2.2 Adapter

The adapter was designed to connect the twin screw extruder with the slit die to produce ribbons. The adapter consisted of two parts: the tubular and converging parts (Figure 4.2). According to Lohfink [8], the converging zone enhanced the extensional flow and coalescence in a single screw extruder. In the case of a twin screw extruder, higher mixing is produce than in a single screw extruder. Therefore, coalescence is expected in the converging section. The length of the tubular part depends on the convergence angle, since the external dimensions are set by the extruder and die. Large angles are associated with short tubular zones. Two angles were chosen (70° and 30°) to study the effect of coalescence in the blend and to compare with Lohfink's results. The adapter dimensions are shown in Appendix A.

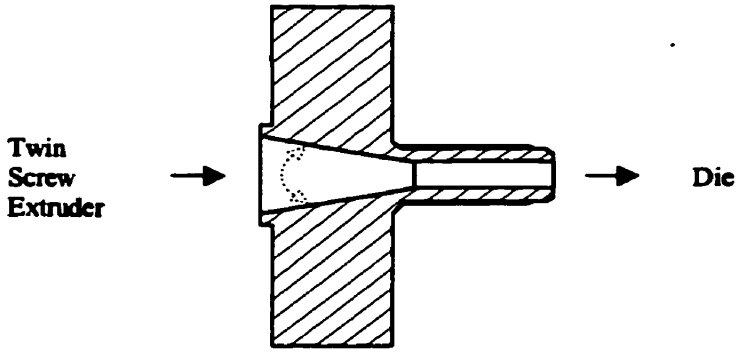

Figure 4.2. Schematic of Adapter

In order to study the morphology of the blend in the adapter, some experiments were conducted with a modified cooled adapter. Three cooling channels were introduced; one near the center for fast cooling of the polymer, and two near the outer walls to reduce the effect of heat conduction from the extruder bands (Figure 4.3). Water at 15 °C was used for cooling.

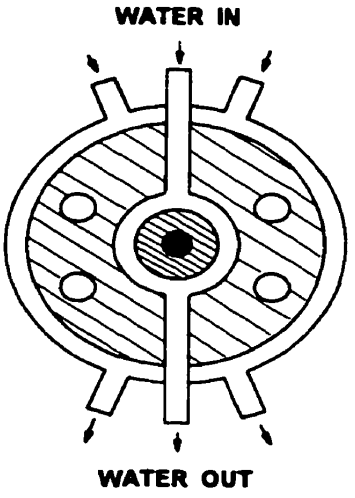

Figure 4.3. Schematic of Cooling Channels of Adapter

4.2.2.3 Extrusion Die

A slit die was used to produce ribbons. The die was designed to produce extensional flow in two directions, in order to enhance the formation of laminar morphology. The die has two converging flow sections, C and E, one diverging zone, D, and a straight slit F. The gap of the die was changed using an adjustable die land gap in sections E and F. (Figure 2.8).

The slit die was heated by a band heater. Two flush mounted thermocouples with pressure transducers were located along the centerline of the adapter, one in the middle and one in the end. Die temperature and pressure were recorded and controlled.

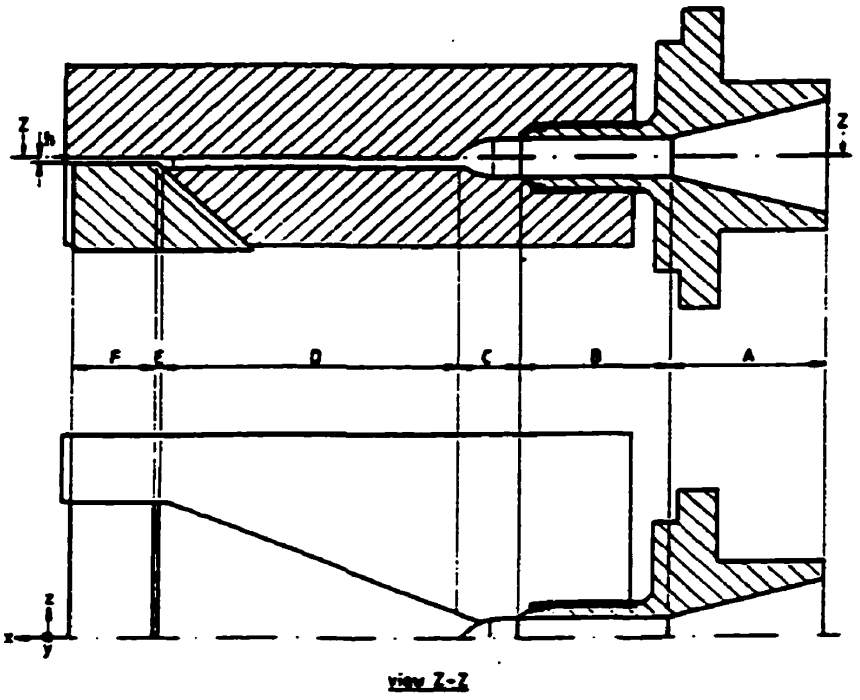

Figure 2.8. Schematic of slit die unit and adapter used by Lohfink to produce laminar morphology [8].

4.2.2.4 Cooling and Take-off system

In order to avoid the moisture absorption by nylon-6, a series of air fans was used for cooling the blends. This system consisted of four fans at the top of a trail made with Teflon coated rods and other four fans at the bottom. After the trail, the ribbon was pulled out by the take-off system, which consisted of a variable-speed flat belt conveyer. The take-off speed was controlled to avoid axial stretching.

4.2.3 Processing Conditions

The following variables were evaluated: adapter angle, die gap, temperature profile, feed rate, and screw speed. For each adapter angle (30° and 70°), two die gaps (1 mm and 0.5

mm) were tested. For each set, the temperature profile, feed rate and screws speed were varied, as shown in Figure 4.4 and Table 4.3. The first temperature profile was chosen according to optimum results obtained with the single screw extruder for the same blend [15]. It was selected so that the dispersed phase would melt just before entering the die.

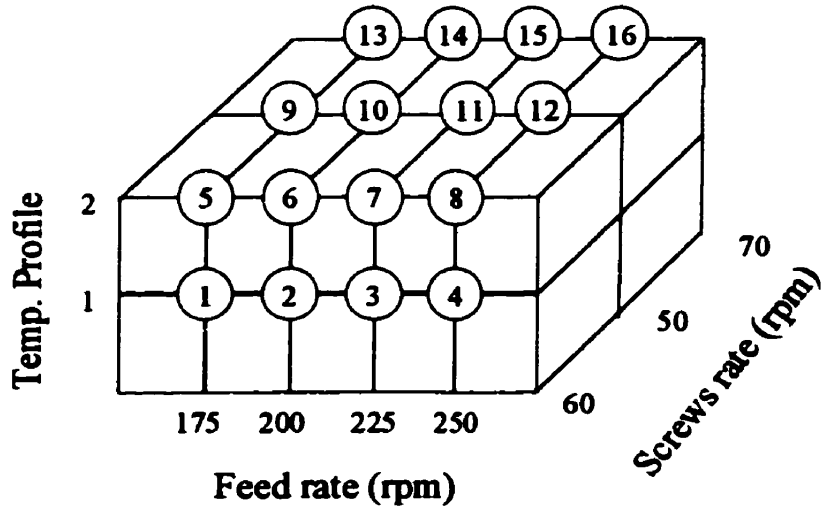

Figure 4.4 Three-dimensional set of variables: temperature profile, feeding rate and screws speed.

Table 4.3 Temperature profile in the twin screw extruder and die

	1	2	3	4	5	6	DIE
T1 (°C)	180	190	200	200	225	230	250
T2 (°C)	180	190	200	200	230	240	250

The selected feed rates: 175 rpm (3.68 kg/h), 200 rpm (4.21 kg/h), 225 rpm (4.72 kg/h) and 250 rpm (5.24 kg/h), represent variations near the limits of laminar development

evaluated during preliminary studies. Increasing the feed rate raises the pressure and torque, but reduce dispersive mixing and residence time.

Three screw speeds were used: 50, 60 and 70 rpm. Extruder speed affects the residence time in the extruder and die. There is an effect on the compatibilizer action, due to the time available for contact. Thus, interfacial adhesion is changed. An increase of screw speed increases the shear rate. When lower screw speeds were tested, poor laminar morphology was observed. At very high screw speeds, unmelted pellets of dispersed phase were obtained.

The following operating procedure was employed during blend extrusion:

a) The extruder and die were heated until the set points were reached. One hour was set for the system to stabilize.

b) High Density Polyethylene alone was extruded for 15 minutes to clean and eliminate any residual degraded material.

c) The dry blend was fed to the extruder, and 15 minutes were allowed to reach steady state.

d) For each experiment, 15-20 samples were collected and cut. They were 25-cm long and 6-6.5 cm wide. The sheets were placed and sealed in plastic bags and stored at room temperature.

The procedure employed to extract blend specimens from the die adapter was as follows:

a.1) Once the machine and blend had reached steady state, the screw rotation and heating of extruder and die were stopped.

b.1) The cooling system in the adapter unit was switched on. It took about 4 minutes to cool down from 250 °C to 135 °C. During this period, the die was removed, but not the adapter.

c.1) The cooling continued until 35 °C was reached. This was done to make sure that the whole blend was solidified at all points.

d.1) The temperature was raised up to 130 °C, just to melt the polymer near the walls. The adapter was disassembled and the specimen was removed for morphological analysis (Figure 4.5).

The processing conditions for these experiments were: 70° adapter angle, 225 rpm for the feed rate, 60 rpm screw speed, temperature profile 2 (Table 4.3), and 1mm die gap.

Figure 4.5 *Extraction of the blend from the adapter*

4.3 Characterization of the blend

4.3.1 Morphological Analysis

4.3.1. Morphology in the adapter

To study the morphology in the adapter, the samples were cut as shown in Figure 4.6: four samples in the transverse direction (T1-4) and one in the axial direction (A1) that included the whole converging section. The specimens were washed and dried. In this case the ultramicrotome could not be used due to the size of the sample, but a Buehler Isomet low speed diamond saw was used. The dispersed phase was etched with 88 % formic acid for 24 h and washed with acetone. Small deformations could occur, but at magnifications of 6.7X to 20X in an optical microscope (Olympus SZ240 Stereo), no scratches were observed.

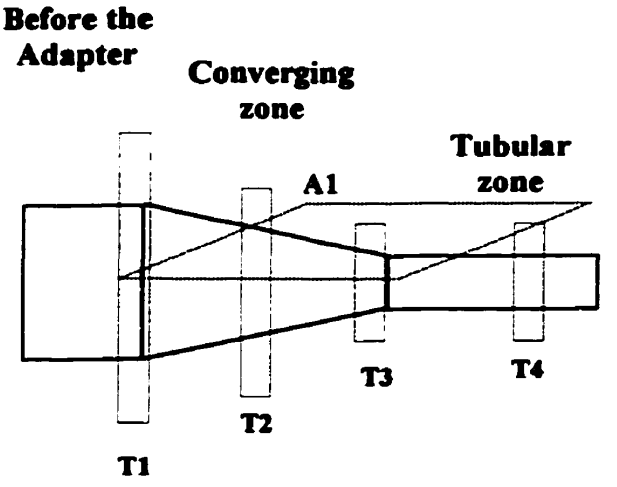

Figure 4.6 OM Sample Locations for adapter (axial and transversal direction)

4.3.1.2 Morphology of the Extrudate Sheets

The morphology was studied in a scanning electron microscope (Joel 840). The samples were prepared as follows. Different locations in the sheets were analyzed (Figure 4.7): a pair in the transverse direction, one in the center (1) and one in the side (2), and another pair in the axial direction, in the center (3) and side (4). These samples were cryogenically cut using a Leica ultramicrotome Ultracut S. The cutting temperature under nitrogen atmosphere, was −170 °C. This temperature is below the glass transition temperature of both polymers, thus reducing possible deformation during the cutting. The samples where washed with acetone to clean all the possible accumulated dust and dried in air. Subsequently, the blends were immersed in 88% formic acid for 2 hours to extract the nylon-6. Later, they were washed and dried again. The specimens were then fixed in a sample holder with epoxy glue, so that the microtomed surface faced upwards. The next step was to coat the specimens with a gold/palladium mixture. This mixture made the sample conductive. The coating was applied by sputtering of the metals under vacuum in an Anatech Ltd. Hummer VI sputtering system.

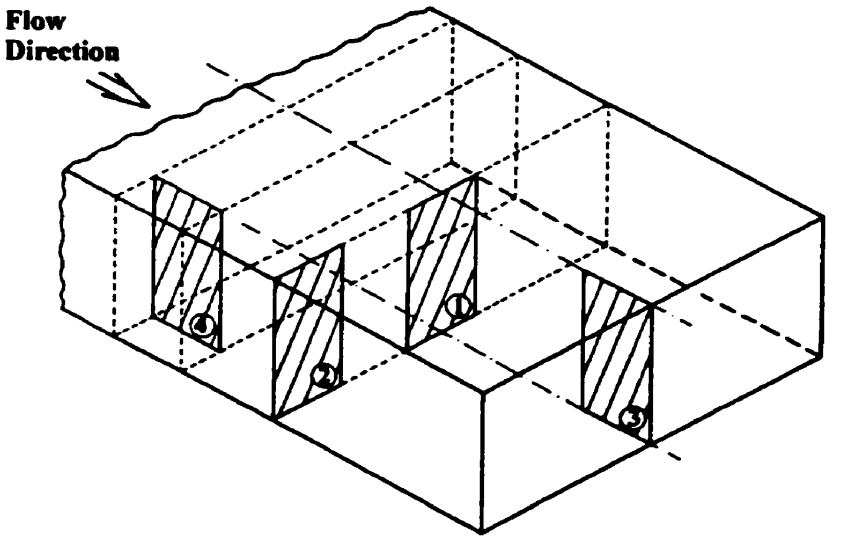

Figure 4.7 SEM Cutting Sample Locations for sheets (axial and transverse direction)

A Joel 840 Scanning Electron Microscope was used to examine the morphology of the samples. An accelerating voltage of 15 kV seemed to produce the best image, so it was used throughout the study. The working distance was adjusted according to the image (37-39 mm). This value depends on the height of the samples. A general magnification of 150X was used for all the samples. In some cases, lower magnifications were applied to show the length of the lamellas. higher magnifications were used to study the drops of the dispersed phase.

4.3.2 Toluene Permeability

The permeability of the extruded blends with respect to toluene was measured. Toluene has been used as a typical hydrocarbon to measure the permeabilities of different barrier materials.

In order to reduce the effect of surface imperfections and to have samples of comparable dimensions, squares of 6 cm long were compression molded using a Carver model 2114-2 Laboratory Press. A maximum change of 15% in the compression molded samples from the original area was set. According to Garmabi [15], less than 5 % change of the permeability was observed for compressed samples. The conditions of compression molding were: 120 ° C (below the melting point of both polymers), 22.4 Newtons, 3 min. preheating, 2 min. heating under pressure, and 5 minutes of cooling. It was found that longer preheating times could degrade the specimens.

The toluene permeability measurement was done according the ASTM F739 standard test method. This method was designed to study the permeation of liquids through protective clothing materials. The samples were stored at constant temperature (21-22 °C) for several days, but the humidity could not be controlled. The thickness of the samples was measured at 9 different locations to obtain an average. The specimen was mounted in the test cell (Figure 4.8). This cell was divided into two chambers. The chamber was filled

with toluene on one side and connected to the collecting medium (helium) in the other side. The toluene that passed through the blend was carried out by helium and went to a Hewlett Packard Gas-Chromatograph type 5890 series II, where the concentration of toluene was monitored. Two different cells were connected to the chromatograph and every 50 minutes the solvent concentration of each cell was recorded.

The permeability was calculated according to the ASTM F-739 and no temperature correction was applied because room temperature was always constant (22 °C).

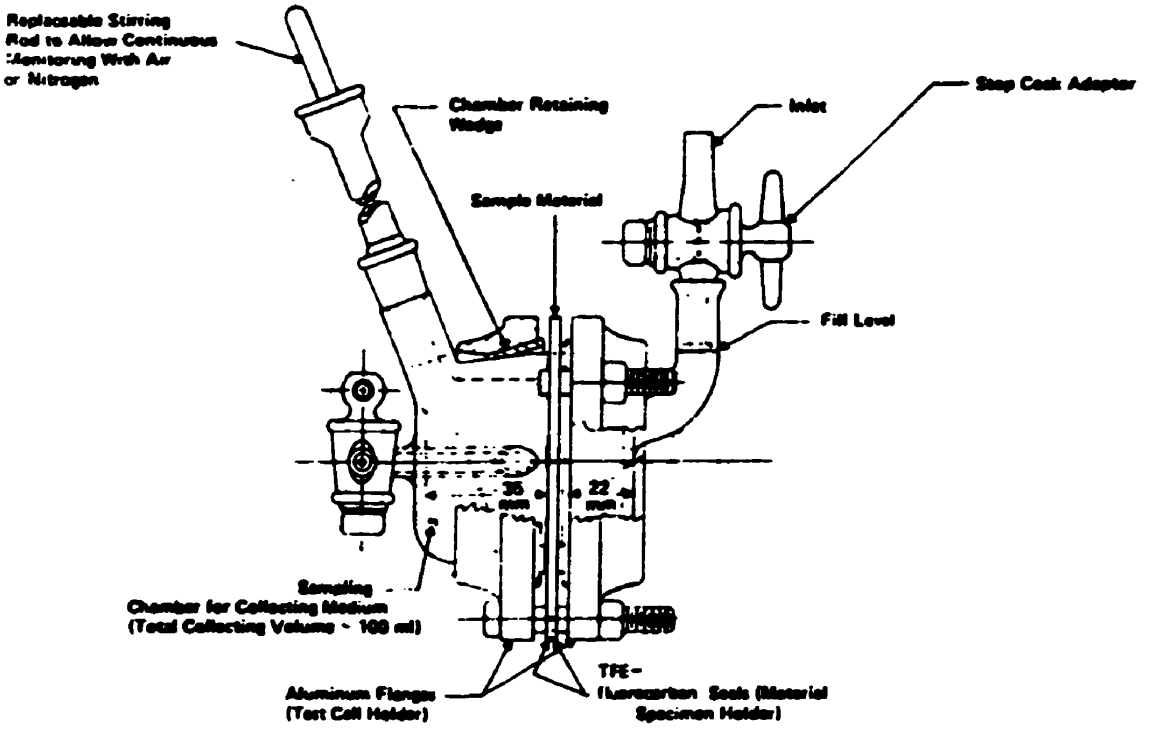

Figure 4.8 ASTM Permeation Test Cell [ASTM F-739]

4.3.3 Impact Testing

The evaluation of the impact behavior of the blends was performed in a Rheometrics RIT 8000 high-speed impact tester, in which a dart stroke the extruded sample at a constant velocity until the rupture. A square sample of 6 x 6 cm was fixed with retaining rings. The velocity was set at 1000 in/min for all the experiments. Before testing, the thickness of the samples was measured with a micrometer at nine different points, and an average was taken.

The force exerted on the rod, as a result of the impact, was measured and a curve of force versus displacement was produced on the screen. The points to calculate the slope, yield stress and break point were selected manually. The curve was plotted and the obtained results at the yield and break point were force, energy and displacement. The slope was also obtained.

4.3.4 Tensile Testing

An Instron Tensile Tester, Model 1123, equipped with pneumatic grips was used to measure the tensile properties of the blend. ASTM D-638M was followed to achieve the testing. The samples were conditioned at 22 °C for more than 40 h. The relative humidity was not controlled, but it varied from 40% to 60%. Ten specimens in the flow direction were machined in dumbbell form, type M-III. (Figure 4.9). The test was conducted at room temperature. For each sample, accurate measurement of width and thickness was done. Centerlines in the vertical and horizontal direction were drawn as a guide for the grips. The grips were adjusted to avoid toe compensation in the final curves. The lower grip was hardly attached to the base of the machine to avoid lifting. A testing speed of 10 mm/min was set, since it produced rupture in less than five minutes. A load-displacement curve was obtained on the screen and values of modulus, stress and strain at maximum and rupture points were calculated. For the purposes of this research, the elastic modulus and tensile strength were the most representative values because after the yield point,

necking occurred in all the samples due to the heterogeneous morphology of the blend. The values at break showed significant variability.

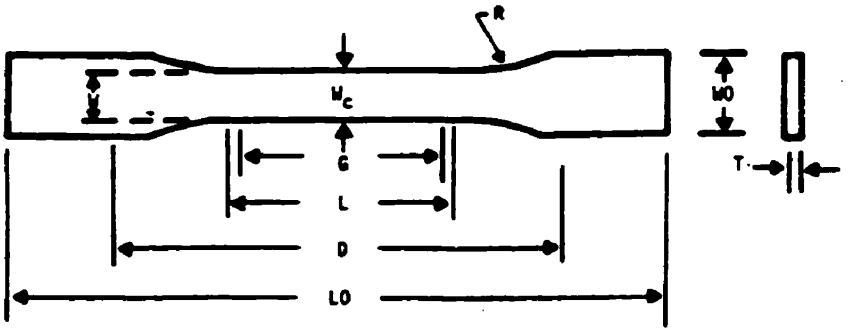

Figure 4.9 Tensile Test Specimen Measurements

Unless otherwise indicated, the specimen dimensions were as follows:

W	width of narrow section	2.5 mm
L	length of narrow section	10.0 mm
WO	width of overall	10.0 mm
LO	length of overall	60.0 mm
G	gage length	7.5 mm
D	distance between grips	25.0 mm
R	radius of fillet	15.0 mm

5.0 RESULTS AND DISCUSSION

The main objective of this research was to obtain ribbons exhibiting laminar morphology in a twin screw extruder. This would have advantages over single screw extrusion of dry blends because it would produce better distributive mixing and smoother surface in the final product.

Five variables were considered: adapter angle, die gap, temperature profile, feed rate, and screw speed. The combination of these variables showed general trends in the analyzed properties. Statistical analysis was used to determine the optimum conditions to obtain a sample that combines good morphology-permeability with good mechanical properties.

5.1 Morphology

The morphology of the blend at the exit of the screw zone, in the adapter and in the final products was investigated. The results are presented below.

5.1.1 Morphology in the adapter

The adapter angle chosen for this part was 70°. Originally, it was thought that the dispersed phase might have been broken up due to the intensive mixing of the twin screw extruder, and that a large angle could help in causing the dispersed phase droplets to coalesce. The samples were cut according to Figure 4.6. It should be noted that the viscosity ratio in the adapter is higher than one. The temperature in this zone was about 245°C and the maximum shear rate calculated in the converging zone was 26.7 s^{-1} (see appendix B).

Figure 5.1 and 5.2 show micrographs of the blend morphology evolution in the adapter in both the axial and transverse directions. These photographs were taken with an optical microscope (Olympus SZ240 Stereo). The PA-6 was extracted for 24 h from the matrix

with formic acid. The processing conditions were: 60 rpm screw speed, 225 rpm for feed rate, temperature profile 2, 1mm die gap and 70° adapter angle. The blend samples, before extraction of the dispersed phase, showed a smooth surface; no flow lines were visible. However, when the PA-6 was extracted; gaps in form of lines were observed.

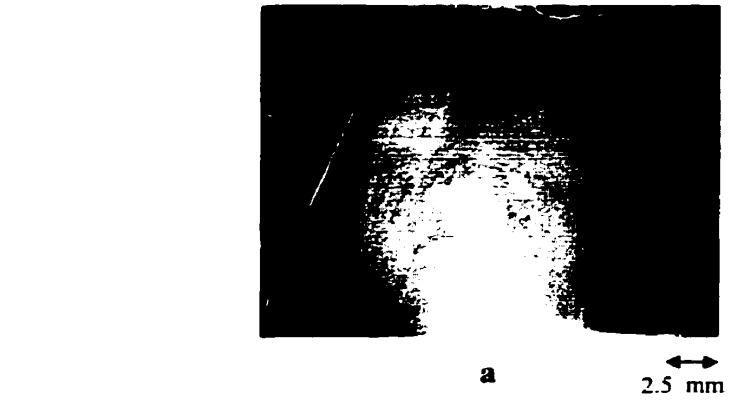

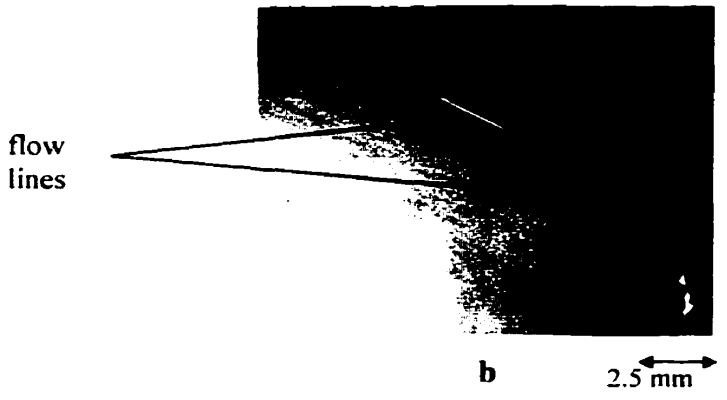

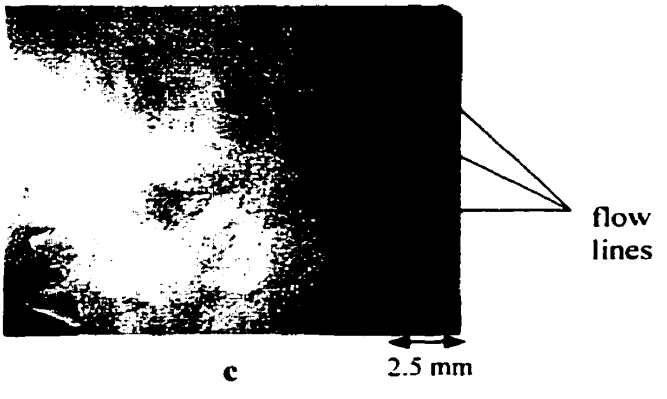

continue next page

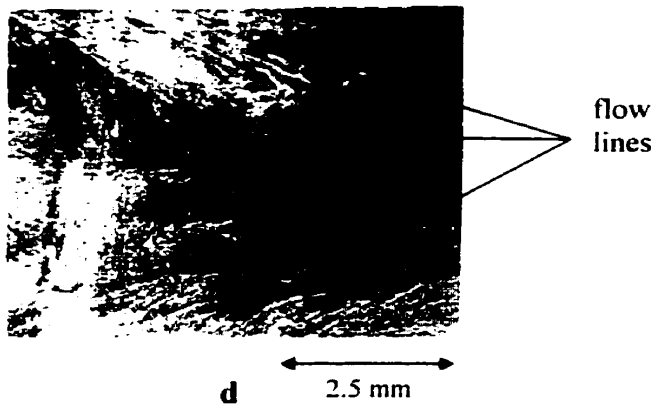

Figure 5.1: *OM Micrographs of the blend morphology in the converging section of the adapter (axial direction): a) whole converging section (6.7X), b) side view (10X) c) center of the sample (10X), d) center of the sample (22X)*

The morphology along the axial direction in the converging zone of the adapter zone is shown in Figure 5.1. Different magnifications for the same sample were taken. The whole converging zone is seen in Figure 5.1a. At the bottom, some disturbance in the center, mainly at the beginning of the converging section, is observed. The inertia from the co-rotating screws of the extruder produced this effect. On the other hand, near the wall, the lines of dispersed phase are oriented in the flow direction. A better view (10X) of the layers near the walls is shown in Figure 5.1b. Some gaps, in the form of lines produced by the extraction of PA-6, are extended from the beginning to the end of the converging zone.

At a magnification of 10X in Figure 5.1c and at higher magnification (22X) in Figure 5.1d, one can see the converging flow lines of the dispersed phase as it enters in the tubular section. Also some breakup of these lines is noted at the end of the converging zone, due to the high elongational and shear stresses and strains experienced in the converging section. Utracki and Shi [31] observed that elongational flow enhanced the breakup of the dispersed phase of viscoelastic polymers into droplets

Figure 5.2 shows the evolution of the blend morphology in the adapter along the transverse direction. In these micrographs, the presence of lines in transverse direction and the lines observed in axial direction in Figure 5.1 confirm the existence of the layers, instead of fibers, of the dispersed phase.

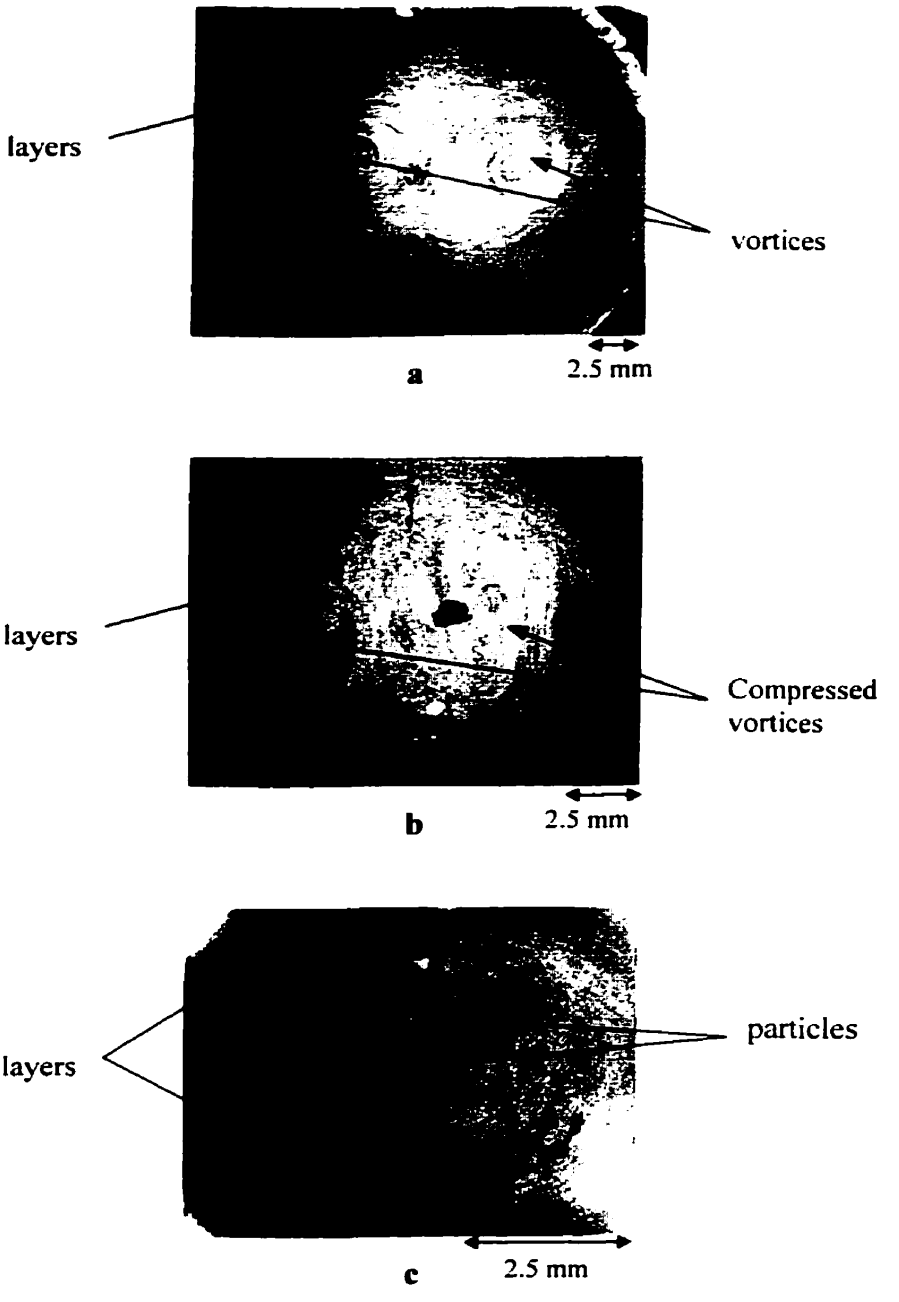

continue next page

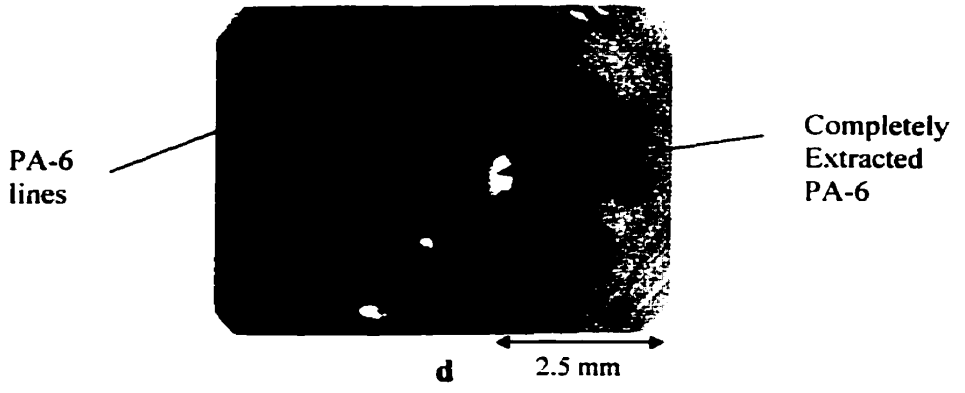

Figure 5.2: *OM Micrographs of morphology evolution across the adapter (transverse direction): a) before the adapter (6.7X), b) in the middle of the converging zone (10X), c) in the end of the converging zone (22X), and d) in the tubular zone of adapter (22X).[see figure 4.6]*

Figure 5.2a shows the morphology of the blend (6.7X) just before entering the adapter, i.e. at the end of the screws. The inertia generated by the movement of the screws is evident, and the thin continuous layers produced by extraction of PA-6 are seen. The layers of dispersed phase are distributed over the whole cross-section. These continuo layers are similar to the Poincaré pattern observed by Raynal and Gence [74] for two co-rotating agitators in a cylindrical tank in laminar flow (Figure 2.14). The micrograph shows the elliptical and hyperbolic points characteristic of chaotic mixing, as described by Ottino [71] and Aref [73]. This figure shows for the first time, the existence of layers of the dispersed phase as the melt leaves the screw zone. Macosko et al [44] and Vanio et al. [45] observed layers near the melting section of a twin screw extruder, just after the feeding zone. These layers were broken up later in the mixing section. The dimensions of the layers observed by Macosko et al. were in the range of 1 to 10 microns. In this research, the layers near the walls of extracted PA-6 are in the range of 0.5 to 1 cm length. These layers are formed around the screws and persist as they travel inside the converging zone.

Figure 5.2b shows both the persistence and the compression of the vortices and layers due to convergence (10X). This leads to orientation of the layers, as shown in Figures 5.1c and 5.1d, and the rupture of some layers. There are still several layers near the walls. A possible migration to the center and coalescence of the dispersed might take place because the reduction of the area. The black point in the center was due to the cutting, so it should be ignored. Figure 5.2c shows the morphology obtained at the end of the converging part (22X). Some layers are still visible near the walls, but there are several large particles of the dispersed phase, black dots, resulting from the breakup of the layers due to the excessive deformation caused by the large converging angle. Bourry et al [28] showed that high shear and extensional deformations are experienced by the viscoelastic dispersed phase, when it enters in the converging zone.

Figure 5.2d shows the morphology in the tubular part, between the exit of the converging zone and the die entrance. Few thin layers remain near the walls, but mostly large particles are seen. The particles are distributed over the whole cross-section, with slightly higher concentration observed in the center. When the dispersed phase was extracted, a small hole was produced in a 2-mm thick sample in the center indicating the concentration of PA-6 in that location. Although PA-6 is also seen in other locations. Lohfink [8] also observed that the dispersed phase in the converging zone tends to coalesce along the central axis. In this study, the coalescence effect along the central axis was observed mainly with the high adapter angle.

A high convergence angle, 70° in this case, appears to cause breakup of the layers formed in the twin screw extruder. A smaller angle would involve less stretching of the dispersed phase, thus reducing the breakup. On the other hand, the coalescence effect in this study was not very pronounced as in single screw extrusion. The viscosity of the dispersed phase, associated with the low temperature profile in the extruder, tended to slow down the migration of the dispersed phase to the center; as Utracki and Toma [53] described.

5.1.2 Morphology of Extruded Sheets

5.1.2.1 Morphology across the thickness

Three different zones have been observed across the thickness of extruded and injection molded samples: core, intermediate, and skin [8-15, 54-55]. In the core and intermediate zones, well-developed laminar morphology was seen, but not near the walls. Spheres and ellipsoids formed by the rupture of layers have been found in the skin layer. The aspect ratio (length/thickness) of the layers showed large differences mainly between the center and walls.

The morphology in each zone depends on the distribution and size of the dispersed phase which, in turn, depends on the processor, the die/adapter design, and the operation conditions. In the adapter, as seen in section 5.1.1, the particles of dispersed phase are distributed throughout the matrix, but in the center the concentration is somehow higher. A typical sample that results from this kind of distribution can be seen on Figure 5.3a (50X). The layers of dispersed phase are thicker in the center or core, while near the walls or in the skin, the layers are thinner. In this case, the combination of processing conditions produce distributed layers across the sample thickness, even near the walls.

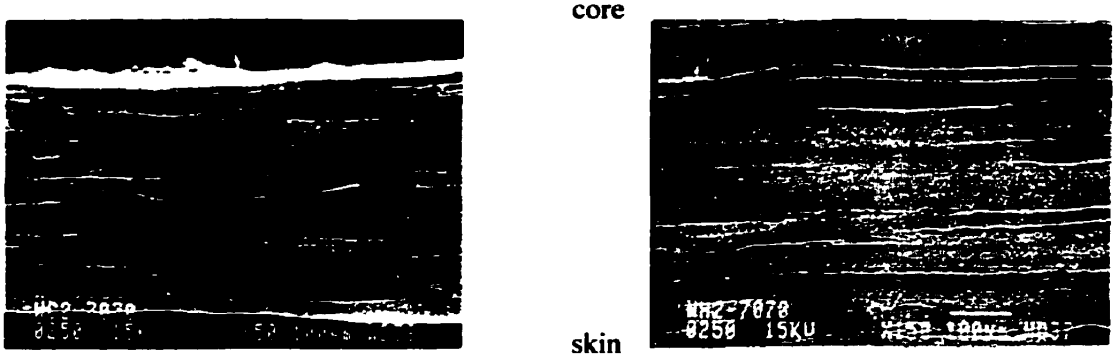

a **b**

Figure 5.3 Micrographs across the sample thickness: a) uniform distributed layers (50X), b) layers concentrated in the center (150X).

In Figure 5.3b (150X), a different behavior is observed. A prominent thick layer in the center is seen, but much thinner layers are seen in the intermediate and skin layers. Coalescence causes accumulation of large particles in the center, while high shear rates cause the breakup of the dispersed phase near the walls. Utracki [53] observed that the most viscous polymer in a blend tends to stay in the center, thus experiencing low deformation.

In general for the twin screw extruder, the layers of dispersed phase were found distributed over the whole thickness. The observations discussed above, made by other researchers, appear to be applicable for this extruder, but not necessarily under all conditions. The viscosity and/or elasticity ratio, shear and elongational rate are factors that determine the thickness of the layers in the sample, but under the right conditions, as seen before, a broad distribution of layers can be achieved even near the walls.

5.1.2.2 Morphology in different locations

The morphology was studied at four different sampling locations (Figure 4.7) in order to confirm the existence of laminar and not fibrillar morphology in the sample. Two specimens were microtomed from the center and two from the sides in transverse and axial directions respectively.

In the micrographs taken in center, Figure 5.4a and b show distributed layers across the thickness. But in the sides, Figure 5.4c and d show layers mostly in the core at both directions, transverse and axial; small spheroids and ellipsoids are also observed in the skin zone. In samples taken from the sides, the presence of a third wall (top, bottom and side) in the die increases the shear rate effect. This contributes to the breakup of layers that produces the ellipsoids and droplets.

These micrographs confirm the existence of layers of PA-6 in polyethylene across the thickness and along the width of the samples, since similar observations are made in both axial and transverse directions.

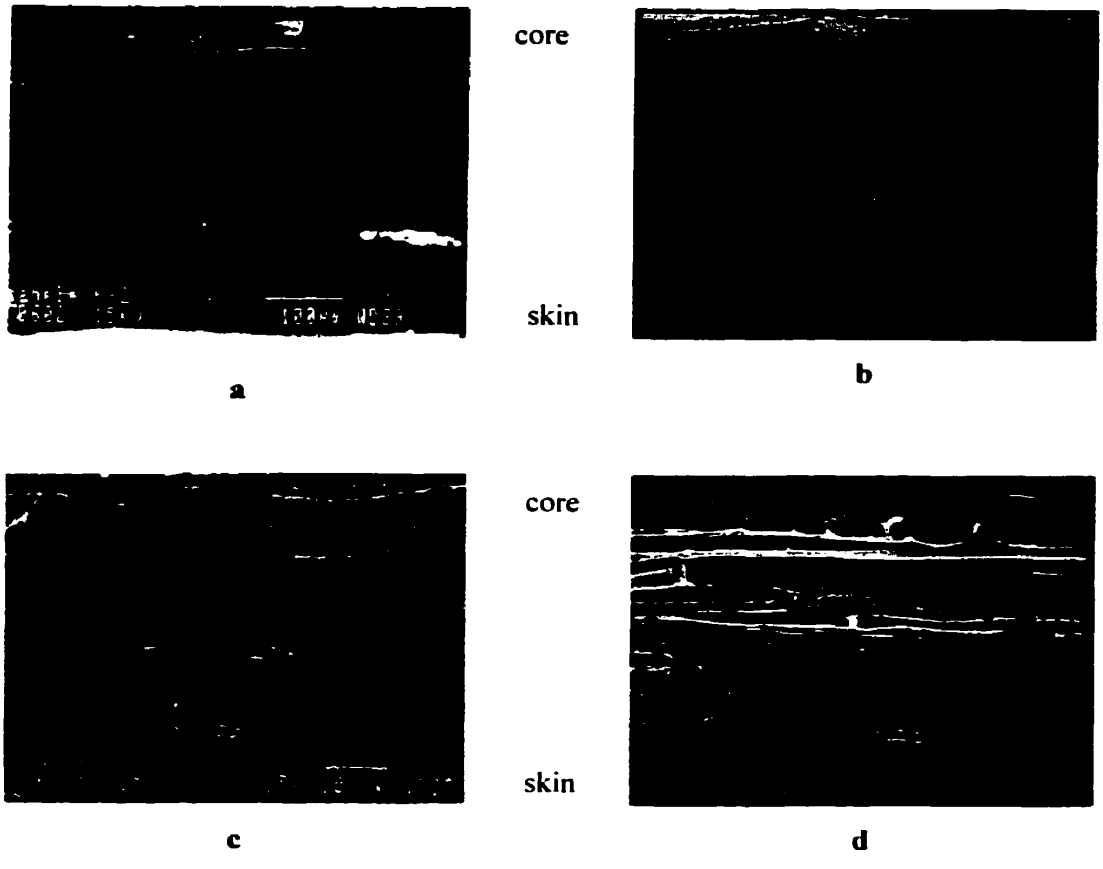

Figure 5.4 SEM Micrographs in four different sampling locations: a) center-transverse direction, b) center-axial direction, c) side-transverse direction and d) side-axial direction. (see figure 4.7)

5.1.2.3 Adapter angle effect on morphology

Two different adapter convergence angles were evaluated to study their effect on the morphology of the blend. Figure 5.5 shows micrographs of the results. It was shown in section 5.1.1, that at the end of the 70° convergence zone, most of the layers of the dispersed phase were broken down into large particles, due to the high shear and

elongational flow produced by the large convergence. At the entrance to the adapter, the particles already formed layers. These layers are stretched and orientated in the adapter and they are again stretched in the die, resulting in ribbons with distributed layers. These layers can be seen in Figure 5.5a. In the intermediate and skin zones, some layers do not cover the entire field, probably because some small particles produced during the breakup of layers in the adapter were extended in the die, but they were too small to produce large layers at the exit of the die.

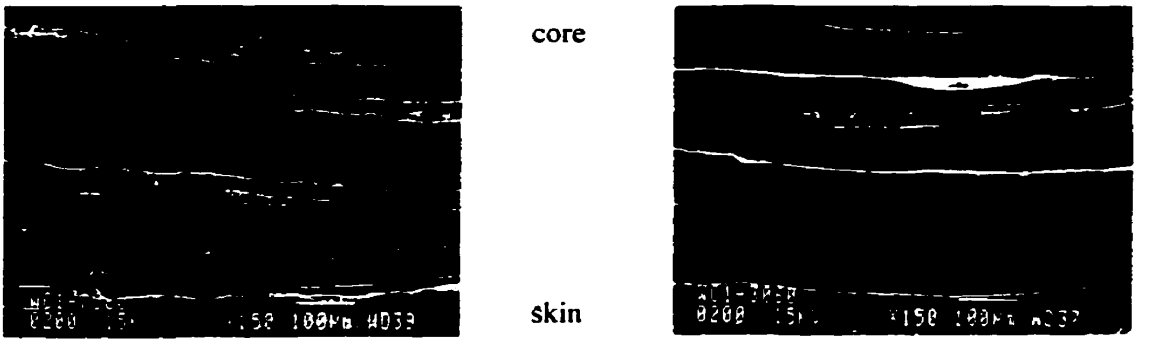

Figure 5.5 *Adapter effect on morphology: a) 70° convergence angle*
b) 30° convergence angle

Figure 5.5b shows the morphology with a 30° adapter angle, at the same die gap and processing conditions as for the 70° angle. In this case, the layers extend over the whole length of the micrograph. A large number of thinner layers is formed. Many of these layers were probably formed already at the front of the twin screw extruder, as discussed in section 5.1.1.

Lohfink [9] evaluated the 30° and 70° adapter angles in a single screw extruder. He observed that with both metering and mixing screws, a higher angle resulted in extensive coalescence in the short converging section of the adapter, creating large and extended

dispersed phase agglomerates along the axis. He suggested that coalescence is required for development of laminar morphology, so a large convergence angle would help to produce layers in the core, where coalescence is most pronounced. His results might appear to contradict the observations presented here. However, the mechanism of mixing plays an important role in the ultimate morphology that is formed. It should be noted that the twin screw extruder used in this work was operated to produce distributed mixing with minimum breakup of the particles, and the temperature profile was low enough to prevent earlier melting of PA-6. But, the adapter with the large convergence angle tended to break down the layers to smaller particles. In the case of single screw extrusion, droplets enter the adapter from the extruder. These particles coalesce and are then stretched in the adapter. Under these conditions, coalescence in the adapter with large converging angle is helpful in forming layers. Under some operating conditions in the twin screw extruder, only droplets were formed in front of the screws, and the role of the adapter in these cases, was similar to that observed in the single screw extruder. When the layers are already built at the end of the extruder, a large convergence angle only increases the breakup of such layers.

Although laminar morphology was obtained with the two angles in this study, the presence of some gaps, along the length, between the layers for the 70° adapter may have a significant influence on the permeability of the blend, because the solvent or gas might diffuse more easily through those gaps.

5.1.2.4 Die Gap effect on morphology

Two different die gaps were studied: 1 mm and 0.5 mm. Figure 5.6 shows that, in the case of the1 mm die gap, several and distributed layers are obtained across the thickness. For the same adapter angle and processing conditions, the 0.5 mm die gap, results in poor lamellas. The layers are mainly in the center, and some very thin layers appear in the intermediate zone. It can be deduced from the micrographs that for small die gaps, high overall shear rates are produced, so high deformation is also obtained and possible

breakup might occur. The breakup of the layers occurs mainly near the wall. The resulting droplets might diminish the barrier properties, but they might contribute to improve the impact properties.

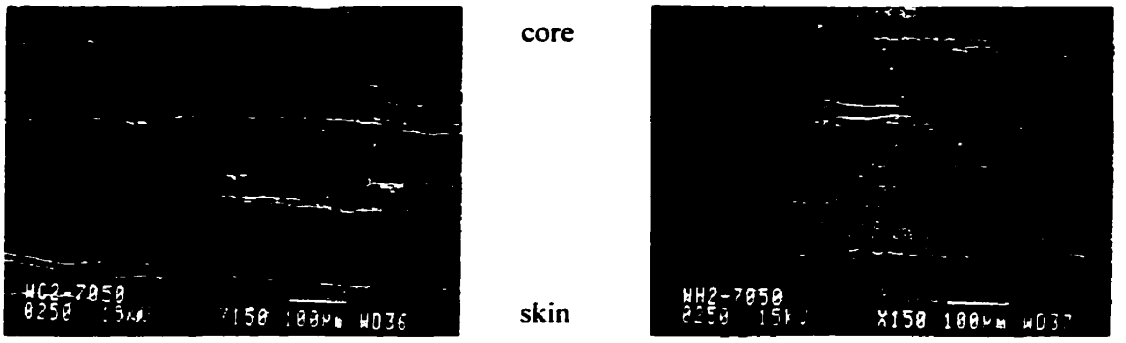

Figure 5.6 *Die Gap effect on morphology: a) 1 mm and b) 0.5 mm*

5.1.2.5 Temperature Profile effect on morphology

The first temperature profile selected for this study was based on the optimum temperature profile found for developing laminar morphology for the same blend system in a single screw extruder. Work with the single screw extruder has shown that delaying the melting of the dispersed phase until the last zone (i.e. metering) of the single screw extruder, produced large particles that could be stretched in the slit die to obtain layers, mainly in the intermediate and core zones.

Another temperature profile was evaluated because the extrudate sheets showed, in some cases, unmelted PA-6. This temperature profile was higher by 5° C in the penultimate zone and 10° C in the last zone of the extruder, compared to the first profile (Table 4.3). The results are shown in Figure 5.7.

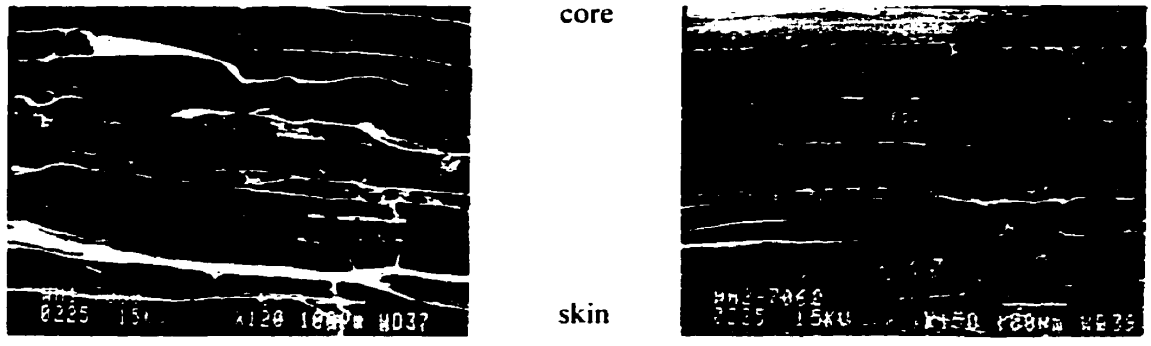

***Figure 5.7** Temperature Profile effect on morphology: a) T1 and b) T2. (refer to Table 4.3)*

The first temperature profile shows thick layers in the core and near the wall, but some unextended ellipsoids in the intermediate zone. This morphology includes some gaps where the permeant can pass. Although the layers are thick, some of them are not long enough to cover the whole micrograph, as in the case of the 70° adapter angle. For the second temperature profile, the layers are well defined and fully extended to cover the length of the micrograph.

In both cases, the laminar morphology is formed. However, it is preferred to have longer and thinner than thicker and shorter layers that are not fully elongated. According to Nielson [60], the tortuosity for the diffusion is higher with longer particles. This results in decreasing the permeability of the system.

It is important to recognize that the morphology strongly depends on the temperature profile. Garmabi [15] showed that changing the temperature from 200 to 240°C in the last zone of a single screw extruder decreases the aspect ratio (L/T) of the layers by almost a factor of 10.

5.1.2.6 Feed Rate effect on morphology

The twin screw extruders are starved-fed. Thus, the degree of screw channel fill, i.e. the ratio between the actual output and the screw output capacity, is less than one. An increase in the mass flow rate (feed rate) will increase the degree of screw channel fill, but might decrease the dispersive mixing

Figure 5.8 shows the effect on laminar morphology when the feed rate is increased, while other variables remain constant. For a feed rate of 175-rpm (3.68 kg/h), some layers appear in the center, as shown in Figure 5.8a. In this case, the material has higher residence time and higher probability to interact with the flights and barrel in the extruder, and the walls of the adapter and die. Although the temperature profile is low, the material is exposed to shear and heat for a longer time. Therefore, melting occurs and the particles or layers of PA-6 break into drops, producing spherical rather than laminar morphology. Yang [39] observed the size reduction of the dispersed phase when the residence time was increased.

When the feed rate is increased to 200 rpm (4.21 kg/h), several additional layers are seen in Figure 5.8b, mainly in the intermediate zone. These layers are thin and extended to cover the length of the micrograph. In this case, the residence time is lowered and the contact between the dispersed phase and the walls is reduced. According to Teh and Rudin [38] higher pressure is developed in the extruder that might keep the PA-6 in contact with the matrix. The layers are slightly thicker and well distributed in the sample when the feeding rate is increased to 225 rpm (4.72 kg/h), as shown in Figure 5.8c.

For a feeding rate of 250 rpm (5.24 kg/h), Figure 5.8d shows a micrograph with a magnification of 50X with very thick layers distributed across the thickness. Although the general appearance is promising, there are some gaps where the layers did not extend. So, the layers do not cover the whole sample, and the permeant might easily pass thought the gaps.

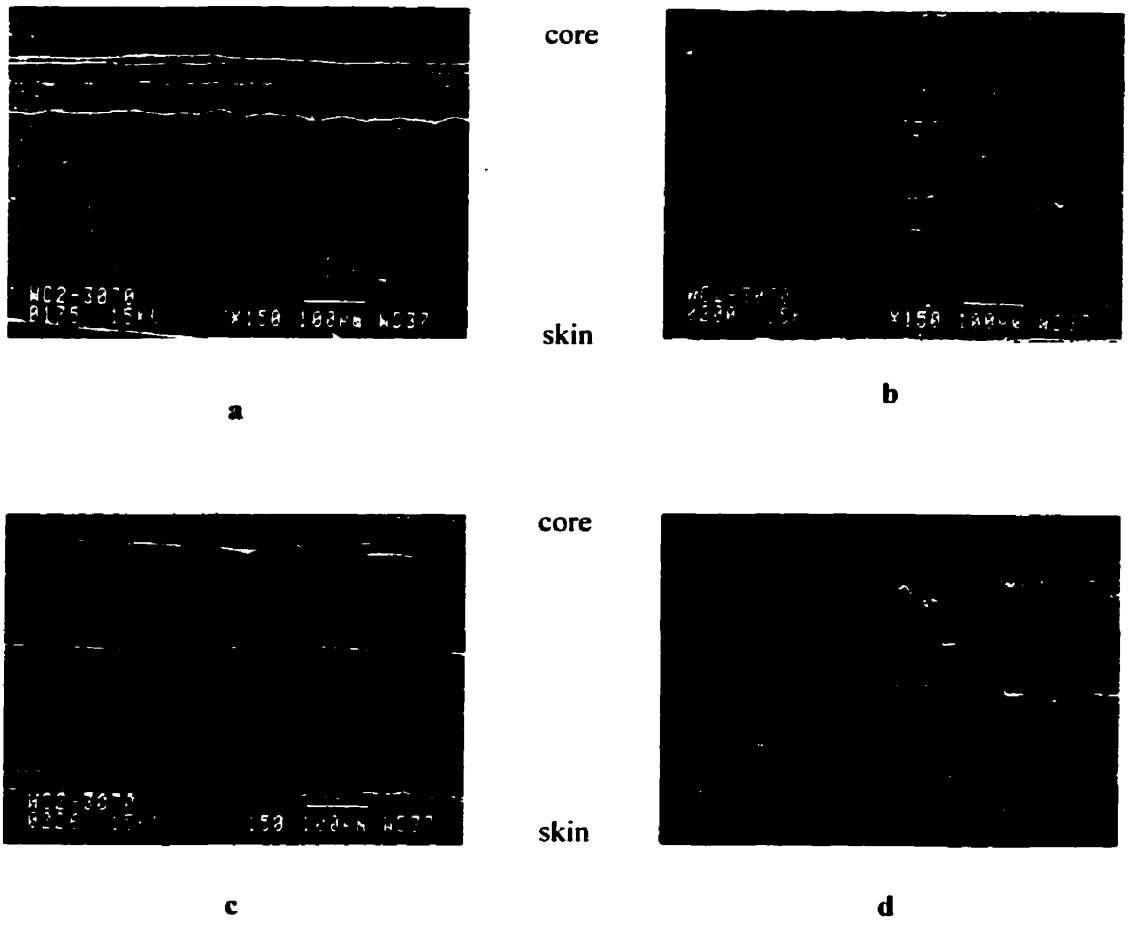

Figure 5.8 Feed Rate effect on morphology: a) 175 rpm, b) 200 rpm, c) 225 rpm and d) 250 rpm

Other feed rates were tested. For 150 rpm, the dispersed morphology was found mainly in the form of drops, and for 300 rpm, the pellets were not melted, thus not elongated (Figure 5.9). The above results showed a significant influence of the mass flow rate on morphology development. Delamare and Vergnes [42] showed that higher feed rates produce lower residence time and are associated with larger particles. In the case of laminar morphology development, the processing window is small. It is desirable to melt the dispersed phase particles and elongate them as much as possible without breaking. Low feed rates normally enhance particle breakup, while high feed rates will leave many particles unmelted.

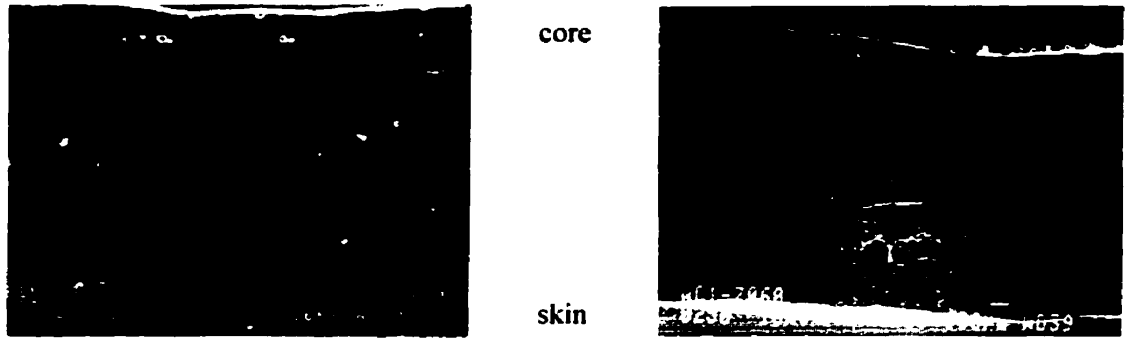

Figure 5.9 Feed Rate effect on morphology: a) 150 rpm (mainly drops) b) 300 rpm (unextended pellets)

5.1.2.7 Screw Speed effect on morphology

Figure 5.10 shows the morphology obtained when the extruder screws speed was varied. For 50 rpm, some accumulated thin layers appear in the center, while near the walls, mainly spheres and ellipsoids are seen. For 60 rpm, many distributed layers are observed across the thickness, even near the walls. When the speed was increased to 70 rpm, several distributed layers are still seen, although the number of layers is reduced.

In the case of dispersed morphology, Shi and Utracki [37] and Delamare and Vergnes [42] showed that increasing the screw speed in a twin screw extruder leads to shorter residence times and higher shear rates and modifies the viscosity ratio. They observed that at very high screw speeds, an efficient breakup occurs, thus reducing the diameter of the particles.

On the other hand, for laminar morphology in a single screw extruder, Lohfink [8] and Lee [41] found that increasing the screw speed from about 20 to 90 rpm, increase the size of the layers. Although, it is contrary to the behavior observed for the development of

spherical morphology due to the blend experience higher shear stress that could ultimately yield a smaller dispersed phase, the authors suggested that these observations are better explained in terms of residence time. Thus, short residence times that are produced at high screw speeds increase the layer size because there is less time of contact with the extruder and die walls.

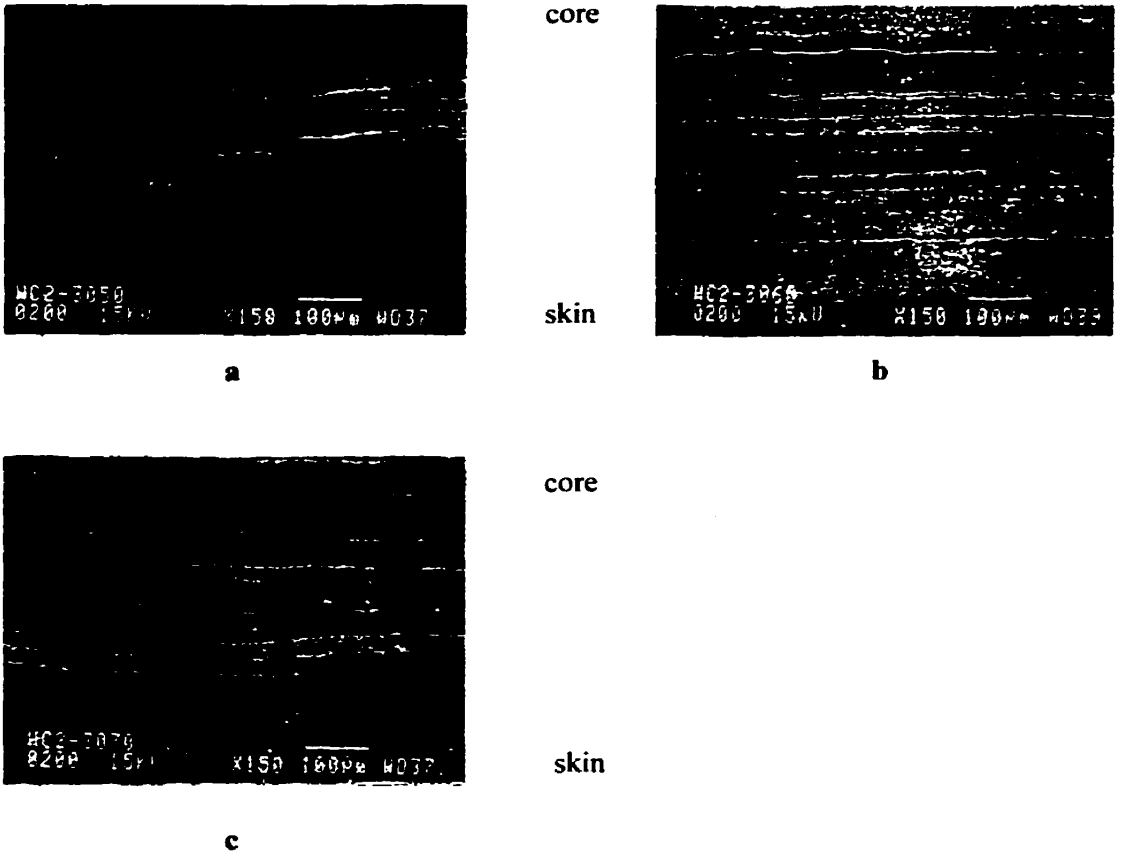

Figure 5.10 *Screw Speed effect on morphology: a) 50 rpm b) 60 rpm c) 70 rpm*

In this research, the laminar morphology in a twin screw extruder showed a small number of layers at very low and very high screw speeds. However, the distribution was more uniform at higher screw speeds. Raising the screw speed above a critical point produced unmelted pellets. It would be desirable to investigate the behavior at higher speeds for

cases where some other variables are changed in order to optimize the development of layers. However, it is also important to note that at higher screw speeds, the contact time between the phases will be shorter, thus reducing the effect of the compatibilizer. This could lead to a reduction in mechanical properties.

5.2 Permeability

Polyamides provide very good barrier against the permeation of hydrocarbons, but they exhibit only average toughness and they are relatively expensive. On the other hand, polyethylene is easily processible and suited for containing aqueous materials. It has the advantage of high toughness and low cost. However, it exhibits high permeability to solvents and vapors. Blending polyamides and polyethylene to produce laminar morphology of polyamide in a polyethylene matrix, in a twin screw extruder, can yield barrier containers or tubing for hydrocarbons. Twin screw extrusion could be a technology to produce articles with uniform and reproducible properties compared to those obtainable in single screw extrusion.

The permeability of blends is intimately related to their morphology. Thus, the tortuosity in laminar morphology is higher than in spherical morphology. In this research, toluene was chosen to investigate the permeability of the HDPE/PA-6 blend. Both design variables (adapter and die gap) and processing variables (temperature profile, feed rate, and screw speed) were considered. Three-dimensional graphs are presented to provide a better understanding of the combined effects of variables on the barrier behavior.

The permeation rate of the blends was calculated according to the ASTM F-739 as follows:

$$q = c\left(\frac{F}{A}\right) = ppm * 0.09993 \qquad (5.1)$$

Where q is the toluene permeation rate (mg/mm^2.min), c is the concentration of toluene that penetrated the extrudate sheet in mg/L (3.769*ppm), where ppm refers to the concentration in parts per million of toluene obtained from the gas chromatograph. A, is the exposed area of the material specimen, normally equal to 18.85 cm^2, and F is the flow of fresh collecting medium through the cell, in this case helium (0.05 L/min).

The permeation rate is related to the permeability by:

$$P = q * t \qquad (5.2)$$

where P is the permeability coefficient (mg.mm/m^2.min) and t is the thickness of the sample in mm.

5.2.1 Influence of Adapter Angle and Die Gap on Permeability

Figure 5.11 shows the effect of the adapter angle on the permeability. As discussed on section 5.1.2.3, the layers of PA-6 were more uniformly distributed and elongated for the 30° angle. In the case of 70° converging angle, some the layers did not cover the complete micrograph. This was attributed to the breakup of the layers produced in the adapter. Although these results affect the permeability, the effect of the adapter angle, compared to other variables, does not seem to be great. In fact, for both die gaps, the differences in permeability due to the adapter angle are around 10-15%. However, the permeability measurement is seen to be in harmony with the morphological results.

In section 5.1.2.4, it was shown that the morphology was changed substantially when the die gap was decreased. The same effect is seen on toluene permeability. For 0.5mm die gap, the spherical morphology, created by the high stretching and breakup of the particles, allows the solvent to penetrate and pass through the sheet easily. For 1mm die gap, the layers are extended and uniformly distributed. Thus, the path that the solvent has to

follow in order to reach the other side of the sheet is longer (Figure 2.10). For an adapter angle of 70°, the permeability at 0.5 mm die gap, is 4.5 times higher than for 1 mm. For 30 °, the difference is 6.5 times. The values change according to the processing conditions employed, but the trend remains the same.

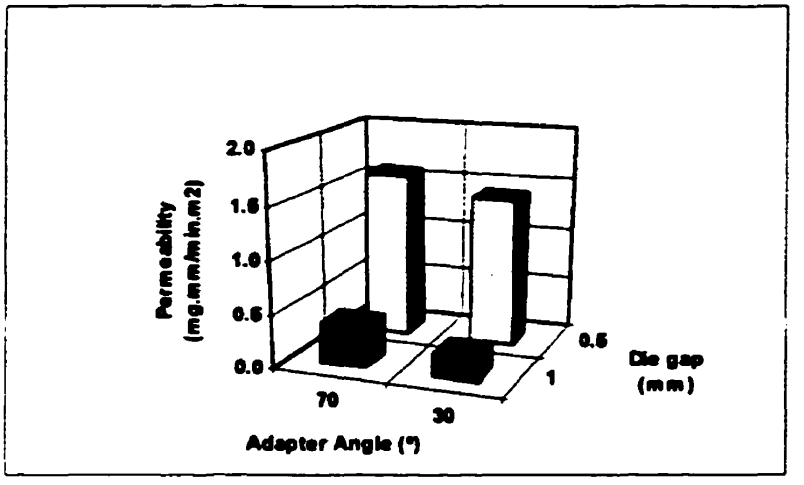

Figure 5.11 Effect of adapter angle and die gap on toluene permeability (feed rate:225 rpm, screw speed: 60 rpm, and temperature profile1)

5.2.2 Influence of Temperature Profile and Feed Rate on Permeability.

In Figure 5.12, the effects of temperature profile and feed rate are shown. The permeability of the polyethylene alone is also given for comparison. At low feed rates, an increase in temperature in the last two zones of the extruder causes an increase in the permeability. Low feed rates are associated with long residence times. Thus, more heat is received from the extruder heaters and shear, which lead to early melting of PA-6. The high shear and elongational effects in the extruder and adapter cause breakup into spheres and ellipsoids, producing high permeability of the blend. When the feed rate is increased, the temperature effect is not as large as before. In this case, the shorter residence times, combined with high feed rates and high temperatures cause the layers to be longer.

The effect of the feed rate on permeability may be explained in light of morphology depicted in the micrographs shown in Figures 5.8. As the feed rate is increased in the range of 175 to 225 rpm, the number of layers increases as well as the thickness and the uniformity of their distribution. This leads to a reduction in permeability. However, at higher feed rates (e.g. 250 rpm), the pellets are not completely melted and extended. As a result, thick and short layers with gaps are produced. This leads to a small increase in the permeability at such high feed rates.

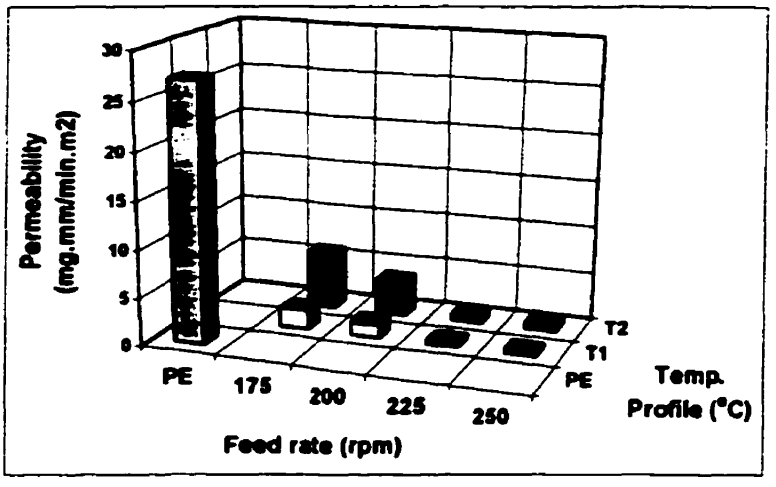

Figure 5.12 Effect of temperature profile and feed rate on toluene permeability (adapter angle: 70° and die gap: 1 mm)

5.2.3 Influence of Screw Speed on Permeability

In Figure 5.13, the effect of feed rate is presented again but in combination with the effect of extrusion screw speed. For low feed rates (175 rpm), the spherical morphology is dominant over the laminar morphology. Thus, there is not a large effect of the screw speed on the permeability. Once the feed rate is increased to 200 rpm, the effect of extruder screw speed becomes important. Thus, higher screw speed produces lower permeability. At higher feed rate (225 and 250 rpm), a large drop in permeability occurs from 50 to 60 rpm screw speed. The permeability appears to level off at higher screw

speed. As indicated earlier, there is a competition between the effects of residence time and screw speed (see section 5.1.2.7). Higher screw speeds are usually associated with large and uniform distributed layers. Lee and Kim [41] also observed that increasing the screw speed decreased exponentially the oxygen permeability for LDPE/EVOH blend.

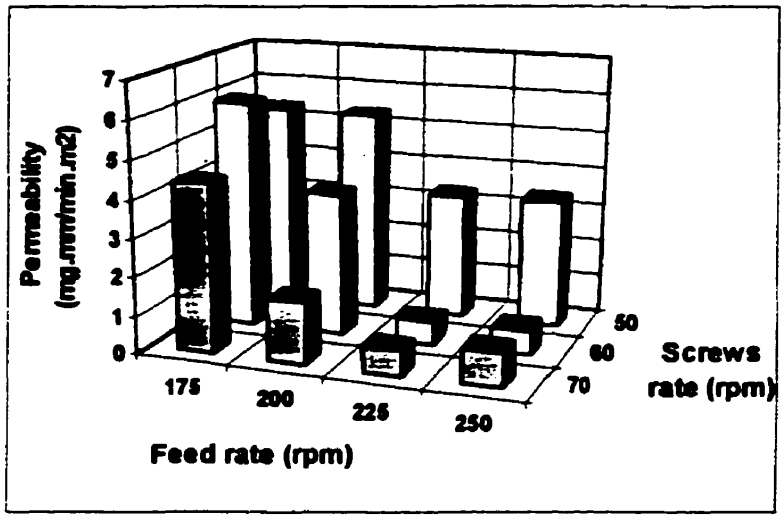

Figure 5.13 Effect of feed rate, screw speed on permeability (adapter angle: 70°, die gap: 1 mm)

5.2.4 Overall Barrier Performance

Two limiting models are available to calculate permeability. The Series Model (equation 2.14) is applicable to continuo multilayer structures or coextruded materials, where several layers of a barrier polymer are sandwiched in layers of another polymer. The Maxwell model (equation 2.13) is useful to estimate the permeability of the dispersed phase when it is in the form of spherical particles. Both models require data regarding the permeabilities of the pure resins. The permeability of toluene in polyethylene is well known (Table 4.1). Garmabi [15] measured the toluene permeability of a compression-molded PA-6 and reported a value of 0.11 mg.mm/min.m^2. In the present work, twin screw extruded sheets of PA-6 were used to measure the toluene permeability. A value of 0.0162 mg.mm/min.m^2 was obtained. It is possible that compression molded samples

were not completely packed leaving voids or bubbles, thus producing higher permeability. Therefore the value obtained in this research for the toluene permeability of PA-6 was used in the application of the Maxwell and Series models.

All the data regarding the permeability of the various twin screw extruded samples are reported in Table C.1 in Appendix C. Also for reference, permeabilities of selected single screw extruded samples are shown in Table C.2 in the same appendix [15]. Figure 5.14 shows a comparison between the measured and calculated permeabilities of various samples. The composition of PA-6 was always at 17.4 %vol. (20 %wt.). The first four specimens show the effect of feed rate (see last three digits). The last two samples show the effect of extruder screw speed (50 and 70 rpm), that can be compared with the second sample (60 rpm). It is seen that increasing either the feed rate or extruder screw speed lowers the permeability. The observations have been discussed in earlier sections in relation to the effects of residence time, shear and morphology.

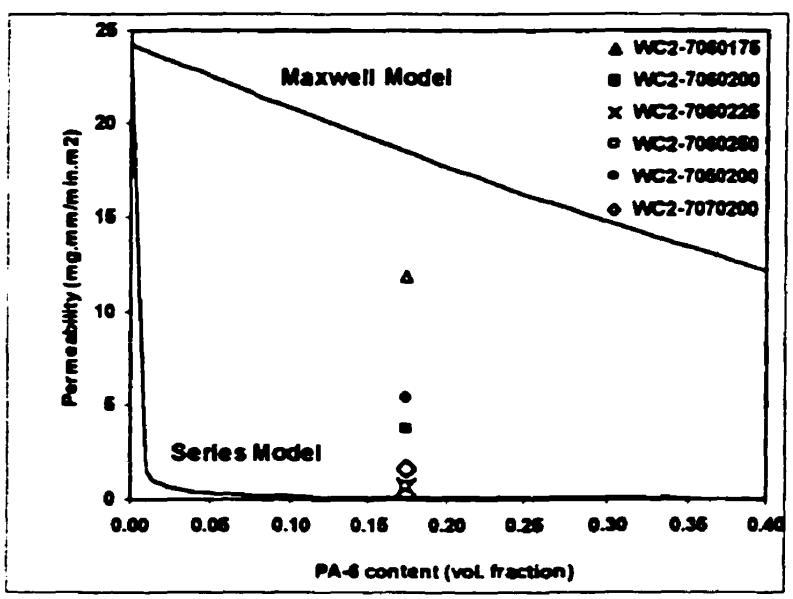

Figure 5.14 Toluene Permeability of HDPE/Nylon-6 along the Series-Maxwell Model

It is important to note that, under appropriate conditions, it is possible to obtain permeability values close to those achievable in co-extruded structures. The ratio between the toluene permeabilities in polyethylene and nylon-6, measured at the same conditions, as in the experiments, was 1500 (Table 4.1). The Series model predicts a permeability ratio of 262, between a co-extruded structure and PA-6, at 17.4% vol. PA-6. The best sample obtained in this research showed a ratio of 113. The best ratio reported by Garmabi, for single screw extruded ribbons, is around 45. Moreover, it should be noted that sample uniformity is not generally adequate in the single screw extruder.

5.3 Impact Properties

The impact strength of a material is defined, as the energy required for fracture across unit cross-section during high speed loading. It gives a measure of the ability of the material to withstand impact loading, and it is important since articles are frequently subjected to such loading during service. The impact strength of blends is a good indicator not only of the strength but also of the quality of adhesion in the system. However, the fracture may reflect not only adhesive (interfacial) failure but also cohesive or mixed failure.

The impact strength of the samples was measured using a high rate impact tester. By definition, the ultimate energy to break gives the impact strength of the sample. In the case of laminar morphology, it has been suggested that other impact test data such as ultimate force, slope and displacement are not as indicative of impact behavior as ultimate energy. In any case, in this section, we present the data for both ultimate force and ultimate energy. In Appendix C, Table C.1 shows a list of all the data for the samples in this study, regarding the ultimate force and ultimate energy. In Table C.3, a list of slope and displacement values is given for all the samples.

The energy and impact values were standardized according to the following equations [12]:

$$E_{1mm} = E_t \frac{E_{N,1mm}}{E_{N,t}} \quad \text{and} \quad F_{1mm} = F_t \frac{F_{N,1mm}}{F_{N,t}} \qquad (5.3)$$

$$E_{N,1mm} = 2.46t - 1.20 \quad \text{and} \quad F_{N,1mm} = 598.5t - 199.1 \qquad (5.4)$$

where E_{1mm} and F_{1mm} are the normalized values of energy (Joules) and force (Newtons) respectively, E_t and F_t are the measured values, $E_{N,1mm}$ and $F_{N,1mm}$ are calculated values for thickness of 1mm and $E_{N,t}$ and $F_{N,t}$ are those values for thickness of t mm for the HDPE/MAPE/PA-6 blend.

5.3.1 Influence of Adapter Angle and Die Gap on Impact Properties

Spherical morphology of the dispersed phase is known to improve mechanical properties, because it helps to distribute the stresses. In the case of laminar morphology, the layers should be distributed not only across the thickness but also along the width and length of the sample.

Figures 5.15 and 5.16 show the effect of adapter angle on ultimate force and ultimate energy. For a die gap of 0.5 mm, the effect of the angle on these properties appears to be smaller than for a die gap of 1 mm. It can be also seen that the effect of die gap, in this range, is larger than the effect of the adapter angle. The larger die gap produces lower impact energy and force at failure. As noted earlier, the deformation associated with the small gap are more effective to cause particle breakup than the large angle. In both cases, the impact properties are improved for an angle of 70°, because higher particle breakup

occurs in the case of the high converging angle. The changes in the ultimate energy are more pronounced than those observed in the ultimate force.

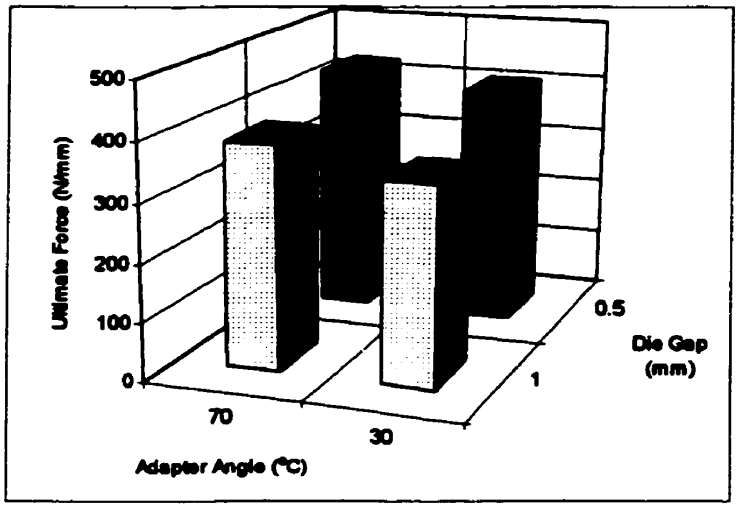

Figure 5.15 Effect of adapter angle and die gap on Ultimate Force (feed rate:225 rpm, screw speed: 60 rpm, and first temperature profile)

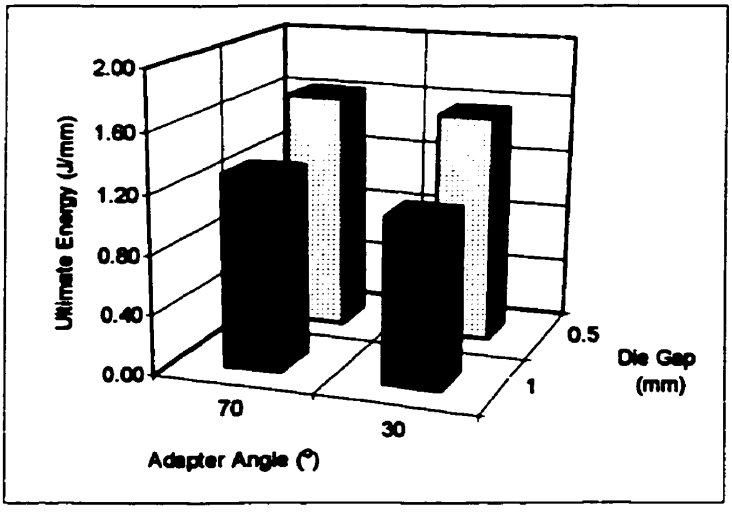

Figure 5.16 Effect of adapter angle and die gap on Ultimate Energy (feed rate:225 rpm, screw speed: 60 rpm, and first temperature profile)

The factors that enlarge impact behavior are the same as those that contribute to increase the permeability, as a consequence of the resulting morphology. It should be remembered that low permeability is preferred. However, ideally it is desired to obtain both good impact and barrier properties.

5.3.2 Influence of Temperature Profile, Feed Rate on Impact Strength

Figures 5.17 and 5.18 show the variation of impact strength with the temperature profile and feed rate. It is desired to maintain impact characteristics comparable to those of polyethylene. The ultimate impact force is of the same order of magnitude as for polyethylene. However, when the ultimate energy is analyzed, a significant drop is observed. This is more likely due to poor adhesion between the two phases.

Both Figures show, in most cases, that higher force and energy are obtained at the higher temperature profile (T2), especially for energy. This is probably due to the improved interaction between the compatibilizer, the disperse phase and the matrix phase. The interfacial tension between the two components is reduced at high temperature. Similarly, the viscosity is lower, causing improved diffusion that results in enhanced impact behavior. Low feed rates produce long residence times that induce to a high interaction of the dispersed phase and the matrix phase with the compatibilizer, so good adhesion between the phases results in higher impact properties.

High mechanical properties are obtained when the dispersed phase is in the form of drops due to the distribution of the mechanical stresses. An increase in the size of the dispersed phase produces a reduction of mechanical properties [13]. In the case of laminar morphology, thin and long layers, i.e. high aspect ratio, increase the path where the failure can occur, thus decreasing the ultimate energy. Although the platelets were biaxially extended in the flow and transverse direction in the slit die, an increase of 10 % in the ultimate energy was observed in the flow direction. This might be due to the slight

stretching to remove blend from the extruder that is produced by the take-off system during the processing.

In this work, it was observed that increasing the feed rate results in a large decrease of impact energy. It was also observed that the temperature profile (T2) at high feed rates produces better development of layers, as seen in section 5.1.2.5. Moreover, this might result in an increase of the dispersed phase aspect ratio. Figure 5.18 shows, for the temperature profile T2, a decreasing trend along the feed rate. This behavior can be also explained by the aspect ratio increment. Similarly, the ultimate energy at low temperature profile (T1) and low feed rates shows the same the trend as that observed for T2, but at 250 rpm an increase instead of decrease of the impact energy is produced. This could be due to the presence of small and unmelted particles of PA-6 that reduce the area exposed to failure.

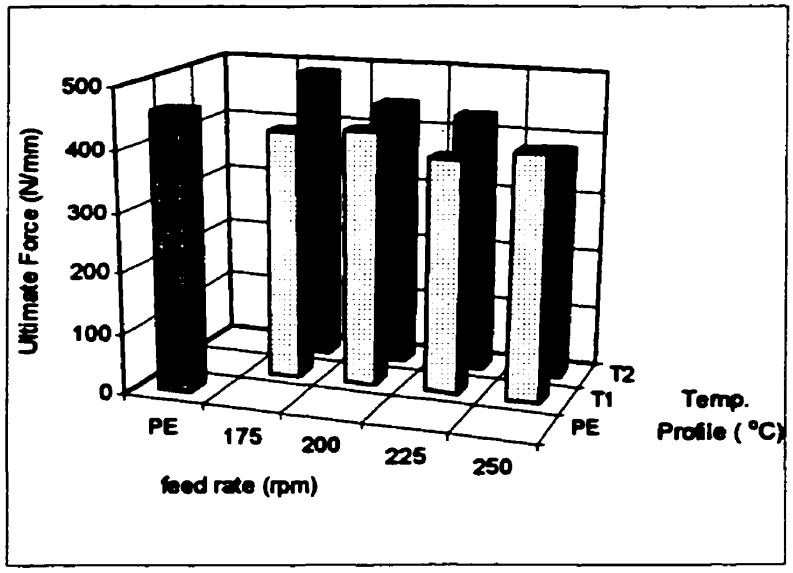

Figure 5.17 Effect of temperature profile and feed rate on ultimate force (adapter angle: 70° and die gap: 0.5 mm)

The ten load-displacement curves obtained from the impact measurement for each sample provide some insight, regarding homogeneity or uniformity of the samples. Appendix D

shows the results of the complete impact load vs. displacement curves, when the feed rate was varied. For 175 and 200 rpm, the ten test results almost coincide. As the feed rate was raised to 225 rpm and later to 250 rpm, significant variations are observed reflecting lack of uniformity of the extrudate obtained at these rates.

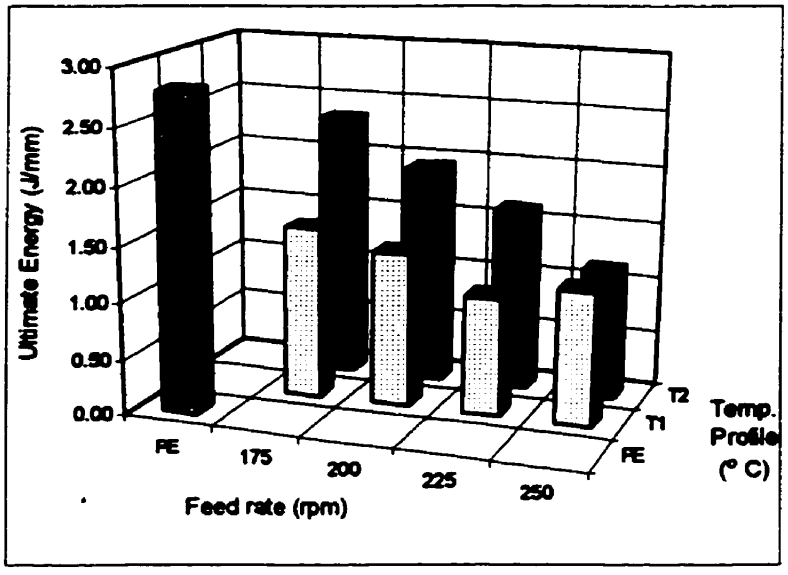

Figure 5.18 Effect of temperature profile and feed rate on ultimate energy (adapter angle: 70° and die gap: 0.5 mm)

5.3.3 Influence of Screw Speed on Impact Properties

Increasing the speed of screws in the twin screw extruder lowers the residence time but raises the shear rate. Figures 5.19 and 5.20 show that the ultimate energy and force are decreased when the feed rate increases, but the effect of the screw speed appears to be negligible. At lower and higher feed rates, the impact strength values show small changes. These small variations with screw speed might be attributed to experimental error (below 5% in most cases). In section 5.1.2.7, it was shown that the effect of screw speed on morphology is not as notorious as other variables, e.g. feed rate. A similar behavior is seen in the impact properties.

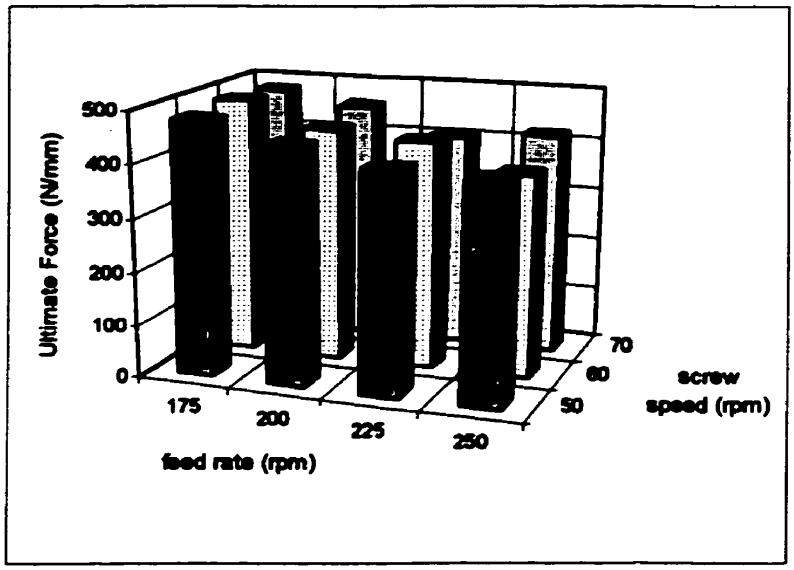

Figure 5.19 Effect of feed rate and screw speed on ultimate force (adapter angle: 70° and die gap: 0.5 mm)

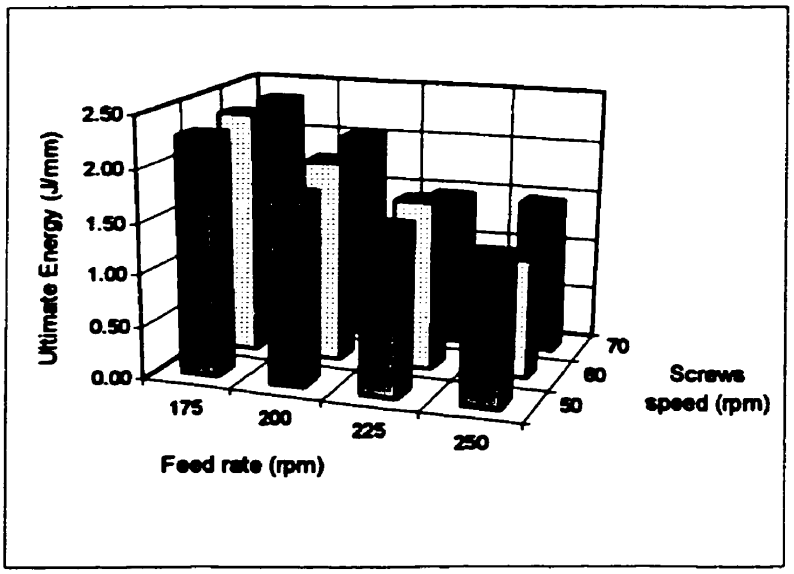

Figure 5.20 Effect of feed rate and screw speed on ultimate energy (adapter angle: 70° and die gap: 0.5 mm)

5.4 Tensile Properties

Tensile testing involves moderate rate measurement of uniaxial deformation under the influence of an applied uniaxial load. This test was conducted with an Instron Tester Model 1123. The data obtained from the test were tensile strength and elongation at yield, tensile stress, elongation and energy at break, and elastic modulus.

The laminar morphology is characterized by good barrier properties, but suffers from heterogeneity that could lead to deterioration of mechanical properties. This was clearly reflected in impact behavior of the blends. In the case of tensile properties, necking was observed for all the samples. Again, the necking can be result of the heterogeneity of the samples. The tensile properties at break showed large deviations in the individual specimens. The necking occurred at different points, depending on the distribution of the layers along the sample. Because the recommended area by ASTM method during the stretching is small (Figure 4.9), the size and distribution of the layers could be a significant factor in tensile measurements. In the case of impact testing, this is not so serious, because the testing area is much larger (section 4.3.3). Therefore, it was decided to take only the properties before the necking to minimize uncertainty. Thus, tensile strength at yield and elastic modulus were analyzed. Typical tensile curves for the blend system are shown in Appendix D. All the data concerning the tensile strength at yield and elastic modulus are shown in Table C.1 of Appendix C.

5.4.1 Influence of Adapter Angle and Die Gap on Tensile Properties

Figures 4.21 and 4.22 show that the adapter angle and die gap do not have a significant effect on the tensile strength and elastic modulus. The variability can be attributed to experimental errors, because in most cases, the deviation is lower than 5%.

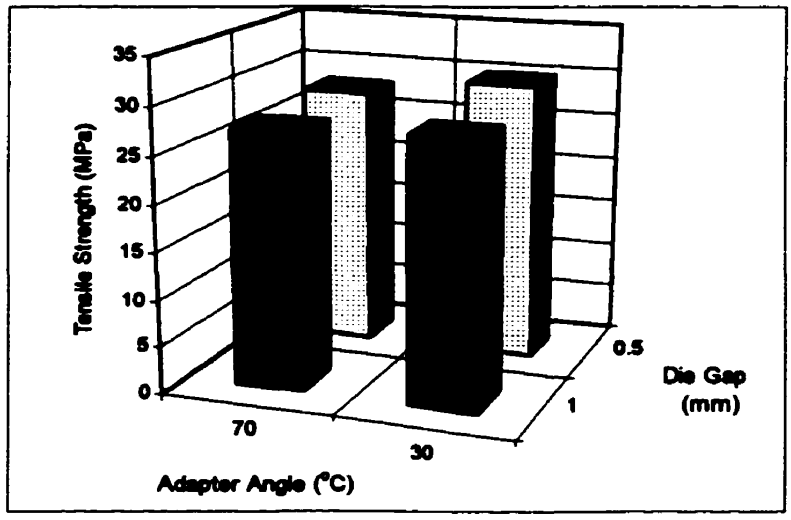

Figure 5.21 Effect of adapter angle and die gap on Tensile Strength (feed rate:225 rpm, screw speed: 60 rpm, and first temperature profile)

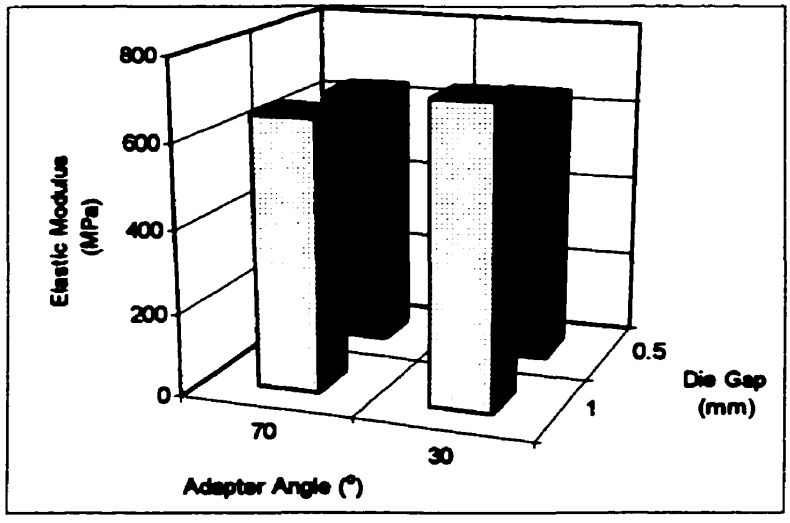

Figure 5.22 Effect of adapter angle and die gap on Elastic Modulus (feed rate:225 rpm, screw speed: 60 rpm, and first temperature profile)

5.4.2 Influence of Temperature Profile, Feed Rate on Tensile Properties

Figures 5.23 and 5.24 show the tensile strength and elastic modulus values of the polyethylene and blends. For the blends, the tensile strength values are very close to the polyethylene values, but the polyethylene modulus is slightly higher than the blend modulus. The effect of the feed rate and temperature profile on tensile properties appears to be negligible, although, a slight increase of tensile modulus may be associated with the higher temperature profile.

Tensile test results show that polyethylene and blend samples before the necking can handle similar uniaxially applied loads, i.e. tensile strength at yield. The comparable stiffness values of the blends before necking, given by the tensile modulus, suggest that the tensile properties are not affected by the morphology of the system.

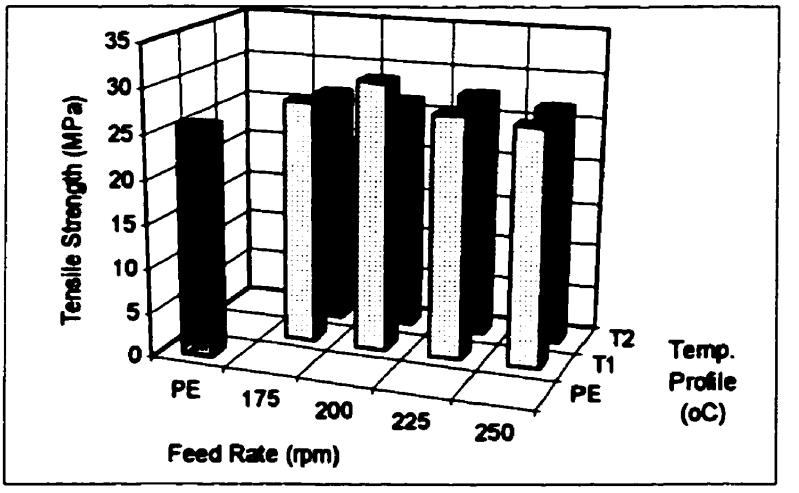

Figure 5.23 Effect of temperature profile and feed rate on Tensile Strength (adapter angle: 30° and die gap: 1 mm)

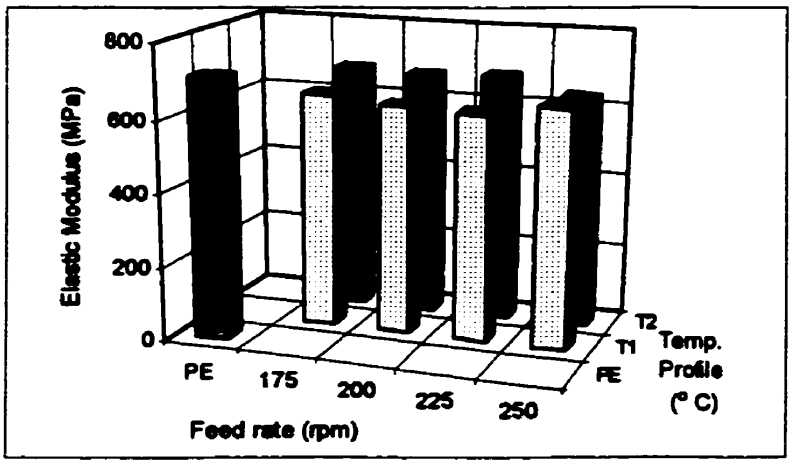

Figure 5.24 Effect of temperature profile and feed rate on Elastic Modulus (adapter angle: 30° and die gap: 1 mm)

5.4.3 Influence of Screw Speed on Tensile Properties

Following the same pattern, the screw speed does not seem to affect the tensile strength and elastic modulus. Some variations occur, but they are small and may be attributed to experimental errors.

The tensile test results, in general, do not provide a basis for screening of the blends in relation to the five variables discussed before. They do not appear to depend significantly on the morphology of the blend and PA-6 is not even contributing to improvement in the mechanical behavior as a reinforcement of the polyethylene. However, it is interesting to note that the tensile modulus and the tensile strength of the blends are close to the properties of the matrix. This is different from the impact results reported earlier. Similarly, Teh and Rudin [38] observed that for blends produced in the twin screw extruder, the impact properties were closely related to the blend morphology, but tensile testing did not provide such a relation. It should be noted that their results were evaluated for samples exhibiting spherical morphology.

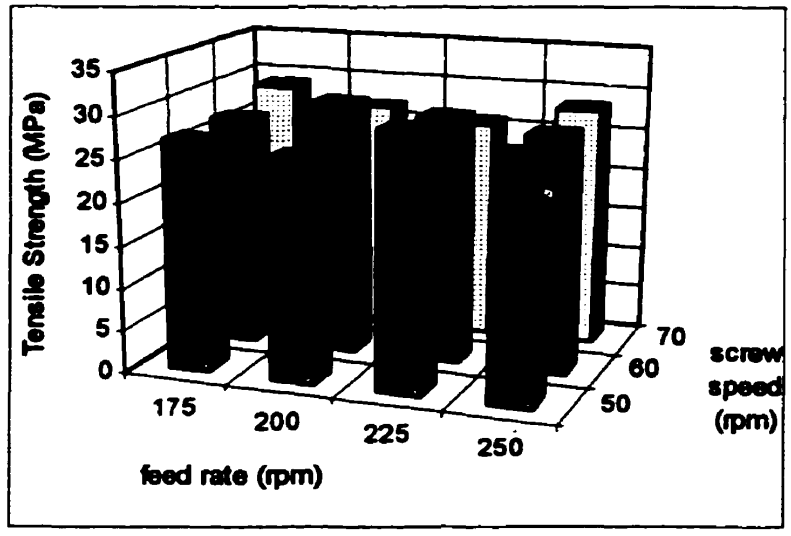

Figure 5.25 Effect of feed rate and screw speed on Tensile Strength (adapter angle: 30° and die gap: 0.5 mm)

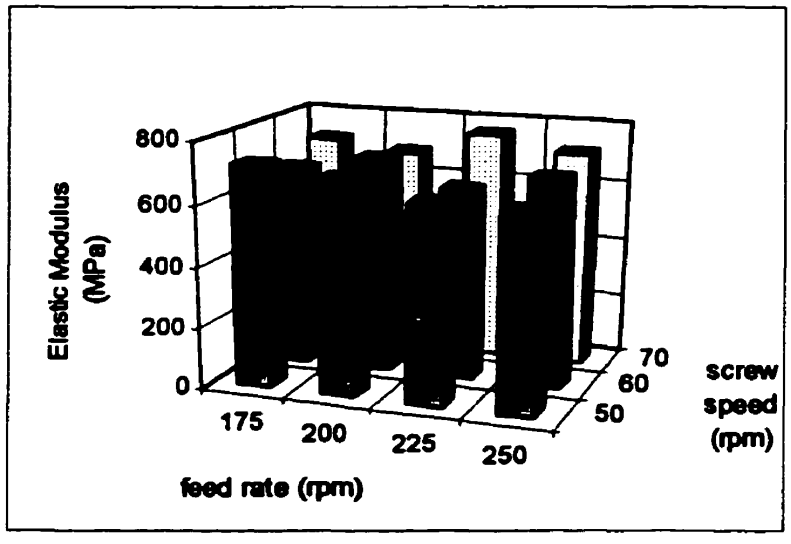

Figure 5.26 Effect of feed rate and screw speed on Elastic Modulus (adapter angle: 30° and die gap: 0.5 mm)

5.5 STATISTICAL ANALYSIS

The results of this work have shown that the best samples for permeability exhibited poor mechanical properties. A statistical analysis was carried out to find a sample with optimum balance of barrier and mechanical properties. The method, developed by Harrington [75], is called Desirability Function.

The desirability function method consists of assigning a desired value, *de*, to each property, e.g. permeability, impact strength, elastic modulus, etc. The best sample will have a desirability value of one, and the worst value will be zero. Based on these two limits, the desirability for the other samples is calculated for that specific property. The transformed data, y', are calculated taking into account the desirability value using the following formula:

$$de = \exp\left[-\exp\left(-y'\right)\right] \qquad (5.3)$$

y' is calculated for each sample and for each property and it is related to the actual value, y, as:

$$y' = b_1 + b_2 y \qquad (5.4)$$

The parameter b_1 and b_2 are calculated from the low limit (0.2) and high limit (0.8) of *de* for each property (Figure 5.27). This is done to avoid errors for choosing boundaries near one or zero. A new desirability function, d, based on the actual value is calculated as:

$$d = \exp\left[-\exp\left[-\left(b_1 + b_2 y\right)\right]\right] \qquad (5.5)$$

The value of "d" is again calculated for each sample for one property. The sample procedure is done for all the other properties. Harrington proposed to take the square root of the product of all d's for each sample and take the maximum as the optimum value. If this criterion is used, the same weight will be given to all the properties. In this research, the permeability plays a more important role than the mechanical properties. So, the values of d's, were standardized, d_{std}, to the same lower and upper limits, and the typical addition of terms multiplied by preference to the property, x, was followed. Thus,

$$D = \sum x \cdot d_{std} \qquad (5.6)$$

where x = 0.6 for permeability, x= 0.3 for ultimate energy and x = 0.1 for tensile modulus desirabilities. More emphasis was placed on permeability and ultimate impact energy, because they showed strong correlation with the morphology development, in the five variables analyzed. In fact, 60% of preference is for permeability and 40% for mechanical properties. Using this criterion, the maximum value of D will give the compromise or optimal conditions to develop laminar morphology with very good barrier and good mechanical properties.

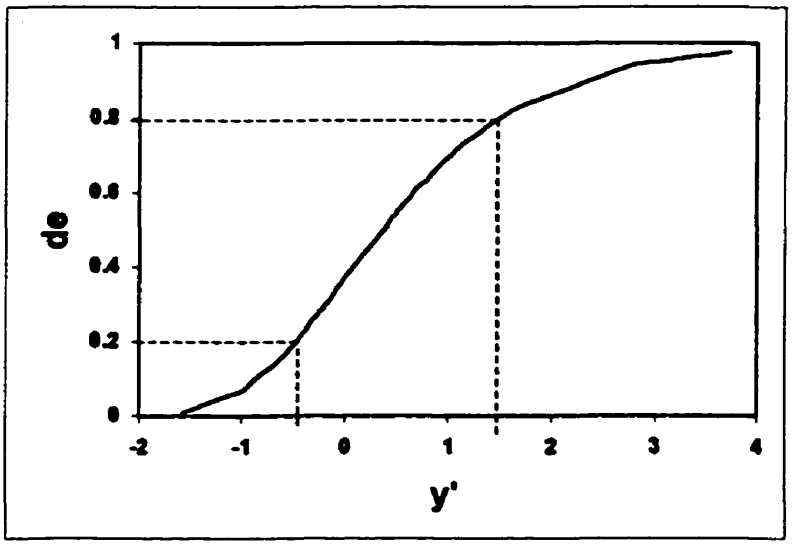

Figure 5.27 Desirability function, de, vs. transformed desirability value

Table 5.1 Ten best samples according to the statistical analysis

	Sample	Die Gap (mm)	Adapter Angle (°)	Temp. Profile (°C)	Screw Speed (rpm)	Feed Rate (rpm)
1	WC2-3070225	1.0	30	2	70	225
2	WH2-7070200	0.5	70	2	70	200
3	WH2-3070225	0.5	30	2	70	225
4	WC2-7060225	1.0	70	2	60	225
5	WC1-3060200	1.0	30	1	60	200
6	WH2-3060225	0.5	30	2	60	225
7	WH2-7070225	0.5	70	2	70	225
8	WH1-3060225	0.5	30	1	60	225
9	WC1-3060225	1.0	30	1	60	225
10	WC2-7060250	1.0	70	2	60	250

Table 5.1 shows the best ten out of sixty-four samples obtained from the statistical analysis. The ten best samples are listed in order to evaluate the effects of the design and processing variables on the properties discussed in earlier sections. The best sample is obtained at the feed rate of 225 rpm, the highest screw speed of 70 rpm, the die gap of 1 mm, the adapter angle of 30° and second temperature profile. Using these conditions an improvement of 52 times in toluene permeability, relative to polyethylene alone, is achieved. If not only the first sample but also the ten best samples are analyzed, it can be concluded that a feed rate of 225 rpm and temperature profile 2 are the best conditions to develop material with good properties. In the case of the adapter angle, 30° shows advantages over 70°. This was observed in the morphology and permeability results, where 30° appeared to produce better behavior. For the screw speed, 60 and 70 rpm appear to be equivalent. It is important to note that the first three samples refer to 70 rpm, while the others were mostly for 60 rpm screw speed. Finally, the die gap showed a competition between permeability and mechanical properties. The balance of both effects is obtained in the top ten samples listed, where no real preference is noted for these two

die gaps. An illustration of the procedure to obtain the desirability function for one sample, the complete list of the data obtained from the statistical analysis and the ranking for all the samples are shown in Appendix E.

6.0 CONCLUSIONS AND RECOMMEMDATIONS

6.1 Conclusions

1. For the first time, laminar morphology of HDPE/PA-6 blends was obtained and reported in the product of a co-rotating twin screw extruder (TSE).

2. Laminar morphology was observed in front of the screws of the TSE, with layers of dispersed phase distributed around the tips of the screws.

3. A large converging angle in the adapter can result in breakup and high orientation of the dispersed phase layers.

4. Using an appropriate combination of design and processing variables, it is possible to obtain many well-distributed layers across the thickness of the extruded ribbons.

5. Feed rate and temperature profile in the extruder are the most important variables for the development of laminar morphology in the product. Die gap, screw speed and adapter angle have moderate effects.

6. An improvement of up to 113 times on the toluene permeability of the polyethylene has been achieved in the twin screw extruder with a 17.3% vol. PA-6/polyethylene blend. This value is close to the values attainable with co-extruded materials (262 times), for the same system and composition, and it is 2.5 times better than the best value reported with the single screw extruder (45 times).

7. Impact properties are more sensitive than tensile properties to variations in processing conditions and morphology.

8. A HDPE/PA-6 blend obtained at 225-rpm feed rate, 70-rpm screw speed, 1mm-die gap, 30° adapter angle and the second temperature profile (higher temperature) yields an extrudate with good balance between permeability to hydrocarbons and mechanical properties.

6.2 Recommendations

1. Other blends systems and other die designs (i.e. annular) should be tested in a TSE for the development of laminar morphology blends.

2. A detailed theoretical study to understand the mixing mechanism and the development of laminar flow in the twin screw extruder should be valuable.

3. An on-line morphology characterization technique to evaluate and/or control the size and distribution of the disperse phase layers in the TSE would be of great value.

4. A combination of twin screw extrusion with blown film or blow molding machines is worthy of consideration for producing films or bottles with laminar morphology, thus good barrier properties.

REFERENCES

1. P. M. Subramanian and V. Mehra, Polym. Eng. Sci., 27 (9), 603 (1987)
2. L. A. Utracki, "Polymer Alloys and Blends", Hanser Verlag, New York (1989)
3. P. J. Flory. "Principles of Polymer Chemistry", Cornell University Press, Ithaca, NY (1953)
4. D. R. Paul, "Polymer Blends", Academic Press, Vol. 1 (1978)
5 P. M. Subramanian, "Process for Making Laminar Articles of Polyolefin and Condensation Polymer", US Patent No. 4,410,482, Oct 18, 1993
6 P. M. Subramanian, "Laminar Articles of Polyolefin and Condensation Polymer", US Patent No. 4,444,817. Apr. 24 1984
7 P. M Subramanian. Polym. Eng. Sci., 25 (8), 483 (1985)
8 G. W. Lohfink, Ph D. Thesis, Department of Chemical Engineering, McGill University (1989)
9 G. W. Lohfink and M. R. Kamal, Polym. Eng. Sci. 33 (21), 1404 (1993)
10 M. R. Kamal, H. Garmabi, S. Hozhabr and L. Arghyris, Polym. Eng. Sci., 35 (1), 41 (1995)
11 M. R. Kamal, H. Garmabi, S. Hozhabr and L. Arghyris. "Process for Laminar Extrussion". US. Patent No. 5,188,784. Feb 23 (1993)
12 S. Hozhabr, M. Eng. Thesis. Department of Chemical Engineering, McGill University (1991)
13 L. Arghyris, M. Eng. Thesis. Department of Chemical Engineering, McGill University (1991)
14 H. Garmabi and M. R. Kamal, SPE ANTEC Conference, 2687 (1997)
15 H. Garmabi, Ph. D. Thesis, Department of Chemical Engineering, McGill University (1997)
16 P. M. Lepoutre, M. Eng. Thesis, Department of Chemical Engineering, McGill University (1989)
17 Wu, Polym. Eng. Sci., 27, 335 (1987)
18 H. Van Oene, J. Colloid Interface Sci., 40, 448 (1972)

19 N. Demarquette, , Ph D. Thesis, Department of Chemical Engineering, McGill University (1993)

20 A. Luciani, M. F. Champagne and L. A. Utracki. J. of Polym Sci. Part B, 35 (9) 1393 (1997)

21 G. I. Taylor, Proc. Roy. Soc. A146, 501 (1935)

22 R.G. Cox, J. Fluid Mech. 37, 601 (1969)

23 S. Tomotika, Proc. R. Soc., A153, 302 (1936)

24 H. A. Stone, B. J. Bentley and L. G. Leal, J. Fluid Mech., 173, 131 (1986)

25 J. F. Palierne, Rheol, Acta, 29, 204 (1990)

26 I. Delaby, B. Ernest, D. Froelich and R. Muller, Rheol. Acta, 34, 525 (1995)

27 J. J. Elmendorp and A. K. Van de Vegt, Polym. Eng. Sci., 26, 1332 (1986)

28 D. Bourry, F. Godbille, R. E. Khayat, A. Luciani, J. Picot and L. A. Utracki, Polyblend Conference/ SPE RETEC, 314 (1997)

29 W. Bartok and S G. Mason, J. Colloid Sci., 14, 13 (1959)

30 R. S. Allen and S. G. Mason, J. Colloid Sci., 17 383 (1962)

31 L. A. Utracki and Z. H. Shi. Polym. Eng. Sci., 32 (24), 1824 (1992)

32 I. Fortelny and A. Zyvny, Polymer, 36, 4113 (1995)

33 K. Wallheinke, P. Pötschkle, C. Macosko, H. Stutz, Polyblends Conference / SPE RETEC, 509 (1997)

34 S. Lim and J. L. White, Polym. Eng. Sci., 33, 923 (1993)

35 D. K. Setua, S. Lim and J.L. White, Polym Eng. Sci., 26, 34 (1986)

36 S. Lim and J. L. White, Polym. Eng. Sci., 34 (3), 221 (1994)

37 Z. H. Shi and L. A. Utracki, Polym Eng. Sci, 32 (24), 1834 (1992)

38 J.W. Teh and Rudin. SPE Antec Conference, 1124 (1991)

39 L. Y. Yang, D. Bigio and T. G. Smith, SPE ANTEC Conference 2010 (1995)

40 C. Lacasse and B. Favis. Polyblends / SPE RETEC, 448 (1997)

41 S. Y. Lee and S. C. Kim, Polym. Eng. Sci., 37 (2), 463 (1997)

42 L. Delamare and B. Verges, Polym. Eng. Sci., 36(12), 1685 (1996)

43 C. E. Scott and C. W. Scott and C. W. Macosko, Polym. Bull, 26, 341 (1991)

44 U. Sundararaj and C. W. Macosko, Polym. Eng. Sci., 32, 1814 (1992)

45 T.P Vanio, A. Harlin and J.V. Sepala, Polym Eng. Sci, 35(13), 225 (1995)

46 J. T. Lindt and A. K. Ghosh, Polym. Eng. Sci.,32 (24), 1802 (1992)

47 L. Levitt, C. W. Macosko and S. D. Pearson. Polym. Eng. Sci., 36, 1647 (1996)

48 M. Getlichermann and C. David. Polymer 35, 2542 (1994)

49 A. Y. Polishchuck and G. E. Zaikov. "Multicomponent Transport in Polymer Systems for Controlled Release". Gordon and Breach Science Publishers. The Netherlands (1997)

50 W. J. Koros. "Barrier Polymer and Structures". ACS Symposium Series 423, Texas (1989)

51 Y. Thakore, "Barrier and Selective Barrier Plastic Based Material and Structures for Packaging". Business Comunications Company Inc., Norwalk CT (1994)

52 M.R. Kamal, I. Jinnah and L.A. Utracki, Polym Eng. Sci, 24, 1337 (1984)

53 L. A. Utracki, P. Toma, Polym Eng. Sci., 26 (1), 34 (1968)

54 N. Walling, M. Eng. Thesis. Department of Chemical Engineering, McGill University (1991)

55 N. Walling and M. R. Kamal. Advances in Polymer Technology, 5 (4), 269 (1996)

56 Y. G. Lee, M. S. Lee and Y. G. Cho. "Polyolefin Base Blend Containing Reactive Low Molecular Weight Compound and Process for Making the Same". European Patent No. EP 0 526 230 B. Oct 16, 1996

57 S. Y. Lee and S. C. Kim, International Polymer Processing, 11 (3), 238 (1996)

58 J. Comyn. Polym. Permeability, Ch. 1 Elsevier Applied Science Publisher, London (1985)

59 J. C. Maxwell. "Electricity and Magnetism" Vol. 1, Dover. New York (1940)

60 L. E. Nielson. J. Macromol. Sci. (Chem), A1(5), 929 (1967)

61 L. M. Roberson, A. Noshay and M. Matzner, Makromol. Chem. 29 (30), 47 (1973)

62 E.L. Cusler, S.E. Hughes, W.J. Ward and R. Aris, J. Memb Sci, 36, 161 (1988)

63 J. L. White. "Twin Screw Extrusion. Techology and Principles". Hanser Publishers, New York (1991)

64 M. J. Stevens and J. A. Covas. "Extruder Principles and Operation". Chapman and Hall, London (1995)

65 Rauweendaal. "Polymer Extrusion" Hanser Publishers, New York (1986)

66 M. A. Huneault, M F. Champagne, L. E. Daigneault and M. M. Dumoulin. SPE ANTEC Conference, 2020 (1995)

67 C. Maier, M. Lambla and K. Ilham, SPE ANTEC Conference, 2015 (1995)

68 V. Bordereau, Z. H. Shi, L. A Utracki, P. Sammut and M. Carreaga. Polym. Eng. Sci., 32 (24), 1846 (1992)

69 I. Manas-Zloczower and Z. Tadmor. Mixing and Compounding of Polymers. Theory and Practice, Ch-4. Hanser Publishers. New York (1994)

70 A. Lawal and D. Jaylon. Polym. Eng. Sci, 35 (17), 1325 (1995)

71 J.M. Ottino, The kinematics of mixing: stretching, Chaos and Transport, Cambridge Univ. Press. Cambridge UK (1989)

72 C. Rauwendaal. Mixing in Polymer Processing. Marcel Dekker Inc.. New York (1991)

73 H. Aref., J, Fluid Mech, 143, 1 (1984)

74 F. Raynal and J.N. Gence. Chem. Eng. Sci., 50(4), 631 (1995)

75 E.C. Harrington Jr. Ind. Quality Control, 109(21), 494 (1965)

76 Z. Tadmor and C. Gogos, "Principles of Polymer Processing". Wiley-Interscience Publication. New York (1979)

APPENDIX A

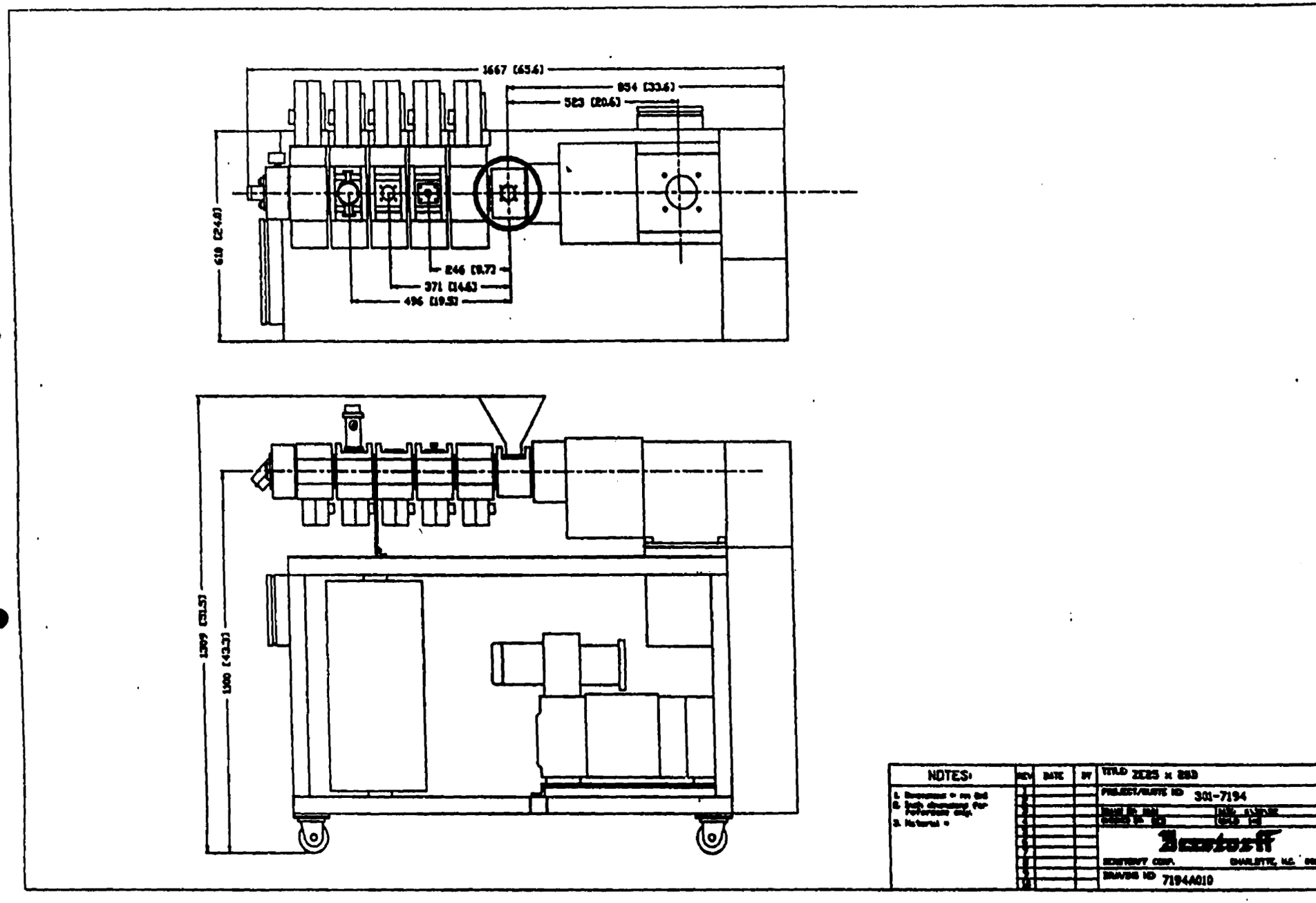

Twin Screw Extruder

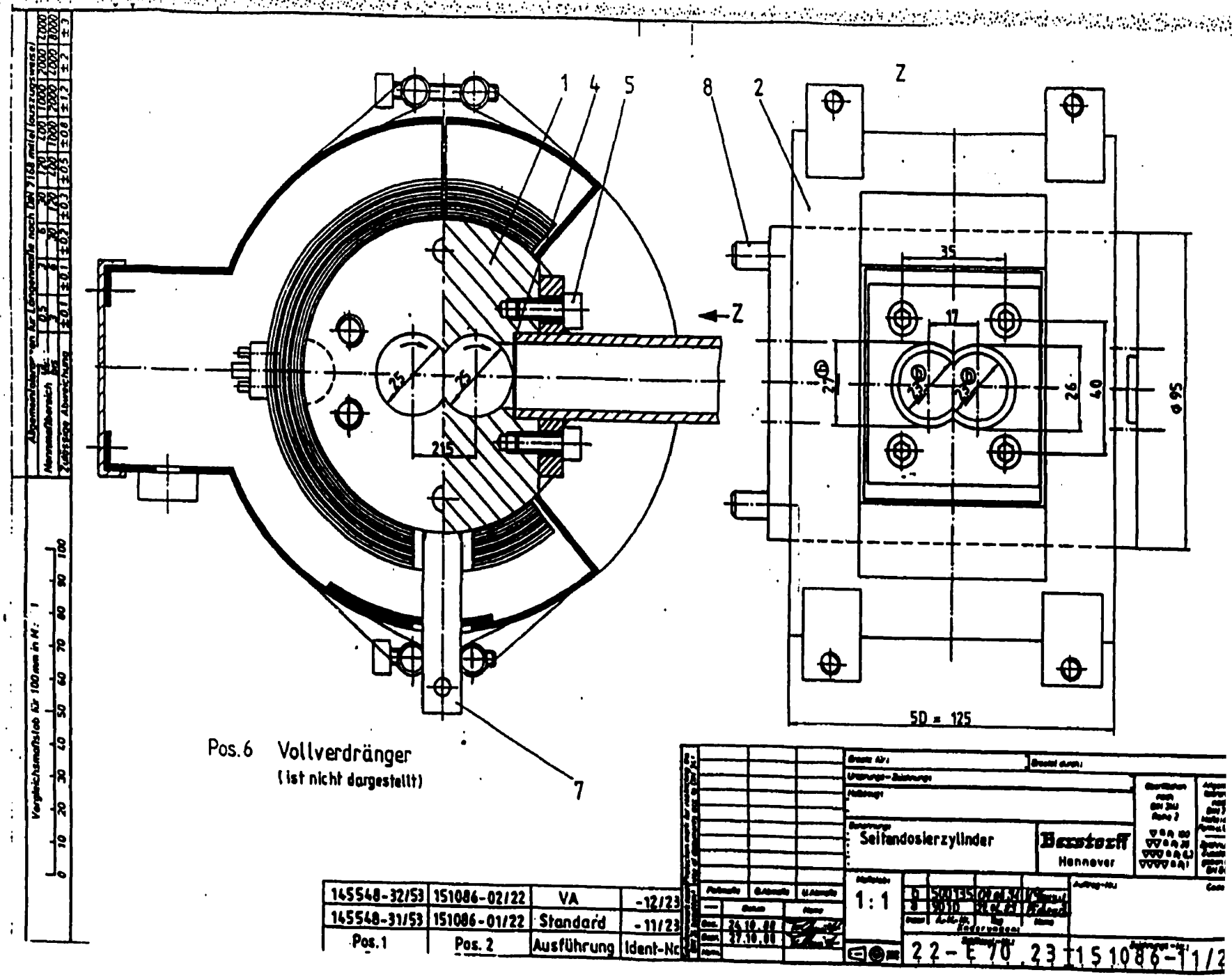

Last Zone of Twin Screw Extruder

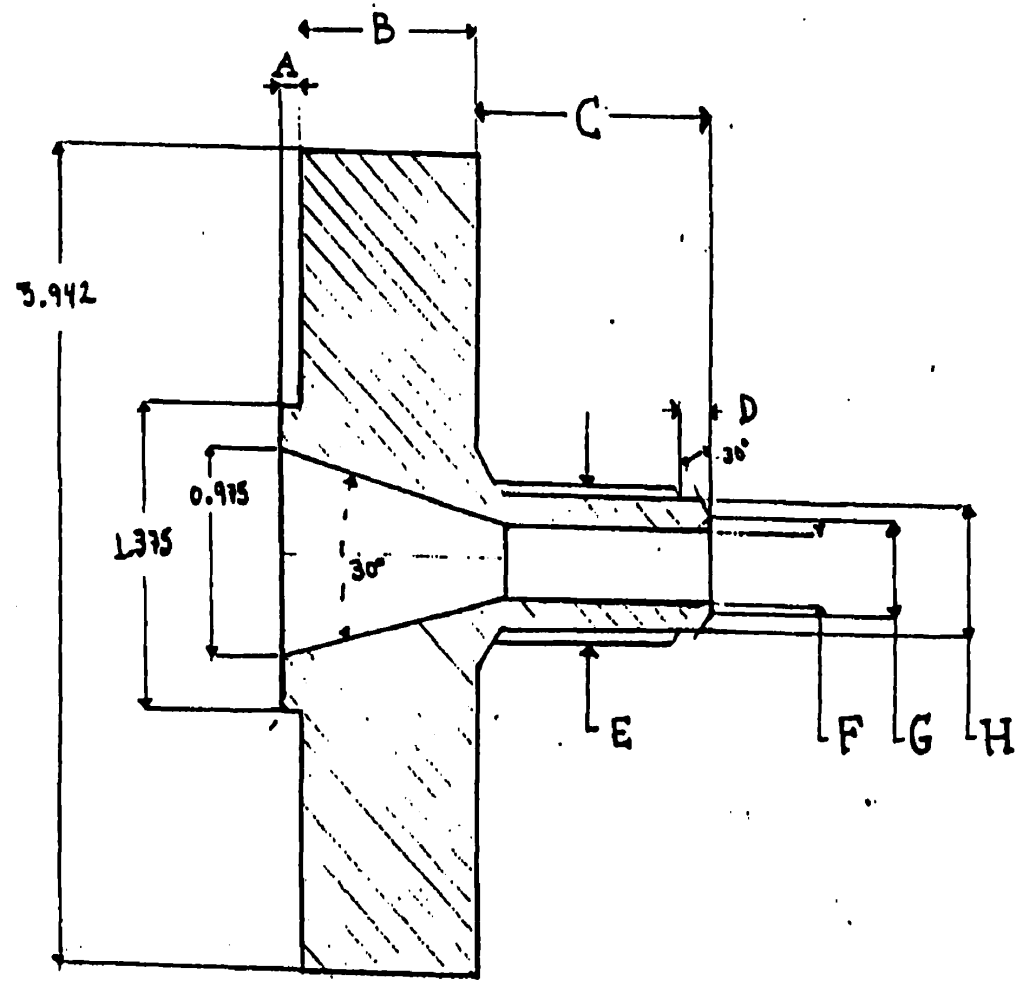

	inch
A	0.197
B	0.915
C	1 1/4
D	3/16
E	3/4-16
F	0.375
G	7/16
H	5/8

Adapter Schematic with dimensions

Rodrigo Vela

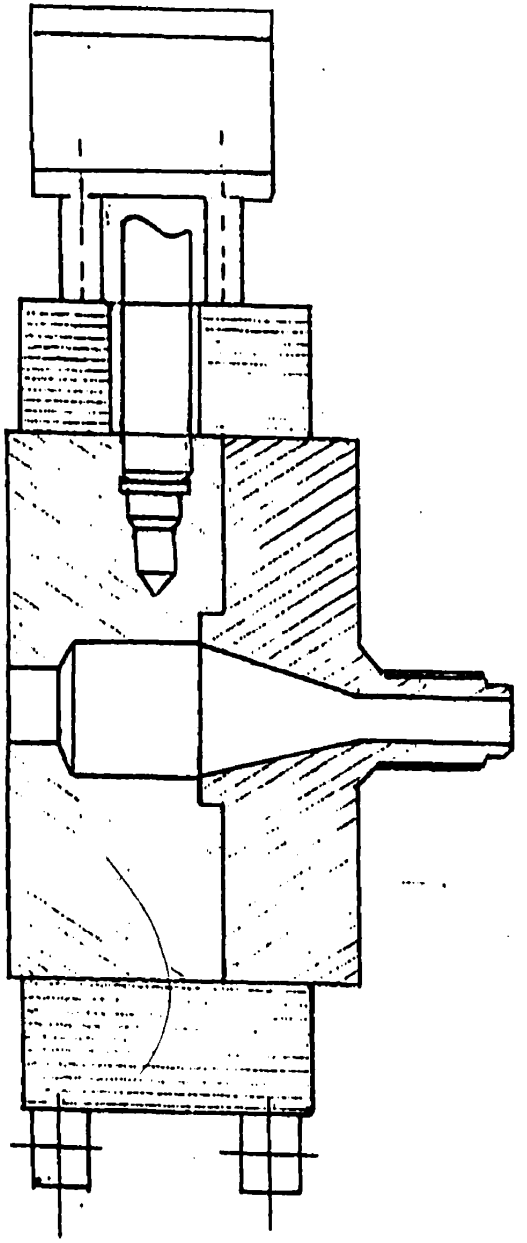

Adapter with last zone of
Twin Screw Extruder

Rudiger Klee

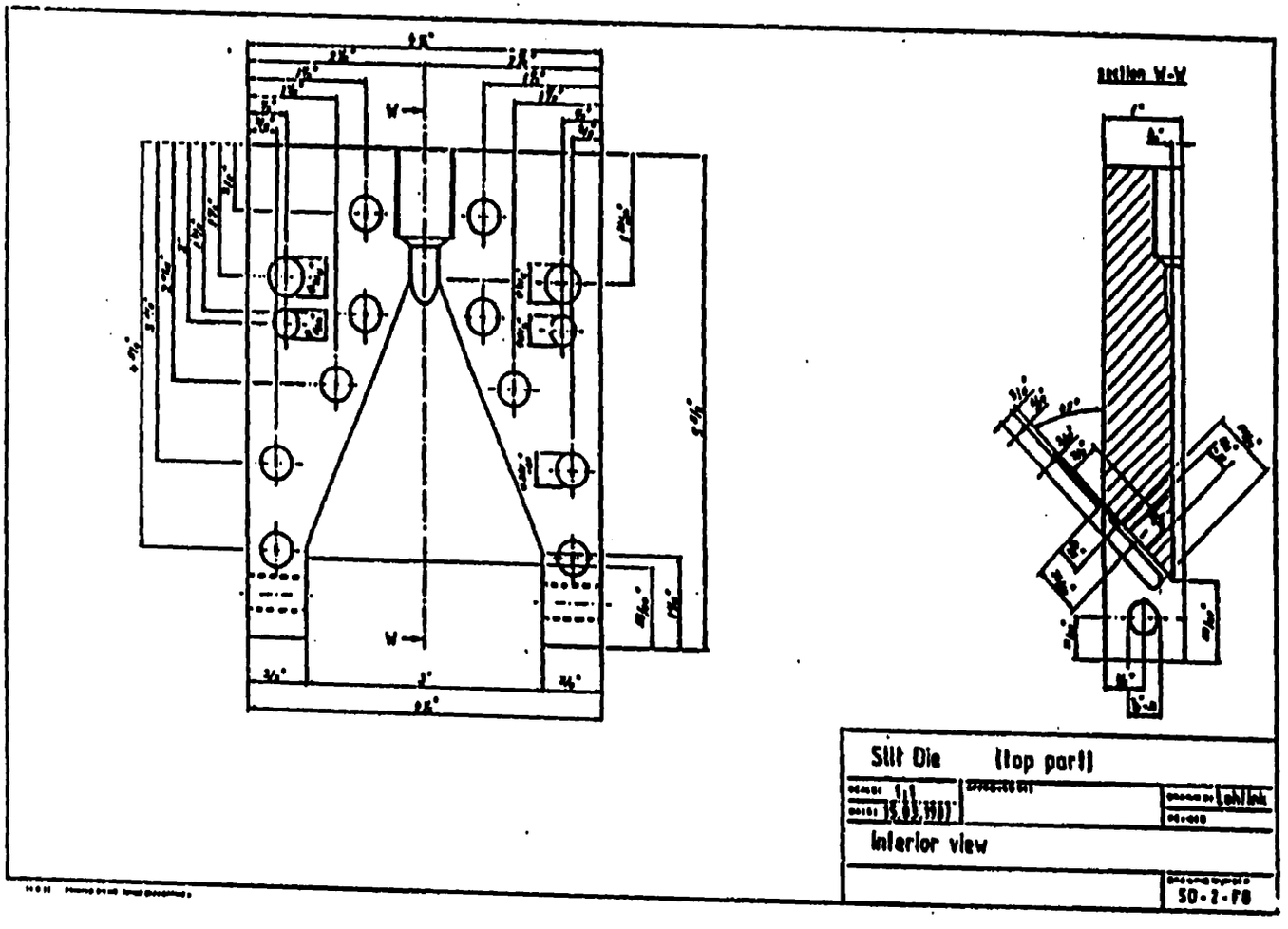

Top view of Slit Die

APPENDIX B

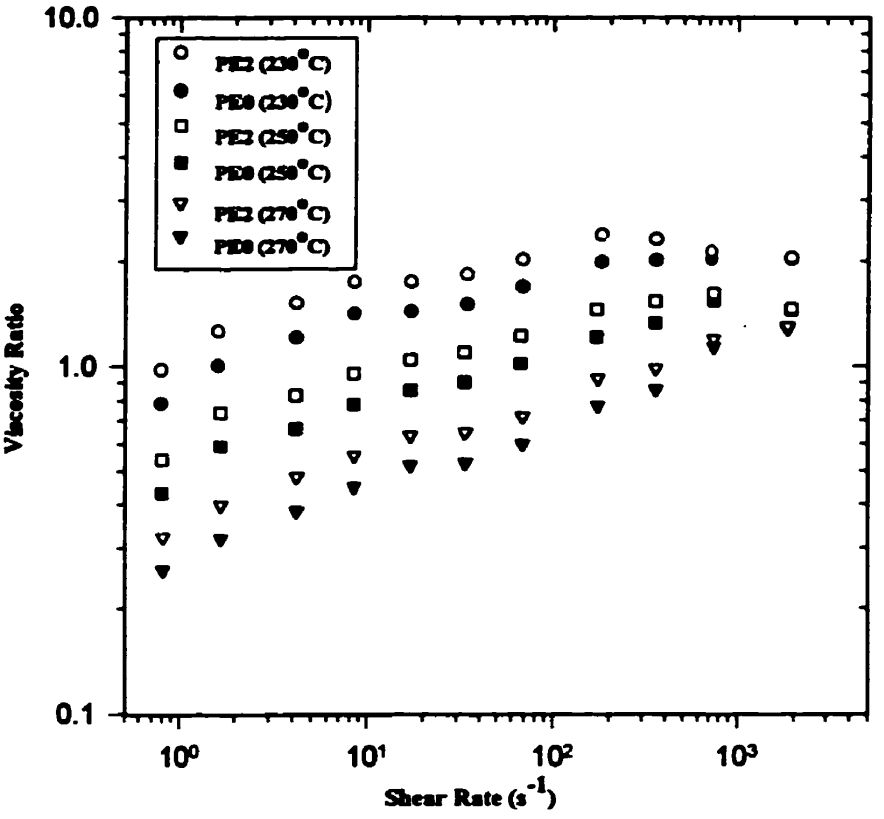

Viscosity Ratio Curve for Nylon-6 and HDPE (PE0); and MaPE (PE2) at different temperatures [15]

Shear rate estimation in the adapter

The shear rate estimation was made at the entrance and the end of the converging zone in the adapter.

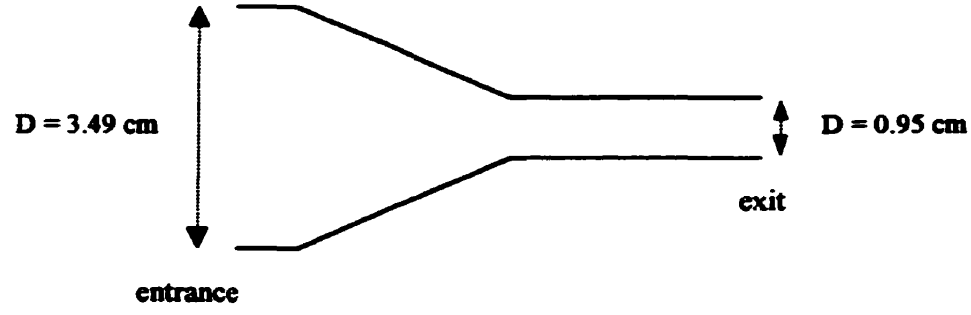

The shear rate was calculated according to the capillary flow equation considering a power law fluid (equation B.1) [76]. The specific volume of resins, for the flow rate estimation, were calculated using Tait (equations B.2 to B.4) and Spencer-Gilmore (equation B.5) state equations at the pressure of 110.31 bar and the temperature of 250 °C.

$$\gamma^{\bullet}_{w} = \left(\frac{3n+1}{4n}\right)\left(\frac{4Q}{\pi R^3}\right) \qquad \textbf{(B.1)}$$

$$V(T,P) = V(0,T) \times [1 - C \ln (1 + P/(B(T))] \qquad \textbf{(B.2)}$$

where,

$$B(T) = B_o \exp [-B_1 T] \qquad \textbf{(B.3)}$$

and

$$V(0,T) = Ao + A_1 T + A_2 T^2 \qquad \textbf{(B.4)}$$

$$(P + \Pi)(V - \omega) = R\,T/M \qquad \text{(B.5)}$$

where n is the power law parameter, Q is the flow rate in cm^3/s, R is the radius of the tubular zone in cm, P is the pressure in bars for Tait equation and in Mpa in Spencer-Gilmore equation, T is the temperature in °C for Tait equation and °K in Spencer-Gilmore equation, R is the universal gas constant in cm^3 bar mol^{-1} K^{-1}, B_o, B_1, A_o, A_1, A_2 and C are the parameters for Tait equation, and Π, ω and M are those for Spencer-Gilmore equation.

The power law and Tait and Spencer-Gilmore parameters and the calculated specific volumes for each resin are listed in Table B.1.

Table B.1. Power law, Tait and Spencer-Gilmore parameters for HDPE, MAPE and PA-6 [15]

	HDPE	MAPE	PA-6
n	0.51	0.53	0.69
$B_o \times 10^{-2}$	2.078	2.030	--
$B_1 \times 10^{3}$	5.387	5.290	--
A_o	1.157	1.170	--
$A_1 \times 10^{3}$	0.6855	0.5129	--
$A_2 \times 10^{6}$	0.76814	1.2650	--
C	0.08916	0.08940	--
Π	--	--	4585
ω	--	--	0.7893
M	--	--	33.5
V (cm^3/g)	1.3117	1.2819	1.066

For the estimation of the specific volume of the blend the additive rule was used then, a calculated value of 1.2595 cm^3/g was obtained. The shear rate at the entrance and exit of the adapter was calculated for the four mass flow rates (feed rates) used in this research. The results are presented in Table B.2

Table B.2 Estimated shear rate (s^{-1}) for each resin at the entrance and exit of the adapter

		Entrance			Exit		
	Flow Rate						
	(cm^3/s)	HDPE	MAPE	PA-6	HDPE	MAPE	PA-6
175 rpm	1.2872	0.3817	0.3760	0.3423	18.8106	18.5301	16.8711
200 rpm	1.4724	0.4366	0.4301	0.3916	21.5171	21.1962	19.2985
225 rpm	1.6512	0.4896	0.4823	0.4391	24.1300	23.7701	21.6419
250 rpm	1.8338	0.5437	0.5356	0.4877	26.7985	26.3987	24.0352

The shear rate at the entrance of the adapter ranges from 0.34 to 0.54 s^{-1} and at the end of the converging zone goes from 16.87 to 26.79 s^{-1}.

APPENDIX C

The name of the samples is associated to its processing conditions thus,

W = any letter
C = complete die gap (1 mm) or
H = half die gap (0.5 mm)
1 = first temperature profile or
2 = second temperature profile

After the hyphen, the two first digits correspond to the adapter angle, the following two digits are the screw speed and the last three digits give the feed rate used in the experiment. An example is given below.

WC1-7060175 = it means that this sample was produced under the following conditions: 1 mm die gap (C), temperature profile 1, 70° adapter angle, screw speed of 60 rpm and feed rate of 175 rpm.

Table C.1 Measured properties of twin screw extruded HDPE/PA-6 blends.

	TOLUENE	IMPACT PROPERTIES		TENSILE PROPERTIES	
	PERMEABILITY	Force	Energy	Tensile Strength	Elastic Modulus
	(mg.mm/min.m2)	(N/mm)	(J/mm)	(MPa)	(MPa)
PA-6	0.0162	1128	7.12	67.43	1017
HDPE	24.9300	461	2.79	25.91	709
WC1-7060175	2.0202	422	1.46	26.75	728
WC1-7060200	1.4445	346	0.78	27.40	742
WC1-7060225	0.3824	413	1.24	29.54	586
WC1-7060250	0.4109	358	0.84	30.76	614

Table C.1 Measured properties of twin screw extruded HDPE/PA-6 blends (continued)

	TOLUENE	IMPACT PROPERTIES		TENSILE PROPERTIES	
	PERMEABILITY	Force	Energy	Tensile Strength	Elastic Modulus
	(mg.mm/min.m2)	(N/mm)	(J/mm)	(MPa)	(MPa)
WC2-7060175	5.9566	344	1.03	30.00	765
WC2-7060200	3.7282	348	1.09	29.70	691
WC2-7060225	0.6037	384	1.29	29.37	768
WC2-7060250	0.6449	378	1.16	29.13	703
WC2-7050175	5.3725	357	1.16	24.91	695
WC2-7050200	5.3476	332	0.97	26.90	653
WC2-7050225	3.3103	387	1.37	27.15	652
WC2-7050250	3.3733	366	1.18	28.35	579
WC2-7070175	4.3912	331	1.08	27.58	724
WC2-7070200	1.5949	324	0.87	30.27	703
WC2-7070225	0.6539	317	0.79	29.77	651
WC2-7070250	0.8854	389	1.03	28.51	668
WC1-3060175		550	2.01	27.47	640
WC1-3060200	1.6067	535	1.96	30.24	625
WC1-3060225	0.2157	482	1.28	27.36	617
WC1-3060250		543	1.59	26.69	647

Table C.1 Measured properties of twin screw extruded HDPE/PA-6 blends (continued)

	TOLUENE	IMPACT PROPERTIES		TENSILE PROPERTIES	
	PERMEABILITY	Force	Energy	Tensile Strength	Elastic Modulus
	(mg.mm/min.m2)	(N/mm)	(J/mm)	(MPa)	(MPa)
WC2-3060175		328	0.96	26.73	678
WC2-3060200	2.5379	334	0.86	26.44	672
WC2-3060225	1.2900	342	1.11	27.68	680
WC2-3060250		555	1.71	26.73	633
WC2-3050175		347	1.17	27.70	708
WC2-3050200	1.8355	370	1.14	27.73	657
WC2-3050225	0.4309	356	1.07	27.96	719
WC2-3050250		508	1.59	31.22	556
WC2-3070175		222	0.83	27.73	718
WC2-3070200	1.2672	369	1.07	30.23	711
WC2-3070225	0.4603	556	1.99	27.40	656
WC2-3070250		521	1.65	30.02	621
WH1-7060175		414	1.53	27.43	679
WH1-7060200	1.9579	422	1.38	27.04	659
WH1-7060225	1.4123	386	1.05	26.78	643
WH1-7060250		405	1.18	29.19	694
WH2-7060175		487	2.34	25.86	690
WH2-7060200	4.2189	442	1.94	27.98	684
WH2-7060225	1.3328	430	1.62	29.12	572
WH2-7060250		381	1.15	27.62	633

Table C.1 Measured properties of twin screw extruded HDPE/PA-6 blends (continued)

	TOLUENE	IMPACT PROPERTIES		TENSILE PROPERTIES	
	PERMEABILITY	Force	Energy	Tensile Strength	Elastic Modulus
	(mg.mm/min.m2)	(N/mm)	(J/mm)	(MPa)	(MPa)
WH2-7050175		478	2.29	27.91	714
WH2-7050200	3.3552	442	1.80	27.84	648
WH2-7050225	1.3722	413	1.07	27.98	632
WH2-7050250		407	1.40	25.89	641
WH2-7070175		480	2.35	28.75	672
WH2-7070200	1.2822	457	2.02	29.62	711
WH2-7070225	1.3400	408	1.46	27.30	670
WH2-7070250		420	1.46	31.20	746
WH1-3060175		470	2.21	28.60	649
WH1-3060200	4.2688	431	1.56	27.58	684
WH1-3060225	1.5800	417	1.66	28.63	622
WH1-3060250		378	1.21	29.87	651
WH2-3060175		443	2.14	27.09	665
WH2-3060200	5.9910	399	1.64	29.78	712
WH2-3060225	1.1990	408	1.55	28.88	631
WH2-3060250		419	1.48	27.66	687

Table C.1 Measured properties of twin screw extruded HDPE/PA-6 blends (continued)

	TOLUENE	IMPACT PROPERTIES		TENSILE PROPERTIES	
	PERMEABILITY	Force	Energy	Tensile Strength	Elastic Modulus
	(mg.mm/min.m2)	(N/mm)	(J/mm)	(MPa)	(MPa)
WH2-3050175		424	1.77	26.90	725
WH2-3050200	5.0579	423	1.71	25.84	699
WH2-3050225	3.0344	396	1.47	29.88	642
WH2-3050250		377	1.16	28.01	639
WH2-3070175		435	1.83	29.00	720
WH2-3070200	1.9194	404	1.47	27.16	688
WH2-3070225	0.5652	415	1.45	25.90	763
WH2-3070250		389	1.23	28.39	716

Table C.2 Properties and processing conditions of single screw extruded HDPE/PA-6 blends [15]

	PERMEABILITY (mg.mm/ min.m2)	FORCE (N/mm)	ENERGY (J/mm)	SCREW DESIGN	DIE GAP (mm)	TEMPERATURE PROFILE	SCREW SPEED (rpm)	ADAPTER ANGLE (°)	COMPOSITION (PE0/PE1/PE2/PA-6 wt%)
X143723	22.40			Mixing	1	3	30	70	0/0/70/30
X143713	17.33			Mixing	1	3	30	70	0/70/0/30
T543312	9.74			Metering	0.5	3	30	30	0/80/0/20
X143712	20.30	422.1	2.08	Mixing	1	3	30	70	0/80/0/20
X143312	21.20	382.5	1.85	Mixing	1	3	30	30	0/80/0/20
X1437PE0	20.54			Mixing	1	3	30	70	100/0/0/0
X1437042	18.50	393.0	1.90	Mixing	1	3	30	70	40/0/40/20
X1537022	0.55	420.8	1.70	Mixing	1	5	30	70	60/0/20/20
X1037022	16.03			Mixing	1	4	30	70	60/0/20/20
X5337022	17.20	468.0	2.10	Mixing	0.5	2	30	70	60/0/20/20
X1437022	19.30	402.0	1.80	Mixing	1	3	30	70	60/0/20/20
T1333022	23.80	397.0	1.52	Metering	1	2	30	30	60/0/20/20
X153703	1.39			Mixing	1	5	30	70	70/0/0/30
T133303	3.97			Metering	1	2	30	30	70/0/0/30
X143703	5.44			Mixing	1	3	30	70	70/0/0/30
X133703	5.53			Mixing	1	2	30	70	70/0/0/30
T533303	6.64			Metering	0.5	2	30	30	70/0/030
X1537012	0.87	424.0	1.20	Mixing	1	5	30	70	70/0/10/20
X151TB12	3.07	364.0	1.00	Mixing	1	5	30	70	70/0/10/20
X1037012	3.50	360.0	0.73	Mixing	1	4	30	70	70/0/10/20
X151T012	11.10	317.2	0.80	Mixing	1	5	30	70	70/0/10/20
T1333012	12.02	372.3	1.40	Metering	1	2	30	30	70/0/10/20
X1337012	15.98	368.3	1.24	Mixing	1	2	30	70	70/0/10/20
X5337012	16.26			Mixing	0.5	2	30	70	70/0/10/20

Table C.2 Properties and processing conditions of single screw extruded HDPE/PA-6 blends (continued).

	PERMEABILITY (mg.mm/ min.m2)	FORCE (N/mm)	ENERGY (J/mm)	SCREW DESIGN	DIE GAP (mm)	TEMPERATURE PROFILE	SCREW SPEED (rpm)	ADAPTER ANGLE (°)	COMPOSITION (PE0/PE1/PE2/PA-6 wt%)
X1537052	1.44	323.0	0.65	Mixing	1	5	30	70	75/0/5/20
T1333052	7.18			Metering	1	2	30	30	75/0/5/20
T5333052	13.05			Metering	0.5	2	30	30	75/0/5/20
X1337052	19.81	271.8	0.51	Mixing	0.5	2	30	70	75/0/5/20
X5337052	20.10			Mixing	0.5	2	30	70	75/0/5/20
X1537011	5.42	351.8	1.00	Mixing	1	5	30	70	77.2/0/12.8/10
T1333032	9.31			Metering	1	2	30	30	77.5/0/2.5/20
X133702	4.52	131.3	0.23	Mixing	1	2	30	70	80/0/0/20
X143302	5.56	165.6	0.35	Mixing	1	3	30	70	80/0/0/20
T133302	9.17	135.2	0.26	Metering	1	2	30	30	80/0/0/20
X146702	9.48	153.0	0.28	Mixing	1	3	60	70	80/0/0/20
T543302	9.94			Metering	0.5	3	30	30	80/0/0/20
T533302	10.04			Metering	0.5	2	30	30	80/0/0/20
T143302	11.04	154.3	0.30	Metering	1	3	30	30	80/0/0/20
X153702	11.73	131.2	0.24	Mixing	1	5	30	70	80/0/0/20
X533702	24.40			Mixing	0.5	2	30	70	80/0/0/20
X153701	7.23			Mixing	1	5	30	70	90/0/0/10
X143701	15.47			Mixing	1	3	30	70	90/0/0/10
X133701	17.00			Mixing	1	2	30	30	90/0/0/10
T133301	11.19		1.17	Metering	1	2	30	30	90/0/010

The temperature profile considers four zones in the single screw extruder and the slit die so,

Temperature profile # 2 : 220, 230, 240, 250 Die = 250° C
Temperature profile # 3 : 220, 240, 260, 270 Die = 270° C
Temperature profile # 4: 190, 200, 210, 230 Die = 250° C
Temperature profile # 5: 180, 190, 200, 225 Die = 250° C

Table C.3 Impact slope and displacement for twin screw extruded HDPE/PA-6 blends

	IIMPACT SLOPE		IMPACT DISTANCE	
	(N/mm)	% dev	(mm)	% dev.
PA-6	165.3	6.81	9.70	7.42
HDPE	46.9	4.67	8.66	3.60
WC1-7060175	79.3	2.81	7.11	8.64
WC1-7060200	88.4	2.72	5.89	5.88
WC1-7060225	105.3	6.10	7.16	6.17
WC1-7060250	106.3	5.69	5.79	7.61
WC2-7060175	73.2	5.32	6.60	9.87
WC2-7060200	79.9	7.94	6.68	5.41
WC2-7060225	82.5	4.37	7.62	5.39
WC2-7060250	85.1	5.30	7.16	6.08
WC2-7050175	69.9	8.02	7.42	3.84
WC2-7050200	82.8	2.80	6.50	9.32
WC2-7050225	88.6	4.91	7.42	7.41
WC2-7050250	92.6	5.38	7.44	6.49
WC2-7070175	68.3	4.05	6.91	6.25
WC2-7070200	79.9	3.34	6.45	8.63
WC2-7070225	80.0	3.92	6.53	4.84
WC2-7070250	91.8	7.29	6.93	5.48
WC1-3060175	87.2	5.78	7.34	5.42
WC1-3060200	93.0	3.98	7.52	5.01
WC1-3060225	100.2	5.80	6.32	6.71
WC1-3060250	125.2	3.65	7.14	6.22
WC2-3060175	61.8	6.32	6.17	5.99
WC2-3060200	63.6	4.95	6.12	6.93
WC2-3060225	73.4	8.47	7.04	13.29
WC2-3060250	118.6	7.04	7.21	6.36
WC2-3050175	65.7	4.66	7.19	5.05
WC2-3050200	76.9	7.68	6.78	4.70
WC2-3050225	85.8	3.89	7.19	3.15
WC2-3050250	120.1	5.35	7.32	6.93
WC2-3070175	80.7	14.27	7.87	22.66

	IMPACT SLOPE		IMPACT DISTANCE	
	(N/mm)	% dev	(mm)	% dev.
WC2-3070200	98.4	8.52	7.04	10.06
WC2-3070225	104.6	7.91	7.65	6.44
WC2-3070250	113.7	6.35	7.16	10.15
WH1-7060175	48.5	5.87	6.38	7.22
WH1-7060200	56.2	5.89	6.27	7.62
WH1-7060225	62.7	6.42	6.17	7.54
WH1-7060250	68.1	7.58	6.55	7.73
WH2-7060175	43.8	7.71	6.96	5.20
WH2-7060200	48.3	5.29	6.93	2.93
WH2-7060225	61.8	4.01	7.24	3.84
WH2-7060250	64.1	5.01	6.65	6.41
WH2-7050175	44.7	8.08	7.14	2.02
WH2-7050200	50.8	4.23	7.09	3.83
WH2-7050225	54.8	4.63	7.16	2.66
WH2-7050250	60.8	3.48	6.88	5.64
WH2-7070175	45.4	5.65	7.21	1.51
WH2-7070200	53.1	4.21	7.42	4.30
WH2-7070225	56.9	7.59	7.11	4.20
WH2-7070250	62.9	6.56	6.99	5.75
WH1-3060175	46.4	8.41	6.93	9.55
WH1-3060200	53.4	10.06	6.83	5.84
WH1-3060225	58.7	9.71	7.54	6.49
WH1-3060250	63.9	5.72	6.88	5.13
WH2-3060175	46.2	3.82	7.54	4.10
WH2-3060200	49.6	7.02	7.14	2.67
WH2-3060225	60.6	5.38	7.39	5.40
WH2-3060250	59.5	3.01	6.78	5.63
WH2-3050175	47.1	8.55	6.91	3.56
WH2-3050200	51.1	5.70	7.39	5.85
WH2-3050225	55.9	3.42	6.99	3.65
WH2-3050250	62.7	5.36	6.65	6.38
WH2-3070175	47.5	6.75	6.96	3.29
WH2-3070200	53.6	3.94	6.83	3.29
WH2-3070225	58.1	5.19	6.88	5.70
WH2-3070250	60.2	4.97	6.65	4.55

APPENDIX D

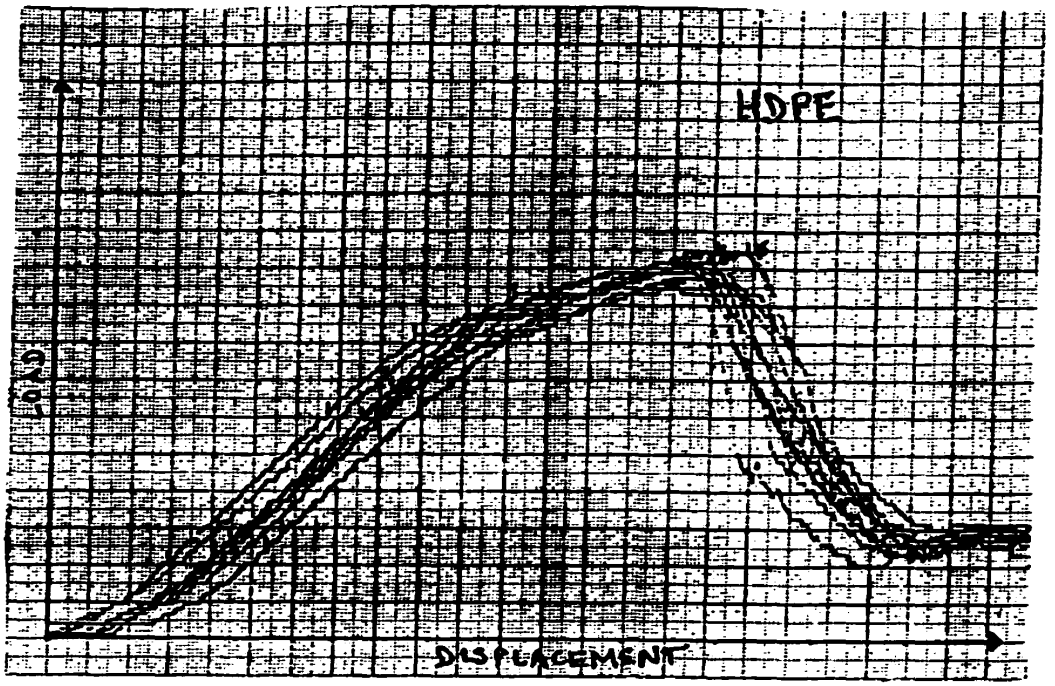

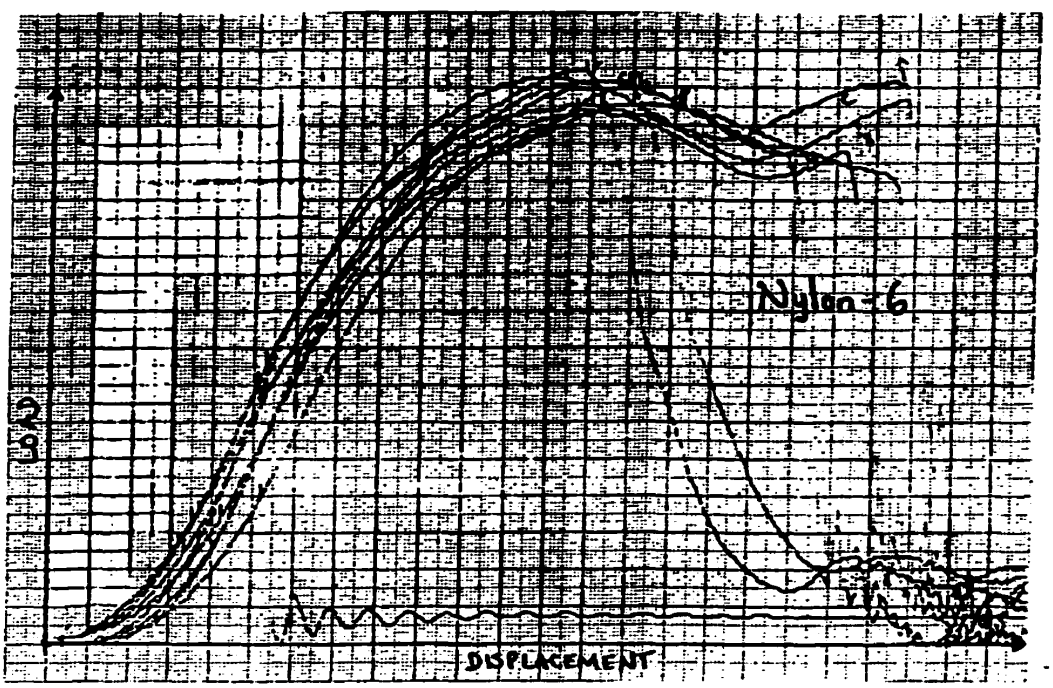

Impact Load-Displacement Curves of HDPE and Nylon-6

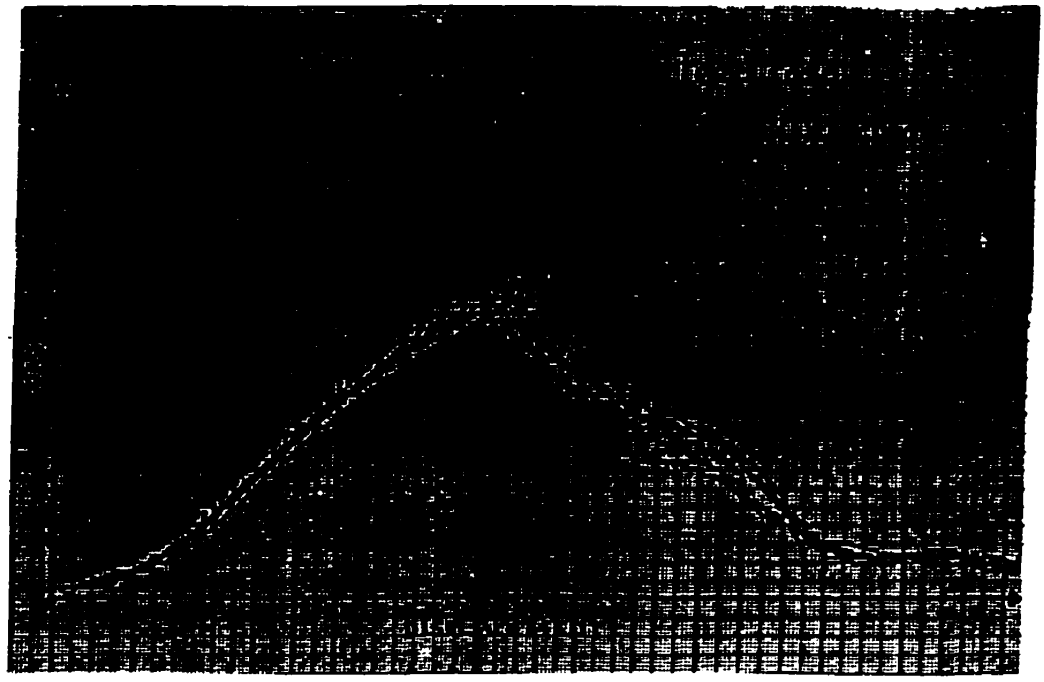

Impact Load-Displacement Curves of HDPE/Nylon-6 Blend
175 rpm and 200 rpm

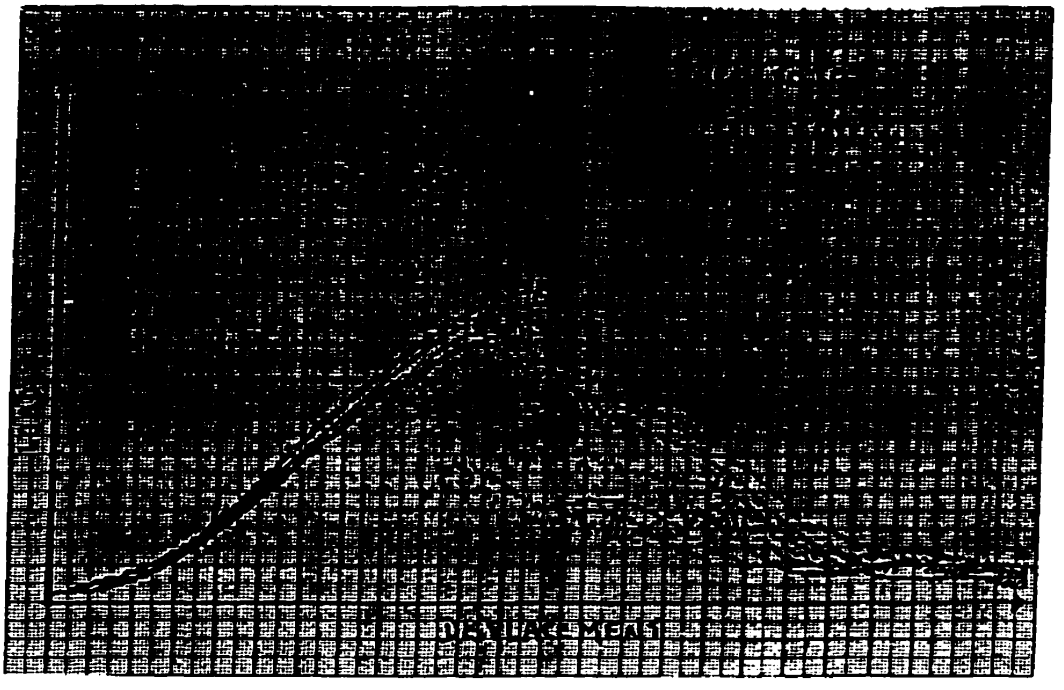

Impact Load-Displacement Curves:
225 rpm and 250 rpm

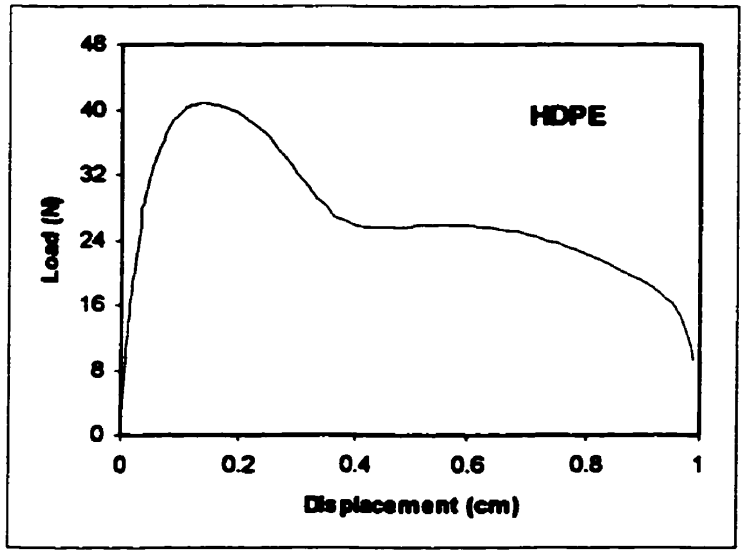

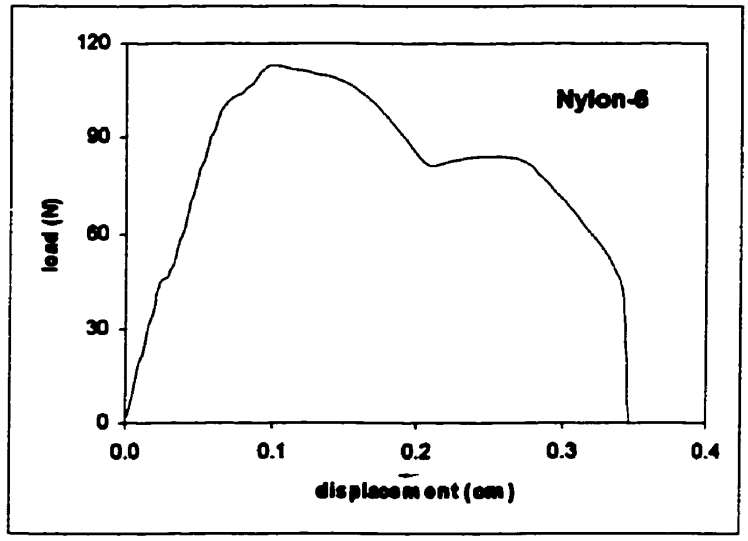

Tensile Load-Displacement Curves of HDPE and Nylon-6

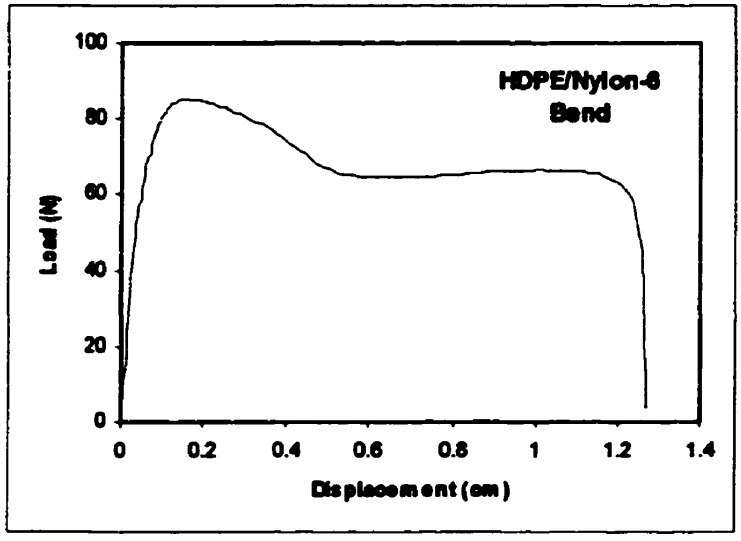

Typical Tensile Load-Displacement Curves of HDPE/Nylon-6 Blend

APPENDIX E

An example and the steps concerning the calculation of the desirability function are given below:

The property to analyze in this case will be the permeability. Values between zero, for the worst sample (WH2-3060200), and one, for the best impermeability (WC1-3060225), are assigned. Based on these limits, the desired values, *de*, for the rest of the samples are calculated (see Table E.1).

Using equation 5.3, the transformed data (y') are calculated for all the samples. As an example, the first sample from the Table E.1, WC1-7060175, will be considered to follow the procedure. So,

$$y'_{WC1\text{-}7060175} = -\ln [-\ln (0.6875)] = 0.9818$$

In order to calculate the parameters, b_1 and b_2, of equation 5.4, a desired value low limit, *de*, near to 0.2 and a high limit near to 0.8 are chosen. This is done to avoid errors for choosing boundaries near zero or one. For permeability, samples WH2-3050200 (0.1616) and WH2-7070225 (0.8053) have the nearest values to those required. Substituting these values in equation 5.4, we have:

For WH2-3050200: $-0.6004 = b_1 + b_2 (5.0579)$

For WH2-7070225 $1.5301 = b_1 + b_2 (1.3400)$

where,

samples	Permeability	de	y'	D
WH2-7070225	1.3400	0.8053	1.5301	0.7535
WH2-3050200	5.0579	0.1616	-0.6004	0.1616

Solving the equations simultaneously, we have that $b_1 = 2.2980$ and $b_2 = -0.5730$. Using equation 5.5 and these constants, the value a desirability function for sample WC1-7060175 is calculated as follows:

$$d_{WC1\text{-}7060175} = \exp \{ -\exp [-(2.2980 - 0.5730 * 2.0202)]\} = 0.7264$$

The desirability values for the rest of the samples are calculated in the same way, using the b_1 and b_2 calculated here. All the desirability values are standardized, taking the highest value for the specific property as one and adjusting the rest. The same procedure is applied for the impact energy and tensile modulus. Finally, equation 5.6 is applied to calculate the final and standardized desirability function, D-std.

Table E.1 Permeability and desirability values of twin screw extruded HDPE/PA-6 blends

Samples	permeability	de	y'	d
WC1-7060175	2.0202	0.6875	0.9818	0.7264
WC1-7060200	1.4445	0.7872	1.4303	0.7946
WC1-7060225	0.3824	0.9711	3.5305	0.8824
WC1-7060250	0.4109	0.9662	3.3702	0.8806
WC2-7060175	5.9566	0.0060	-1.6338	0.0474
WC2-7060200	3.7282	0.3918	0.0651	0.4271
WC2-7060225	0.6037	0.9328	2.6658	0.8676
WC2-7060250	0.6449	0.9257	2.5611	0.8647
WC2-7070175	4.3912	0.2770	-0.2498	0.2883
WC2-7070200	1.5949	0.7612	1.2988	0.7784
WC2-7070225	0.6539	0.9241	2.5395	0.8640
WC2-7070250	0.8854	0.8840	2.0935	0.8463
WC2-7050175	5.3725	0.1071	-0.8038	0.1128
WC2-7050200	5.3476	0.1114	-0.7860	0.1163
WC2-7050225	3.3103	0.4642	0.2646	0.5119
WC2-7050250	3.3733	0.4533	0.2341	0.4995
WC1-3060200	1.6067	0.7591	1.2889	0.7771
WC1-3060225	0.2157	1.0000	—	0.8925
WC2-3060200	2.5379	0.5979	0.6649	0.6505
WC2-3060225	1.2900	0.8140	1.5808	0.8103
WC2-3070200	1.2672	0.8179	1.6046	0.8125
WC2-3070225	0.4603	0.9576	3.1402	0.8774
WC2-3050200	1.8355	0.7195	1.1112	0.7501
WC2-3050225	0.4309	0.9627	3.2709	0.8793
WH1-7060200	1.9579	0.6983	1.0243	0.7346
WH1-7060225	1.4123	0.7928	1.4603	0.7980
WH2-7060200	4.2189	0.3068	-0.1667	0.3240
WH2-7060225	1.3328	0.8066	1.5373	0.8060
WH2-7070200	1.2822	0.8153	1.5889	0.8110
WH2-7070225	1.3400	0.8053	1.5301	0.8053
WH2-7050200	3.3552	0.4564	0.2428	0.5031
WH2-7050225	1.3722	0.7998	1.4985	0.8021
WH1-3060200	4.2688	0.2982	-0.1906	0.3136
WH1-3060225	1.5800	0.7638	1.3112	0.7800
WH2-3060200	5.9910	0.0000	—	0.0446
WH2-3060225	1.1990	0.8297	1.6786	0.8190
WH2-3070200	1.9194	0.7050	1.0511	0.7395
WH2-3070225	0.5652	0.9395	2.7738	0.8703
WH2-3050200	5.0579	0.1616	-0.6004	0.1616
WH2-3050225	3.0344	0.5119	0.4012	0.5646

Table E.2 Desirability standard function form statistical analysis for twin screw extruded HDPE/PA-6 blends

Samples	dper-std	dimp-std	dten-std	D-std	Ranking
WC2-3070225	0.9830	0.9909	0.5213	93.88	1
WH2-7070200	0.9087	1.0000	0.8295	92.36	2
WH2-3070225	0.9751	0.6695	0.9892	90.01	3
WC2-7060225	0.9721	0.5067	1.0000	85.85	4
WC1-3060200	0.8706	0.9811	0.3063	84.18	5
WH2-3060225	0.9176	0.7560	0.3491	82.03	6
WH2-7070225	0.9023	0.6788	0.6115	81.73	7
WH1-3060225	0.8739	0.8359	0.2923	80.63	8
WC1-3060225	1.0000	0.4957	0.2559	79.95	9
WC2-7060250	0.9688	0.3622	0.7913	79.94	10
WH2-7060225	0.9031	0.8087	0.0493	79.41	11
WC2-3050225	0.9852	0.2649	0.8613	79.27	12
WC1-7060175	0.8138	0.6788	0.8917	78.78	13
WH2-3070200	0.8286	0.6879	0.7192	78.24	14
WC1-7060225	0.9887	0.4515	0.0941	76.49	15
WC2-3070200	0.9103	0.2649	0.8255	74.05	16
WH1-7060200	0.8230	0.6015	0.5347	73.88	17
WC2-3060225	0.9078	0.3073	0.6696	73.39	18
WC2-7070250	0.9482	0.2244	0.5993	73.24	19
WC2-7070225	0.9681	0.0509	0.4899	69.10	20
WH2-7050225	0.8987	0.2649	0.3560	68.59	21
WH1-7060225	0.8941	0.2443	0.4349	68.57	22
WC1-7060200	0.8903	0.0467	0.9377	68.42	23
WC1-7060250	0.9866	0.0755	0.2384	68.40	24
WC2-3050200	0.8404	0.3401	0.5255	68.38	25
WC2-7070200	0.8721	0.0932	0.7913	66.93	26
WH2-7050200	0.5637	0.9155	0.4657	64.18	27
WH2-3050225	0.6326	0.6879	0.4289	62.60	28
WC2-7050225	0.5736	0.5913	0.4942	57.01	29
WC2-3060200	0.7288	0.0870	0.6240	55.79	30
WH2-7060200	0.3631	0.9742	0.6921	54.87	31
WH1-3060200	0.3514	0.7640	0.6972	48.91	32
WC2-7050250	0.5596	0.3845	0.0681	46.67	33
WC2-7060200	0.4785	0.2859	0.7326	45.58	34
WH2-3050200	0.1811	0.8670	0.7719	41.17	35
WC2-7070175	0.3230	0.2753	0.8799	36.68	36
WH2-3060200	0.0499	0.8225	0.8324	32.13	37
WC2-7050175	0.1263	0.3622	0.7541	24.81	38
WC2-7060175	0.0531	0.2244	0.9943	19.00	39
WC2-7050200	0.1303	0.1687	0.5002	17.69	40